NASA TECHNICAL TRANSLATION

NASA TT F-598

ASTROMETRY AND ASTROPHYSICS

No. 3 - Problems of Astrophysics

Edited by A. F. Bogorodskiy

"Naukova Dumka" Press, Kiev, 1968

NATIONAL AERONAUTICS AND SPACE ADMINISTRATION • WASHINGTON, D. C. • NOVEMBER 1971

ASTROMETRY AND ASTROPHYSICS

No. 3 – Problems of Astrophysics

Edited by A. F. Bogorodskiy

Translation of "Astrometriya i Astrofizika, No. 3, Voprosy Astrofiziki"
"Naukova Dumka" Press, Kiev, 1968

NATIONAL AERONAUTICS AND SPACE ADMINISTRATION

For sale by the National Technical Information Service, Springfield, Virginia 22151
$3.00

This collection contains articles dealing with solar and stellar physics as well as with the structure of the galaxy. Nonstationary stellar processes, the theory of stellar rotation, certain problems of physics of the solar atmosphere and its active formations are considered.

This collection is intended for scientists working in the fields of theoretical and practical astrophysics, as well as for graduate and undergraduate students.

TABLE OF CONTENTS

A NEW TYPE OF SOLAR FLARE

E. A. Gurtovenko

ABSTRACT. Unusually intense emission in the D_1, D_2 lines was registered photoelectrically in an undisturbed region near the center of the solar disk on July 28, 1966. Various aspects of the possibility that the emission is due to the processes of resonance scattering or fluorescence are analyzed using both natural and artificial comets. It is shown that the observed emission is of solar origin. The appearance of a spot group in the same place after its passage over the solar disk seems to indicate a connection between the sodium flares and the formation of an active region on the sun.

An unusual sodium emission was observed photoelectrically at the Main /7* Astronomical Observatory of the Academy of Sciences of the Ukrainian SSR on July 28, 1966, using the new ATsU-5 telescope. The principal features of the telescope are as follows: the diameters of the coelostat and main mirror are 440 mm; the focal length of the main mirror is 17 m; the focal length of the spectrograph mirrors is 7 m; the diffraction grating is 140 x 150 mm 600 scanning lines/mm. The Abbe number near the D_1 and D_2 sodium lines is approximately equal to 0.11 Å/mm in the fifth order of double transmission.

Recordings were begun for D_2 lines in an undisturbed region near the center of the disk at 0622 UT. The first recording (Figure 1a) was off the scale at the center of the line, suggesting a malfunction. A second, check, reading was taken at double the scanning rate, that is, at 9.2 Å/sec., instead of 4.6 Å/sec. The second trace (Figure 1b) confirmed the picture. Only a small emission peak in the red range had disappeared. A series of consecutive traces of sodium emission was then obtained with the sun roughly guided into a slit to trace the nature of the change in emission in one particular place. The sun moved perpendicularly to the slit about 1' between the first and second traces. Later on this made it possible to evaluate the lower boundary of the dimensions of the emission region. The height of the slit remained constant while recordings

* Numbers in the margin indicate pagination in the foreign text.

were being made, and was equal to approximately 7.5 mm, or 1.5'.

Figure 1, c-i, shows subsequent traces of the same region. One of them (Figure 1e) was obtained at the D_1 line.

Trace scales varied. The scale along the Y-axis was reduced at the beginning of the observations to avoid off-scale readings of emission peaks. The Y-axis scale was also changed when changes were made from the D_1 line to the D_2 line, and vice-versa. In all cases, the intensity I, was tied in with the units of the adjacent continuum. In those cases when the far D_2 wings did not register, they were tied in with the continuous spectrum with an accuracy of a few percentage points.

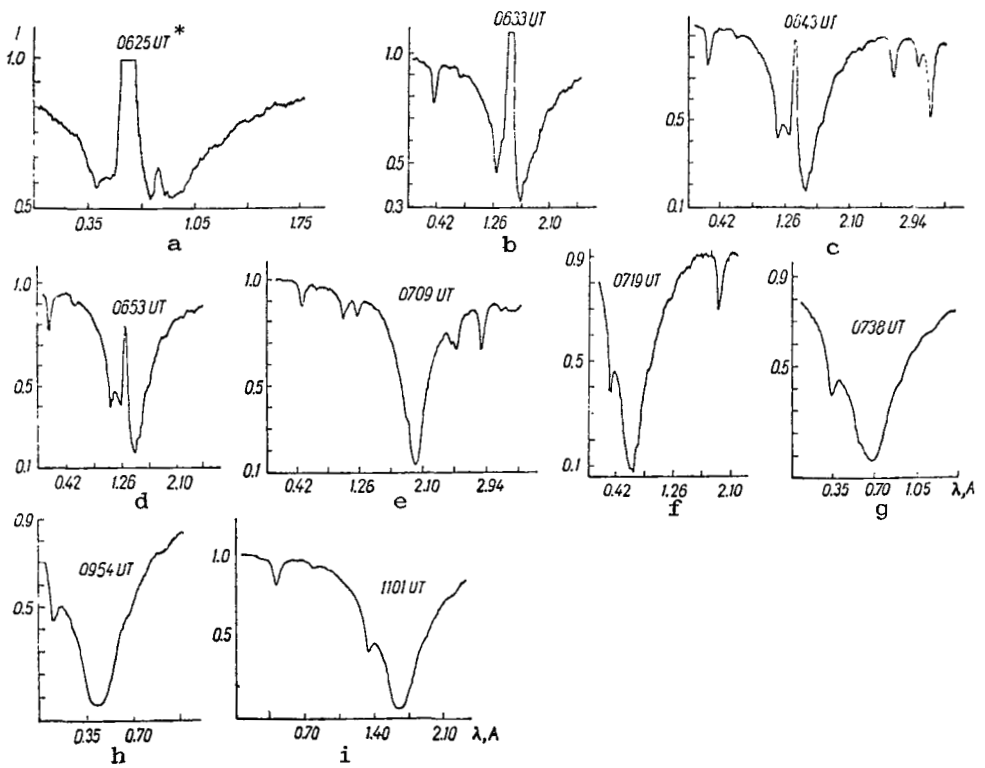

Figure 1. Copies of traces of sodium emission on July 28, 1966, in an undisturbed region of the solar disk.

Traces were obtained over different time intervals, because of variable cloudiness. Observations were completely impossible for this reason between

*Translator's Note: UT - universal time, or Greenwich mean time (GMT).

0740 and 0950. It should be pointed out that cloudiness was the primary reason for our inability to obtain more extensive observations of this phenomenon. In particular, we were unable to conduct spectrographic analysis. /9

The most unusual fact was that sodium emission was observed in an undisturbed region. H_α motion pictures of the disk during this same period and during preceding hours of the day, failed to detect any evidence of activity in this region. Figure 2 shows an H_α filtrogram with the slit of the spectrograph drawn on the disk for the moment of registration (the dash shows the position of the spectrograph slit in the region where the sodium flare was observed). The coordinates of the center of the slit are $\varphi \approx +8°$, $L \approx 252°$.

The rarity of this phenomenon caused many people to doubt the solar origin of this emission. Sodium emission also can be observed from comets, artificial or natural, as well as from the sun. Therefore, we will analyze, briefly, the possibility of such emission from a quantitative point of view.

An Artificial Comet in Interplanetary Space or in the Upper Atmosphere of the Earth

The wavelength of the center of emission was established with respect to telluric lines of water vapor, for which, from reference [1], we have: λ = 5877.226, 5887.664, 5888.708, 5891.186, 5891.665 Å. The wavelength of the emission on traces Nos. 2-4 was 5889.838, 5889.849, and 5889.853 Å, with an error not in excess of ±0.005 Å, and the corresponding radial velocities were -7, -6.5, and -6 km/sec.

The mean altitude of the sun during the observation period was about 44°, so the radial velocity of the emission source relative to the earth was approximately 5 km/sec. We can assume to be unrealistic the possibility of so high a radial velocity for a sodium cloud ejected from a rocket, or from an artificial earth satellite.

The only way an artificial sodium cloud can be observed on the disk of the sun under the usual conditions prevailing in the upper atmosphere, or in interplanetary space is in absorption (resonance scattering). However, let us suppose that it is possible to artificially excite the sodium in such a cloud. The total intensity of the F emission in the D_2 line, computed from the first

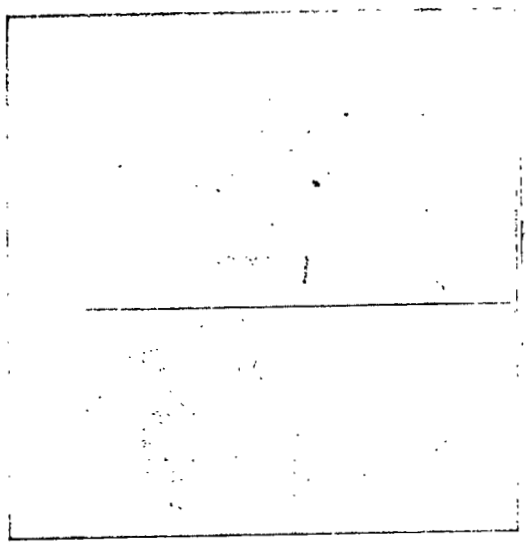

Figure 2. H_α filtrogram of the solar disk on July 28, 1966, at 0630 (the dash shows the position of the spectrograph slit in the region in which the sodium flare was observed).

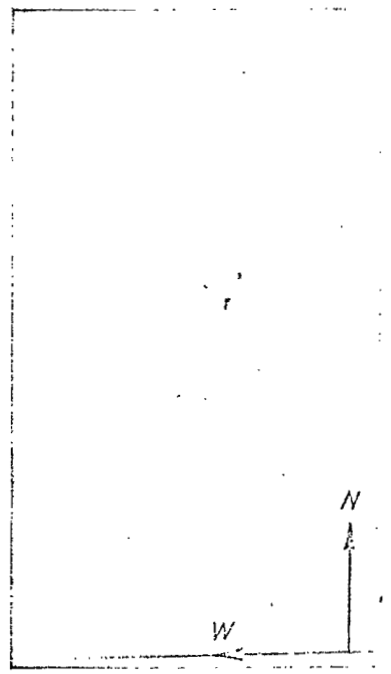

Figure 3. A young sunspot group that formed on August 29, at 0528 in the region in which the sodium flare was observed.

/10

trace (see Figure 1a), is 0.27 equivalent A, or $7.3 \cdot 10^5$ erg $\cdot$ cm^{-2} X sec^{-1} ster^{-1}. This magnitude is the lower boundary of the emission. /11

The total energy flux from 1 cm^2 on the boundary of the emitting cloud was $\pi F > 2.3 \cdot 10^6$ erg $\cdot$ cm^{-2} $\cdot$ sec^{-1}. The angular size of the cloud was at least 1' at the start of the observations. A sharp emission peak was observed for about 30 minutes, and during this time the emission had a radial velocity with respect to the earth of about -5 km/sec. Consequently, the distance to the cloud at the start of the observations was at least 9000 km, and its diameter was $d > 2.7$ km. The total power radiated by the cloud in the D_2 line was $\pi d^2 \cdot \pi F > 5 \cdot 10^{17}$ erg/sec, or $5 \cdot 10^7$ kw. It is quite obvious that no artificial excitation of the sodium in a cloud such as this could provide so powerful a radiation in the D_2 line.

The excitation of sodium lines by ultraviolet solar radiation (the fluorescence mechanism) can be assumed. It is perfectly clear that this mechanism

could be effective only when strong emission lines are present in the spectral region near the boundary of the main sodium series (λ = 241 millimicrons). However, let us make a quantative appraisal. Let us introduce a sodium atom scheme with three energy levels and a continuum. Let us designate levels 3^2S, 3^2P, and 4^2S as 1, 2, and 3 respectively, and ignoring excitation and ionization by electron collision, as well as the effect of line radiation, let us write the equations of stationarity for three levels:

$$\left.\begin{array}{c} n_1 C_1 = n_2 A_{21} + R_1 n^+ n_e, \\ n_3 A_{32} + R_2 n^+ n_e = n_2 A_{21} + n_2 C_2, \\ R_3 n^+ n_e = n_3 A_{32} + n_3 C_3. \end{array}\right\} \quad (1)$$

The recombination coefficients, R_i, only differ by a factor of three for temperature values T = 200 and 2000°.

The density of the radiating field required to find the photoionization coefficients was determined by taking dilution at a distance of 1 atomic unit into consideration. The basic parameters for computing the coefficients C_i and R_i, were taken from Allen's handbook [2]. Assuming $n^+ = n_e$, Eq. (1) yields $n_2 \approx 5 \cdot 10^{-13} n_1$.

Let us assume the maximum weight of the artificial comet to be $5 \cdot 10^6$ grams. It is easy to show that the total number of sodium atoms in a unit column on the line of sight to such a comet is $N_1 < 10^{18}$. The mechanism of fluorescence provides a total number of radiating particles in a unit column for this N_1 of $N_2 < 5 \cdot 10^5$. From observations $N_2 = 4\pi F/A_{21} h\nu > 6 \cdot 10^{10}$ in the sodium flare. /12

A Natural Comet

It should be pointed out that no comet was observed near the sun on or about July 28, 1966. However, cases of passage of faint comets, those in positions that are unfavorable for observation as they approach the sun, are not excluded.

What follows from the data on the total mass of the head (for example, the data in reference [3]) and from the data on the total number of particles in the comet, or on the density distribution of particles at various distances from the nucleus [4, 5] for comets observed at distances from the sun on the order of 1 atomic unit, is that in the line of sight, the total number of particles of atoms, or molecules of various compounds, is not in excess of 10^{11}

to 10^{13}. Undoubtedly the condition $N_1(Na) \leq 10^{13}$ also is satisfied for sodium atoms. The D_1 and D_2 lines are rarely observed in the spectra of these comets, and emission in the most intense lines and in the CN, C_2 and other bands [6], are many orders of magnitude less than in the sodium flare of July 28, 1966.

Cases of comets passing through the solar corona at perihelion are extremely rare. In these comets emission in the D_1 and D_2 lines is intense. The first quantitative results of spectral investigation of the comet Ikeya-Seki 1965 f to appear in print [7] make a detailed discussion of this question unnecessary. The comet was at perihelion on October 21, 1965 at 0430 at a distance of 350,000 km from the photosphere. According to the data from the spectral analysis of photoelectric observations of this comet made on October 20, 1930, the total emission in the D_2 line is about 500 erg $\cdot$ cm^{-2} $\cdot$ sec^{-1} $\cdot$ $ster^{-1}$, and the total number of particles in a 1 cm^2 column on the line of sight is $N_2 \approx 3 \cdot 10^7$. This value is at least three orders of magnitude less than the lower boundary of the value of D_2 emission in the sodium flare of July 28, 1966, and approximately one order of magnitude less than the sodium emission in the bright "metallic" prominences [8].

Thus, if we ignore considerations based solely on guesses as to the possibility of a collision with the sun, or of the passage of some hypothetical cosmic body through the corona, we should conclude that the sodium flare was of solar origin. /13

The emission shift due to radial velocity (-0.13 Å), brought out in the telluric lines, has the same order of magnitude with respect to the lines of the solar spectrum because the radial velocity of the earth's orbital motion with respect to the sun was approximately -0.2 km/sec on July 28, 1966. Given this shift, hydrogen emission undoubtedly would be observed with an H_α-filter, the halfwidth of whose transmission band is 0.5 Å.

A strong sodium emission such as this, and without hydrogen emission, could occur in a layer of the solar atmosphere with a comparatively low temperature ($T < 8000°$), in which hydrogen excitation is determined only by the field of photospheric radiation. Moreover, compaction of material accompanied, possibly, by a reduction in temperature, should occur in the area of the sodium flare. The $n_1(Na)$ and n_e concentration increases with an increase in the compaction

of the material. The density of the upper levels of the D_1 and D_2 lines increases proportionally with $n_e \times n_1(Na)$, the result of excitation by electron collision. An increase in n_e, decreasing the degree of sodium photoionization, results in an additional increase in $n_1(Na)$, and in addition, increases the number of recombination transfers, thereby increasing the brightness of the D_1 and D_2 lines. Now, if there is a temperature decrease in the sodium flare region the sodium ionization by electron collision will also decrease. The decrease in collision transfers $1 \rightarrow 2$ is insignificant when the temperature decreases because, according to the computations in [9], the drop in z_{12} takes place more slowly than does that in z_{1i} when there is a reduction in temperature.

However, a detailed discussion, and final conclusions as to the mechanism involved in sodium excitation in these flares, can only take place and be arrived at in a sufficiently broad spectral range on the basis of photographic observations. There is no doubt that emission in the sodium flare should be observed in the metal lines, the excitation conditions for which are close to the excitation conditions for the D_1 and D_2 lines.

We should note one more striking fact. After one rotation of the sun, a large field of H_α-flocculae was observed in the same region in which the sodium flare was recorded. The field was relatively weak, its boundaries indistinct. Individual flocculae had a friable and fissured structure. The configuration of /14 the flocculae changed significantly during the day. A small filament appeared in the floccular field on August 23, and by August 29, a young active region with a sunspot group had appeared (Figure 3). In a subsequent passage across the disk, the same active region was seen from September 14 to 20, and was observed as part of PFP-ALERT, the international program. An anomaly of this region is a latitude that is low for an initial cycle. Its appearance can probably be related to the continuing activity of the old cycle.

The most interesting phenomena in this region, according to lookout H_α observations at the Main Astronomical Observatory of the Academy of Sciences of the Ukrainian SSR should be pointed out. A large filament appeared in the region $\varphi \approx +3°$, $L \approx 257°$ on September 15, near a large sunspot, and disappeared on September 16. On September 20, three flares and four recurrent surges were observed. One of the flares had a reading of 2n (Figure 4).

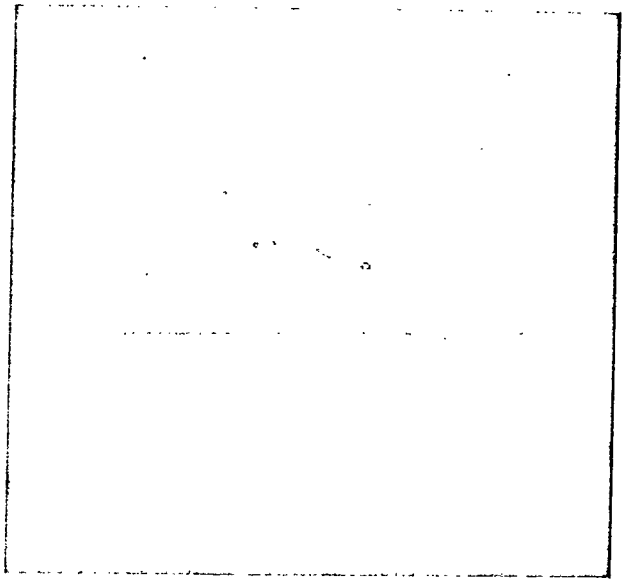

Figure 4. The active region in which the sodium flare was observed in H_α light during subsequent passage across the disk on September 20, 1966, at 1051.

A possible connection between the sodium flare and subsequent formation of an active region in the same place is of particular interest, not only from a scientific point of view, but also in connection with practical problems of long-range forecasting of solar activity. /15

REFERENCES

1. Charles, J. E., et al., Revision of Rowland Preliminary Table of Solar Spectrum Wavelengths, 1928, p. 171.

2. Allen, K. U., Astrofizicheskiye velichiny [Astrophysical Magnitudes], Foreign Literature Press, Moscow, 1961.

3. Kostyakova, Ye. B., IN: Aktivnyye protsessy v kometakh [Active Processes in Comets], "Naukova Dumka" Press, Kiev, 1967.

4. Konopleva, V. P., Problemy kometnoy fotometrii (Informatsionnyy byulleten' No. 10) [Problems of Comet Photometry (Information Bulletin No. 10)] "Naukova Dumka" Press, 1966, p. 77.

5. Swings, P., Quart. Journ. Royal Astro. Soc., Vol. 6, 1965, p. 1.

6. Kostyakova, Ye. B., Problemy kometnoy fotometrii [Problems of Comet Photometry] Vol. 10, 1966, p. 65.

7. Curtis, G. W., Astro. Journ., Vol. 71, 1966, p. 3.

8. Morozhenko, N. N., Solnechnyye dannyye, Vol. 10, 1965, p. 45.

9. Alikayeva, K. V., Solnechnyye dannyye, Vol. 7, 1966, p. 63.

THE PROBLEM OF THERMAL EXPLOSION IN A DEGENERATE GAS

V. V.Porfir'yev and Yu. N. Redkoborodyy

ABSTRACT: The process of hydrogen burning in a stream of matter penetrating the degenerate nucleus of a white dwarf is considered.

Widespread attention has recently been given to an idea advanced by Mestel [1], which is that the outburst of a Nova is caused by the burning of hydrogen penetrating from the shell of a white dwarf to the region of the degenerate nucleus. The process of hydrogen burning under these conditions has never been examined in detail. The purpose of this article is to investigate the possibility of a thermal explosion under these conditions. /16

We will assume that a hydrogen flow in the form of a limited stream penetrates the region of the degenerate nucleus from the shell and that the temperature, and the density, of the stream are automatically established as the same as in the surrounding gas. To be definite, it is assumed that the flow rate satisfied the condition

$$\rho v = \text{const.} \tag{1}$$

The rate of hydrogen depletion is determined by the expression

$$\frac{dX}{dt} = -\frac{\varepsilon_{pp}}{E_p^*} - \frac{\varepsilon_{cc}}{E_C^*}, \tag{2}$$

where X is the relative content of hydrogen in the stream material.

Since it can be assumed as a first approximation that the thermal conductivity of the degenerate gas is infinitely high, the stationary problem of hydrogen distribution in the stream can be examined. After substituting the expressions for ε_{pp} and ε_{cc} in Eq. (2), it can be converted into

$$\frac{dX}{dr} = -\frac{1}{\rho v}\left\{\frac{2{,}5\cdot 10^6\rho^2X^2\left(\frac{10^6}{T}\right)^{\frac{2}{3}}\exp\left[-33{,}8\left(\frac{10^6}{T}\right)^{1/3}\right]}{E_p^*}f_p + \right. \tag{3}$$

$$\left. + \frac{9{,}5\cdot 10^{28}\rho^2XX_{CN}\left(\frac{10^6}{T}\right)^{2/3}\exp\left[-152{,}3\left(\frac{10^6}{T}\right)^{1/3}\right]}{E_C^*}f_c\right\},$$

where f_p and f_c are factors that take the electron shielding of the nuclei into consideration. Eq. (3) was solved numerically on a "Promyn" electronic computer. /17 The concrete computation posited that the degenerate nucleus was isothermal, that its temperature was 10^7°K, that the density distribution was approximated by the polytropic curve for n = 1.5 and that central density was taken as $3.7 \cdot 10^6$ g/cm^3. The electron shielding was taken into consideration by approximate formulas [2].

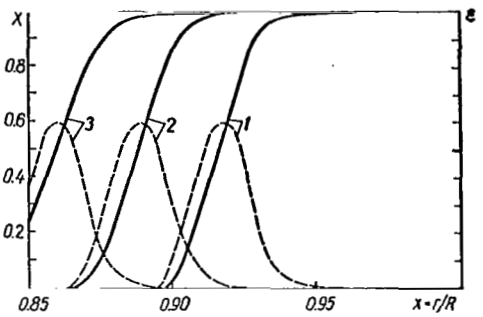

Hydrogen distribution in a stream for ρv = 0.01 (1), 1 (2), and 100 (3). The solid lines show the hydrogen distribution, and the dashed lines the power distribution of the energy sources (in relative units).

Penetration into the degenerate nucleus by the hydrogen stream leads to the appearance of a layer source (see figure) of extremely small geometric thickness (of the order of a few percent points of the radius of the white dwarf). Hydrogen burning takes place almost exclusively in this layer.

The position of the layer source has little relationship to stream velocity. Practically, it can be assumed that the layer source appears at geometric depths where the density of the material reaches values of the order of 10^5 g/cm^3. This can be explained by the fact that given the comparatively low temperature used, the reaction rate can be determined by conditions of nucleic shielding. Apparently, the position of the layer source will not vary very much with small changes in temperature.

It is probable that the results obtained will not change if some other mechanism (diffusion, movement of the boundaries of the degenerate region, and the like) is considered as the reason for hydrogen penetration into the nucleus, rather than a stream. The appearance of a thin layer source in the depths of /18 a star results in heating of the material. An interesting question is that of the space-time distribution of temperature in the immediate vicinity of the layer source. A possible approach to the solution of this problem will be discussed in a later article.

REFERENCES

1. Mestel, L., MN, Vol. 412, 1952, p. 598.

2. Frank-Kamenetskiy, D. A., Fizicheskiye protsessy vnutri zvezd [Physical Processes Inside Stars], Fizmatgiz, Moscow, 1959.

A THEORY OF NONSTATIONARY NONADIABATIC SHOCK WAVES

I. A. Klimishin

ABSTRACT. The Chiznell-Wizem method, which permits finding approximate changes in parameters at the shock wave front is generalized to account for energy losses attributable to ionization and radiation. These losses are estimated for the particular case of shock wave motion in the shell of a red giant. The case of isothermal shock waves is considered. It is shown that the velocity distribution of a shock wave in the atmosphere of an RR Lyrae type variable can be explained by a solution based on the assumption that the shock wave is not completely isothermal.

A number of approximate methods have been developed over the past 10 to 15 /19 years to solve equations of cosmic hydrodynamics because every year the number of investigations made of the physics of nonstationary stars (outbursts of novae and supernovae, pulsations, the efflux of matter from stellar atmospheres, and others) grows ever larger. A summary of these approximate methods is contained in references [1-3], which discuss their shortcomings and list in brief the problems, solutions of which were obtained by some one particular method. However, most of these methods are limited to the concept of adiabatic motion of a shock wave.

Possible energy losses due to ionization and radiation can be accounted for by the Brinkley-Kirkwood (B-K) method. But it is easy to show that this method is totally unsuited for a description of the motion of a shock wave in the outer layers of a stellar shell and in stellar atmospheres, because the force of a shock wave is greatly overestimated as compared with that found by other methods; by the Chiznell-Wizem (C-W) method, for example.

The simplicity of the Chiznell-Wizem method (the convenience in making the computations) makes it appropriate to generalize it for the case of nonadiabatic shock waves. This presents an opportunity to analyze the influence of energy losses attributable to ionization with motion of the shock wave in the cold shell of a star of late spectral class, and of energy losses attributable to

luminescence when the shock wave reaches the surface of the star. We will generalize this method for the case of nonstationary isothermal shock waves, as well, in order to interpret the observation data on the motion of shock waves in the atmospheres of a number of pulsating variable stars (the RR Lyrae, RV Tauri and others).

We should mention, in passing, that the big discrepancy in the intensity of the shock wave obtained in reference [2], when this method is compared with other methods, is not that this method is any worse than the others, but rather that it is practically insensitive to an almost abrupt stopping of a piston, moving after the wave front. This is confirmed by Case 1, cited in reference [2], for which the results of the computation by the C-W method are close to the automobile method, and are obtained more precisely by the B-K method.

Ionization Energy Losses at the Front of a Nonstationary Shock Wave

Let us, in order to account for energy losses attributable to ionization, /20 write the conditions for the conservation of mass, impulse, and energy satisfied at the front of the shock wave:

$$\left.\begin{aligned} \rho_1 u_1 &= \rho_2 u_2, \\ p_1 + \rho_1 u_1^2 &= p_2 + \rho_2 u_2^2, \\ \rho_1 u_1 \left(w_1 + \frac{u_1^2}{2}\right) &= \rho_2 u_2 \left(w_2 + \frac{u_2^2}{2}\right), \end{aligned}\right\} \qquad (1)$$

where

ρ, p are the gas density and pressure, respectively;

u is its velocity relative to the wave front;

$w = \gamma p/(\gamma-1)\rho + w_0$ is the enthalpy;

$w_{01}-w_{02} = Q$ is the energy absorbed ($Q < 0$) at the front of the shock wave in the computation per gram of matter (the subscripts "1" and "2" designate parameters before, and after, the wave front).

The Eq. (1) system can be solved easily for $u_2/u_1 = \rho_1/\rho_2$. As a result, we find the equation of the shock adiabat in the form

$$\frac{u_2}{u_1} = \frac{\rho_1}{\rho_2} = \frac{\frac{\gamma+1}{\gamma-1} + \frac{p_2}{p_1} + 2Q\frac{\rho_1}{p_1}}{\frac{\gamma+1}{\gamma-1}\cdot\frac{p_2}{p_1} + 1} \qquad (2)$$

We can convert the last term in the numerator into the form $2\gamma Q/a^2$, where $a = \sqrt{\gamma RT}$ is the speed of sound in an undisturbed gas. The energy absorbed in the computation per gram of matter can be estimated by the expression

$$Q = \frac{\sum_i n_i (x_{i2} + x_{i1})\varkappa_i}{\sum_i n_i m_i}, \qquad (3)$$

where /21

x_{i2} and x_{i1} are the ionization levels for the i-th element after and before the front of the shock wave;

$\varkappa_i$ is the ionization potential;

n_i is the number of particles of the i-th variety per unit of volume;

m_i is the particle mass.

In the case of what is purely a hydrogen shell $Q = (x_2 - x_1/m_H)\chi$ and, in particular, when $x_1 = 0$ and $x_2 = 1$, we find that $Q = 1.3 \cdot 10^{12}$ e/g.

In the case of the real stellar shell of a red giant [4], when $r/R = 0.9$, $x_1 = 0.94$, $a^2 = 4.5 \cdot 10^{12}$, and the ratio when $x_2 = 1$ proves equal to 0.098; when $r/R = 1$ and $x_1 = 0$, $2\gamma Q/a^2 = 6.4$.

$2\gamma Q/a^2 \approx 10$ for the shells of red supergiants of the Mira Ceti type ($T \approx 2000$-3000). From whence it follows that if $p_2/p_1 = z$ is not too great, the consideration of energy losses in Eq. (2) can significantly alter the ratio ρ_1/ρ_2, and, possibly, the velocity of the shock wave itself.

The essence of the Chiznell-Wizem method, as we know, is that the inhomogeneous medium in which a shock wave is propagated is a set of an infinite number of thin, homogeneous layers, on the interfaces of which pressure and density change abruptly. When a shock wave crosses an interface such as this, a rarefaction wave will travel back toward the denser medium [5]. Let us introduce the following notations. Let two thin media be separated by an in-

finitely thin layer of mass $\Delta m = \rho\Delta x$. The values for the undisturbed parameters to the left of this layer will be denoted by the subscript "1", and those to the right by the subscript "5". The gas parameters after the shock wave front will be denoted by the subscript "2" to the left of the layer, and by the subscript "4" to the right. The rarefaction wave travels toward the denser medium. The parameters after the front of this wave will be denoted by the subscript "3". The equality $u_1 = u_5$ is satisfied because the gas is at rest prior to passage of the shock wave. Furthermore, the rarefaction wave velocity u_3 is equal to the gas motion velocity to the right of the infinitely thin layer, u_4. The pressure difference $p_5 - p_1$ is determined by the condition of hydrostatic equilibrium:

$$p_5 - p_1 = -g\rho\Delta x = \Delta p.$$

Since $u_3 = u_4$, the following equality, too, must be satisfied:

$$p_4 - p_3 = \Delta p = p_5 - p_1.$$

Introducing the notations $z_{12} = p_2/p_1$, $z_{54} = p_4/p_5$, $z_{23} = p_3/p_2$, and $\lambda^2 = \gamma-1/\gamma+1$, from the identity $p_3 = p_4 + p_1 - p_5$, we find

$$z_{12}z_{23} = \left(1 + \frac{\Delta p}{p_1}\right) z_{54} - \frac{\Delta p}{p_1}, \tag{4}$$

and from Eq. (2) /22

$$\frac{\rho_2}{\rho_1} = \frac{z_{12} + \lambda^2}{1 + \lambda^2 z_{12} + \frac{2\lambda^2\gamma Q}{a^2}} \tag{5}$$

Furthermore, from the known shock wave theory relationship

$$u_2 - u_1 = \pm \sqrt{(p_2 - p_1)\left(\frac{1}{\rho_1} - \frac{1}{\rho_2}\right)} \tag{6}$$

after substituting Eq. (5) in it and making simple transformations, we find

$$u_2 = u_1 \pm (z_{12} - 1)\left\{p_1 \cdot \frac{1 - \lambda^2}{\rho_1} \cdot \frac{z_{12} + \lambda^2}{(z_{12} + \lambda^2)(z_{12} - 1)} - \frac{2\lambda^2 Q}{(z_{12} + \lambda^2)(z_{12} - 1)}\right\}^{1/2} = \tag{7}$$
$$= u_1 + \Phi(z_{12}, p_1, \rho_1).$$

Analogously to Eq. (7) we can write

$$u_5 = u_4 + \Phi_{54}; \quad u_3 = u_2 + \Phi_{23}, \tag{8}$$

where Φ_{54} and Φ_{23} are obtained from Eq. (7) by the corresponding exchange of subscripts. Using the condition of the equality of velocities ($u_1 = u_5$, $u_3 = u_4$), we find from Eqs. (7) and (8) that

$$\Phi(z_{12}, p_1, \rho_1) - \Phi(z_{23}, p_2, \rho_2) = \Phi(z_{54}, p_5, \rho_5). \tag{9}$$

At the same time, it should be borne in mind that in the expression for Φ_{23}, corresponding to the rarefaction wave, Q = 0, since there are no energy absorption processes at the front of this wave.

The systems of Eqs. (4) and (9) will yield a differential equation establishing the change in the intensity of the shock wave, z, with distance. To do this, let us rewrite Eq. (5) in the explicit form

$$\begin{aligned}(z_{12}-1)\left\{\frac{p_1(1-\lambda^2)}{\rho_1(z_{12}+\lambda^2)} - \frac{2\lambda^2 Q}{(z_{12}+\lambda^2)(z_{12}-1)}\right\}^{1/2} - (z_{23}-1)\times \\ \times\left\{\frac{p_2(1-\lambda^2)}{\rho_2(z_{23}+\lambda^2)}\right\}^{1/2} = (z_{54}-1)\left\{\frac{p_5(1-\lambda^2)}{\rho_5(z_{54}+\lambda^2)} - \right. \\ \left. - \frac{2\lambda^2 Q}{(z_{54}+\lambda^2)(z_{54}-1)}\right\}^{1/2}\end{aligned} \tag{10}$$

Excluding from this equation the magnitudes $p_5 = p_1 + d_p$ and $\rho_5 = \rho_1 + d\rho$, ignoring squares with small magnitudes, and using Eq. (4), we find, after simple algebraic transformations, the following differential equation for the change in the intensity of the shock wave /23

$$\frac{dz}{d\ln r} = -\frac{\left\{\frac{K-1}{K} + 2[\quad]^{1/2}\right\}\frac{d\ln p}{d\ln r}}{\frac{2}{z-1}\{1+[\quad]^{1/2}\} - \frac{1}{\lambda^2+z} - \frac{2\gamma(1+\lambda^2)\lambda Q}{(1-\lambda^2)(z+\lambda^2)(z-1)^2 a^2}}, \tag{11}$$

where

$$\begin{aligned}[\quad] = \frac{1+z\lambda^2}{z(1+\lambda^2)} - \frac{2\gamma\lambda^2 Q}{a^2}\cdot\frac{2(1+\lambda^2)z-(z+\lambda^2)}{z(z-1)(1-\lambda^4)} - \\ - \frac{4\gamma^2\lambda^2 Q^2}{(1-\lambda^4)z(z-1)a^4};\end{aligned} \tag{12}$$

$K = d \log p / d \log \rho$. If there are no energy losses at the front of the shock wave ($Q = 0$), Eq. (11) becomes the well-known equation of the Chiznell-Wizem theory.

The derivation of Eq. (11) assumed that the magnitude of the energy, Q, absorbed at the wave front will not change during the transition of the wave front from medium "1" to medium "5" nor is it a function of shock wave intensity. Therefore, the solution to the problem of the influence of energy losses at the wave front on wave motion should be sought in the following order: first, compute shock wave motion for $Q \approx 0$; then compute the ionization level x_2, in terms of temperature T_2 found after the wave front, using the Saha formula; and, finally, compute the magnitude of Q through Eq. (3). Equation (11) can now be solved. The following approximation can be made, if necessary.

We note that in reference [6], the differential equation for the change in shock wave intensity was obtained on the assumption that $Q = \text{const}(z-1)^n$, when $n = 1$. However, the numerical solutions of this equation are difficult to apply to concrete astrophysical problems.

Eq. (11) was used to estimate the effect of loss of wave energy attributable to ionization on change in the intensity of a shock wave moving in the shell of a red giant. Several years ago it was suggested [7] that a shock wave could be the mechanism providing separation of the shell of a red giant and the subsequent /24 formation of a planetary nebula. However, the emergence of such a wave onto the surface of the star would have to be accompanied by a sharp increase in the brightness of the star, that is, by a flare (this was brought to our attention by D. K. Nadezhin). Since one planetary nebula appears in our galaxy every year, on the average, flares accompanying the formation of planetary nebula should have been recorded. However, the problem of the origin of planetary nebulae still is an enigma.

TABLE 1

r/R	$n=\frac{d\ln p}{d\ln r}$	$z=\frac{p_2}{p_1}$	$M=\frac{D}{a}$	D,km	r/R	$n=\frac{d\ln p}{d\ln r}$	$z=\frac{p_2}{p_1}$	$M=\frac{D}{a}$	D, km
0.30	1.38	4.82	2.01	167.5	0.70	4.74	16.87	3.70	155.4
0.35	1.51	5.35	2.21	162.2	0.75	6.00	23.02	4 31	161.8
0.40	1.68	5.95	2.23	157.4	0.80	7.80	34.38	5.26	169.0
0.45	1.92	6.88	2.36	153.5	0.85	10.62	61.24	7.01	189.4
0.50	2 22	7.52	2.49	150.8	0.90	13.44	120.94	9.85	206.3
0.55	2.62	8.76	2.68	149.2	0.95	25.02	303.15	15.58	241.5
0.60	3.18	10.47	2.93	149.3	0.98	75.00	1027.11	28.67	358.4
0.65	3.88	12.97	3.25	150.2	1.00	- -	20800 00	128.22	1153.9

Table 1 shows the results of the computation to find shock wave velocity in the shell of a red giant with parameters m = 1.30 $m_\odot$, R = 21 $R_\odot$ [4]. Here n = -d log ρ/d log r. The velocity of a shock wave with known z can be determined through (γ = 5/3)

$$D = a\sqrt{\frac{\gamma+1}{2\gamma}z+\frac{\gamma-1}{2\gamma}}. \tag{13}$$

The computations were made using Eq. (11), when Q = 0; at the same time $\Delta r/R = 0.01$ for $0.3 \leq r/R \leq 0.8$ and 0.005 for $r/R > 0.80$.

The sphericity of the shock wave was taken into consideration during the initial stage of motion [8]. As will be seen from Table 1, shock wave velocity is practically constant along the entire shell, and this ensures its compactness, even after separation. However, in those layers of the shell in which ionization losses can be significant, shock wave intensity is high ($z > 100$), so the contribution of the corresponding terms in Eq. (11), proportional to Q/r, is negligibly small. It can be assumed, however, that the equation obtained is useful in computations of motion of low intensity waves in stellar atmospheres, as well /25 as for certain problems of the motion of shock waves in planetary atmospheres, where the ratio Q/a^2 can reach several tens or even hundreds.

Radiation Energy Losses at the Front of a Nonstationary Shock Wave

In the case when the shock wave reaches the upper layer of the shell ($\tau \sim 1$), its motion can be determined to a significant degree by the energy losses by radiation. Let us now present the law of conservation of energy at the wave front of Eq. (3) in the form

$$\rho_1 u_1\left(w_1+\frac{u_1^2}{2}\right)=\rho_2 u_2\left(w_2+\frac{u_2^2}{2}\right)+F, \tag{14}$$

where

F is the energy flux from the front of a wave traveling to infinity,

$w_1 = w_2$.

In this case the differential equation for determining the change in shock wave intensity has the form of Eqs. (11) and (12), but, instead of Q($Q < 0$), determined through Eq. (3), the following magnitude must be substituted

$$Q^* = -\frac{F}{\rho_1 u_1} \quad . \tag{15}$$

A more difficult problem is that of the magnitude of the radiation flux, F, from the wave front. It would be natural to assume, as was done in references [7, 9], that $F = \sigma T_2^4$. However [10], the maximum flux from the wave front in a perfectly transparent gas leading to an isothermic shock wave, is

$$F_{max} = \frac{1}{2}\rho u_1^3, \tag{16}$$

so that its relationship to the temperature after the wave front, computed for the adiabatic case, is determined by the relationship

$$F_{max} = \frac{1}{2}\rho\left(\frac{16RT_2}{3\mu}\right)^{3/2}.$$

Assuming that the luminescence after the wave front is a maximum such that the wave becomes isothermic, we find, from Eqs. (15),and (16) (if the gas before the front of the shock wave was quiescent, $u_1 = D$), that /26

$$Q^* = -\frac{1}{2} D^2,$$

and the magnitude of $2\gamma Q/a^2 = \gamma D^2/a^2 = \gamma M^2$ can attain considerable size. Considering furthermore that for isothermic shock waves $p_2/p_1 = z = \gamma M^2$ (here a, as before, is the adiabatic speed of sound), we obtain $2\gamma Q/a^2 = z$. Substituting this expression in Eq. (11) and (12), we can greatly simplify the latter, after which the numerical solution is elementary.

Using Eqs. (11) and (12), we computed the motion of a shock wave in the $r/R = 0.90$ to 1.0 layer of a model of a red giant, on the assumption of total luminescence. The density on the "surface" of the model was taken as 10^{-10}, the temperature as $T_0 = 4860°$. The optical thickness of this layer was $\tau \sim 1.5$, and the coefficient of opacity was computed using the Beam-Vitense data [11]. A shock wave breaking away from the shell of a red giant will reach the level $r/R = 0.90$ with a velocity of the order of 400 km/sec for the initial assumptions made. On the surface, without loss by radiation taken into consideration,

$D \approx 1200$ km/sec, but when maximum loss by radiation is considered, the velocity of the wave decreases to 970 km/sec upon reaching the surface, that is, by about 15%. Thus, when the shock wave reaches the observed layer of the stellar shell, there is a noticeable decrease in its velocity as a result of luminescence.

We should, however, beam in mind that the optical thickness of an undisturbed gas can increase significantly as a result of heating of the gas ahead by the radiation flux from the wave front. As a result, the radiation produced in the intermediate region of the heating zone [12, 13] tends to infinity, and the drop in velocity of the shock wave upon reaching the surface layer of the star will be less than that found.

Isothermal Nonstationary Shock Waves

As we know, one of the most characteristic anomalies of a series of variable stars (RR Lyrae, W Virgonis, RV Tauri) is the presence of discontinuities in the radial velocity curves for these stars; and a convincing argument can be made for periodic motion in the atmospheres of a number of pulsating variable shock waves of comparatively high intensity. At the same time, apparently due to a sharp decrease in density with altitude, the velocity of the shock wave increases from /27 the speed of sound at the boundary of the photosphere to several tens of kilometers per second in the upper chromosphere.

Since the motion of the shock wave takes place in quite a rarified medium, the optical thickness of which is significantly less than unity, it can be assumed that as a result of sharp luminescence this wave will be isothermal. Here, generalization of the Chiznell-Wizem method for the case of isothermal shock waves is of interest.

In an isothermal shock wave $\gamma = 1$, so we can write Eq. (2) in the form

$$\frac{p_2}{p_1} = \frac{\rho_2}{\rho_1} = M_s^2, \tag{17}$$

where

$M_s = D/a_s$ and $a_s = \sqrt{RT}$ is the isothermal speed of sound.

Substituting Eq. (17) in Eq. (6), we find the following expression in place of Eq. (7)

$$u_2 = u_1 \pm (z_{12} - 1)\, a_s/\sqrt{z_{12}},$$
$$\Phi = (z - 1)\, a_s/\sqrt{z}. \tag{18}$$

so that

Considering that $\sqrt{p_1/\rho_1} = \sqrt{p_2/\rho_2} = \sqrt{p_5/\rho_5} = a_s$, and substituting the values of Φ (z, p, ρ) according with Eq. (18) in Eq. (9), we obtain, in place of Eq. (10)

$$\frac{z_{12} - 1}{\sqrt{z_{12}}} - \frac{z_{23} - 1}{\sqrt{z_{23}}} = \frac{z_{54} - 1}{\sqrt{z_{54}}}, \tag{19}$$

from whence, using Eq. (4), after simple transformations we obtain the following differential equation for determining the change in shock wave intensity with distance

$$\frac{dz}{d\ln r} = -\frac{2\sqrt{z}(z-1)}{z+2\sqrt{z}+1}\,\frac{d\ln p}{d\ln r}, \tag{20}$$

The solution of this equation for a given pressure gradient is easy to obtain in quadratures.

Let us now consider two cases of pressure (density) distribution in the atmosphere of a star.

TABLE 2 /28

z	1.5	2.0	2.5	3.0	5.0	7.5	10.0
$\varphi(z)$	−1.757	−0.363	0.495	1.108	2.655	3.846	4.705
$\psi(z)$	1.581	3.992	5.891	7.571	13.289	20.931	28.403

15.0	20.0	50.0	100.0	200.0	500.0	1000.0
5.985	6.9635	10.680	14.396	19.293	28.485	38.466
44.220	61.240	185.58	457.68	1176.4	4277.1	11609.0

(1) The atmosphere is in equilibrium prior to passage of the shock wave. In this case the density distribution in an isothermal atmosphere can be written in the form

$$\rho = \rho_0 e^{-\frac{gh}{a_s^2}}, \tag{21}$$

where

g is the acceleration of gravity on the "surface" of the star, i.e., at the photosphere-chromosphere boundary.

Then, if R is the radius of the star,

$$\frac{d \ln p}{d \ln r} = \frac{d \ln \rho}{d \ln r} = -\frac{gR}{a_s^2} = A, \tag{22}$$

and the solution of Eq. (20) has the following form

$$\varphi(z) - \varphi(z_0) = A \ln \frac{r}{r_0} \approx A \frac{h}{R} \quad (h \ll R), \tag{23}$$

where

$$\varphi(z) = \sqrt{z} + 2 \ln (\sqrt{z} - 1); \tag{24}$$

z_0 is the value of the shock wave intensity at the point $r = r_0$. Table 2 shows the function $\varphi(z)$ in terms of the argument.

(2) The shock wave moves in an atmosphere already disturbed by a previous shock wave. This is the phenomenon observed in variables of the RR Lyrae, W Virgonis, RV Tauri, and certain other types. At the same time, periodic shock waves can cause the density distribution in the atmosphere of the star to differ significantly from the law of Eq. (21). In the simplest assumption that can be made as to the isothermality of shock waves, the density at given level h, directly before the arrival of the shock wave, can be evaluated by the expression [12]

$$\rho_1 = \rho_{10} e^{-\frac{gh}{a_s^2 M_s^2}}. \tag{25}$$

Then, taking $u_1 = -D$, such that /29

$$p_2 / p_1 = z = 4M_s^2, \tag{26}$$

we obtain a differential equation for shock wave intensity

$$\frac{dz}{d \ln r} = A \frac{2(z-1)}{\sqrt{z}(z + 2\sqrt{z} + 1)}. \tag{27}$$

Its solution is

$$\psi(z) - \psi(z_0) = 4A \ln \frac{r}{r_0} \approx 4A \frac{h}{R} \quad (h \ll R), \tag{28}$$

where

$$\psi(z)=\frac{1}{3}\sqrt{z}[z+3\sqrt{z}+6]+2\ln(\sqrt{z}-1). \tag{29}$$

Table 2 also lists the values of the function $\psi(z)$ for a series of z.

Let us now compare the solutions obtained with the observation data for the star RR Lyrae. The isothermal speed of sound in the atmosphere of this star is a_s = 7.52 km/sec. Taking g = 770 cm/sec^2, and R = $4.6\cdot10^{11}$ cm, we find that A = 632. According to Preston's data [15], when the brilliance of the star is practically at its minimum, a sharp shift occurs in the metallic lines in the violet direction, and 0.015 (736 sec) later the H and K Ca II lines split, and 0.09 (4420 sec) later the H_α line splits. The relative shift in the violet and red components of the absorption lines on the H and K Ca II level is Δv = 76 km/sec; on the H_α level, the shift is 112 km/sec. Converting from radial (star) velocities to radial velocities, with the effect of darkening the disk toward the limb taken into consideration ($u_{rad} = (24/17)\, v_{star}$), and taking the velocity of the gas upward after the wave front to be equal to its gradient downward before the wave front, we find, from the law of convervation /30 of mass, that

$$\left.\begin{aligned}&\rho_1(D-u_1)=\rho_2(D-u_2),\\&D=\frac{24}{17}\cdot\frac{\Delta v}{2}\left(\frac{x+1}{x-1}\right),\end{aligned}\right\} \tag{30}$$

where

$x = \rho_2/\rho_1 = 4$ in the adiabatic case and $x \to \infty$ in the isothermal case. Thus, what follows from observations is that in the isothermal case the shock wave velocity at the level at which the H and K Ca II lines are formed is D = 54 km/sec, and at the level of the formation of the H_α line, D = 79 km/sec.

It can be assumed that at the level of the metals, the shock wave is weak, and its velocity only slightly exceeds the adiabatic speed of sound (a = 9.65 km/sec). We will assume that it is equal to 12 km/sec.

As we know, the height of formation of the H and K Ca II lines in the solar spectrum is approximately twice, and the height of formation of the H_α line is approximately ten times, the height of formation of the metallic lines above the photosphere. We posit that an analogous stratification is sustained in the atmosphere of the RR Lyrae, although the conditions for spectral line

formation here are more complex. Taking the mean velocity of wave motion between the metallic levels and the H and K Ca II lines as D = 33 km/sec, we find the relative distance between these levels to be $0.24 \cdot 10^{10}$ cm. Movement from the H and K Ca II level to the H_α level takes place at a mean velocity of 66.7 km/sec in a time of 3680 sec, the distance between the levels is $2.46 \cdot 10^{10}$ cm, and the height of the H_α level above the metallic level is $2.70 \cdot 10^{10}$ cm. From whence we find the corresponding heights of the levels (in meters of line formation above the photosphere) to be: $h = 0.30 \cdot 10^{10}$ cm, $h_{Ca\ II} = 0.54 \cdot 10^{10}$ cm, $h_{H\alpha} = 3 \cdot 10^{10}$ cm. If $R = 4.3 \cdot 10^{11}$ cm, then $h/R = 0.0065$, $h_{Ca\ II}/R = 0.0117$, $h_{H\alpha}/R = 0.065$.

Now we find the shock wave velocity at the H_α level, proceeding from the solution of Eq. (27). Taking the velocity of the wave at the level of the photosphere to be 10 km/sec, we obtain $z_0 = 7.12$, $\psi(z_0) = 18$, $\psi(z) = 182$, $z = 50$, and $D = (a_s/2)\sqrt{z} = 6.2$ km/sec. This value is one-third the observed value.

But if the solution of Eq. (23) is used, that is, if it is assumed that the density distribution in the atmosphere of the star is close to the equilibrium of Eq. (21), and if it is considered that the downward gradient for the gas is equal to the upward velocity of the shock wave, that is, that $z = 4M_s^2$, then when $z_0 = 7.12$, we find that $\psi(z_0) \approx 3.5$; $\psi(z) = 44.6$, $z = 1400$, $D = 140$ km/sec, which is about twice the observed value. We should note that if we take the atmosphere before the front of the shock wave to be stationary, then $z = M_s^2$ and $D = a_s\sqrt{1400} \approx 280$ km/sec. /31

If, however, we assume the shock wave moving in the atmosphere of an RR Lyrae to be adiabatic, then a more or less acceptable value of the velocity at the H_α level will be obtained only if the density distribution before the front of the shock wave is given by Eq. (25). The values of the stellar parameters taken above from the computation of Eq. (11) when Q = 0, yield a velocity of $D_{H_\alpha} \approx 70$ km/sec. If, however, the distribution of Eq. (21) is used, then $D \approx 2000$ km/sec. Thus we can probably assume that the density distribution in the atmosphere of a pulsating variable in the presence of periodic shock waves is satisfactorily described by Eq. (25), and the moving shock wave is not completely isothermal. And we do not doubt the values of the stellar

parameters g and R. In particular, if we double g, we can obtain better concordance between the observation data and the solution of Eq. (28).

In conclusion, we note that, despite the approximation, the Chiznell-Wizem method does not permit us to draw definite qualitative conclusions even if we consider energy losses attributable to ionization and luminescence. The application of more rigorous methods to the computations will scarcely change the qualitative conclusions arrived at in this article.

REFERENCES

1. Harlehurst, J. Advances Astron. and Astrophys., Vol. 1, 1962, pp. 1-45.

2. Nadezhin, D. K. and Frank-Kamenetskiy, D. A., Astron. Zhurnal, Vol. 42, No. 2, 1965, p. 240.

3. Klimishin, I. A., Problemy kosmicheskoy fiziki, [Problems of Space Physics], Kiev Univ. Press, 1967.

4. Schwarzshield, M., Stroyeniye i evolyutsiya zvezd, [Structure and Evolution of Stars], Foreign Lit. Press, Moscow, 1961.

5. Ono, Y., Sakashita, S. and Yamazaki, H., Prog. Theor., Phys., Vol. 23, No. 2, Japan, 1960, p. 294.

6. Novak, A. F., Vysnik kiyvs'kogo un-tu, seryya astronomyy, Vol. 8, No. 7, 1966, p. 59; No. 8, 1967.

7. Kaplan, S. A. and Klimishin, I. A., Astron. Zhurn. Vol. 36, 1959, p. 410.

8. Sakashita, S. and Tanaka, T., Progr. Theor., Phys., Vol. 27, No. 1, 1962, p. 127.

9. Kogure, T. and Osaki, T., Publs. Astron. Soc., Japan, Vol. 13, No. 3, 1961, p. 250.

10. Sen, G. and Hess, A., B kn: Kosmicheskaya gazodinamika, [IN: Space Gas Dynamics], Foreign Lit. Press, Moscow, 1960. /32

11. Vitense, E., Zs. f. Ap., No. 28, 1951, p. 81.

12. Zel'dovich, Ya. B. and Raizer, Yu. P., Fizika udarnykh voln i vysokotemperaturnykh gidrodinamicheskikh yavleniy, [Shock Wave Physics and High-Temperature Hydrodynamic Phenomena], "Nauka", Moscow, 1966.

13. Klimishin, I. A., Voprosy astrofiziki, [Problems of Astrophysics], "Naukova Dumka", Kiev, 1967.

14. Klimishin, I. A., Astrofizika, No. 3, 1967, p. 2.

15. Frolov, M. S., Avtoreferat kandidatskoy dissertatsii [Author's abstract from a candidate dissertation], Shternberg State Astron. Institute, Moscow, 1965.

EXCITATION SOURCES IN THE CHROMOSPHERIC H_α LINE

R. I. Kostik and T. V. Orlova

ABSTRACT: The distribution of the excitation sources in the chromosphere was determined from the observed contour of the H_α line. Resonance scattering is the principle source of chromospheric excitation up to 3500 km below the photospheric level. Beginning from h = 5000 km, H_α radiation results from intrinsic excitation sources only.

It is customary when studying physical conditions in the chromosphere to assign some definite mechanism of atom excitation and to compute the line contours at different heights [1-3]. Then, after comparing the observed and computed total intensities, it is customary to draw conclusions as to the excitation sources of these lines. It is more difficult to find the distribution of the excitation sources directly from the observed contour. It is to this problem that we devote this article. /33

As we know [4], the energy sources, g(t), can be found through the equation

$$g(t) = B(t) - \frac{\lambda}{2}\int_0^{t_0} K(|t-t'|)\,B(t')\,dt', \tag{1}$$

where

t and t_0 are the optical depth and the thickness of the chromosphere along the line of sight, respectively;

λ is the probability of survival of a quantum during a unit event of diffusion;

$$K(y) = \left[\int_{-\infty}^{+\infty}\alpha(x)\,dx\right]^{-1}\int_{-\infty}^{+\infty}\alpha^2(x)\,E_1[\alpha(x)\,y]\,dx,$$

$$\alpha(x) = e^{-x^2}.$$

In this equation the source function B(t), as well as g(t) is unknown. The source function can be found through

$$I(t_0, \theta, x) = \int_0^{t_0} B(t)\,\alpha(x)\,e^{-\alpha(x)t\sec\theta}\sec\theta\,dt. \tag{2}$$

Eqs. (1) and (2) are valid if the atoms have only two discrete levels, if the frequency of the radiated quantum is completely independent of the frequency of the absorbed quantum, if the indicatrix of diffusion is spherical, and if energy absorption in the frequencies of the continuous spectrum is

negligiby small.

Eqs. (1) and (2) can be replaced by the following system of matrix equations [34] [5]:

$$\left.\begin{aligned} AB + G = 0, \\ I - CB = 0, \end{aligned}\right\} \tag{3}$$

where

A = $[a_{ik} - \delta_{ik}]$; C = $[c_{jk}]$ (i, k = 1, 2, ..., m);

m is the number of subdivisions of the optical thickness, τ_0, in the interval;

δ_{ik} is the Kronecker delta.

The matrices B, G, I are given by the columns

$$B = \begin{bmatrix} B\left(\frac{\tau_1}{2}\right) \\ B\left(\frac{\tau_1+\tau_2}{2}\right) \\ \vdots \\ B\left(\frac{\tau_{m-1}+\tau_m}{2}\right) \end{bmatrix}, \quad G = \begin{bmatrix} g\left(\frac{\tau_1}{2}\right) \\ g\left(\frac{\tau_1+\tau_2}{2}\right) \\ \vdots \\ g\left(\frac{\tau_{m-1}+\tau_m}{2}\right) \end{bmatrix}$$

$$I = \begin{bmatrix} I(\tau_0, \theta, x_1) \\ I(\tau_0, \theta, x_2) \\ \vdots \\ I(\tau_0, \theta, x_m) \end{bmatrix}.$$

Matrix elements A and C are computed through the formulas

$$a_{ik} = \frac{\lambda}{2} \int_{\tau_{k-1}}^{\tau_k} k\left(\left| t - \frac{\tau_{i-1}+\tau_i}{2} \right|\right) dt, \; c_{ik} = \int_{\tau_{k-1}}^{\tau_k} \alpha(x_i)\, e^{-\alpha(x_i)\, t \sec\theta} \sec\theta \, dt.$$

The Eq. (3) system yields

$$G = -AC^{-1} I. \tag{4}$$

The solution of Eq. (4) is unstable [5, 6] in the sense that small changes in $I(t_0, \theta, x)$ correspond to big changes in B(t). Reference [6] proposed an approximate method for solving this problem, one that expands the source function in a power series of the optical depth, and then applies the least squares method. The result is

$$G = -ASI, \tag{5}$$

where $S = [s_{ij}]$; $s_{ij} = \sum_{l=1}^{n} t_i^{l-1} d_{lj}$; $[d_{lj}] = (\tilde{P}P)^{-1}\tilde{P}$; $\tilde{P}$ is the matrix of transposition to the matrix P. The matrix elements $P = [p_{il}]$ are found through ∠35

$$p_{il} = \frac{(l-1)\,p_{i\,l-1}}{\alpha(x_i)\sec\theta} + t_0^{l-1} e^{-\alpha(x_i) t_0 \sec\theta}, \quad l \neq 1;$$

$$p_{i1} = 1 - e^{-\alpha(x_i) t_0 \sec\theta}, \quad i, j = 1, 2, \ldots, m, \quad l = 1, 2, \ldots, n;$$

where n is the number of terms in the expansion of B(t) in summation form in powers of t, with m > n.

Thus with the contours of the chromospheric lines, and with the matrix AS from Eq. (5) available, we can find the distribution of excitation sources in the chromosphere.

Chromosphere observations were made with the ATsU-5 horizontal solar telescope in the Main Astronomical Observatory of the Academy of Sciences of the Ukrainian SSR in November 1966. One spectrogram with an H_α line, obtained on November 23, 1966, was chosen from a series of spectrograms. The angle between the direction of the slit and the tangent to the limb of the disk was about 34°. Photographs were taken in the second sequence, where dispersion in the H_α region was about 1.2 Å/mm.

Photometric processing of the spectrograms was done on an MF-4 microphotometer with an automatic recording attachment which allowed us to record intensities on the recorder tape [9]. Recordings were made of 11 photometric levels, corresponding to heights of 1500, 2000, ..., 6500 km above the level of the photosphere, which latter was established by the method used by V. A. Krat [7]. The profiles of the photometric levels are shown in Figure 1 [h = 1500 (1); 2000 (2); 2500 (3); 3000 (4); 3500 (5); 4000 (6); 4500 (7); 5000 (8); 5500 (9); 6000 (10); 6500 (11) km]. The given geometric heights correspond to particular optical thicknesses. If the number of atoms per unit volume decreases with height above the level of the photosphere according to the law $e^{-\beta h}$, then the optical depth in the direction of the radius is

$$\tau(r) = \int_r^\infty \sigma_0 e^{-\beta r}\, dr, \tag{6}$$

where

σ_0 is the coefficient of absorption in the center of the line;

β is the logarithmic gradient.

The optical thickness along the line of sight at height h above the level of the photosphere can be found through the following equation, as was shown in reference [2] /36

$$t_0(h) = \sigma_0 \sqrt{\frac{2\pi R}{\beta}}\, e^{-\beta h}.$$

Since

$$\tau_0 = \frac{\sigma_0}{\beta},$$

then

$$t_0(h) = \tau_0 \beta e^{-\beta h} \sqrt{\frac{2\pi R}{\beta}}. \qquad (7)$$

We will take the optical thickness of the chromosphere in the radial direction to be equal to unity and three, and we will assume that $\beta = 1.0 \cdot 10^{-8}$ cm (for the H_α line). Then Eq. (7) makes it easy to find $t_0(h)$ for each photometric level (Table 1). The AS matrices were computed for these values of t_0. The integration range [0, t_0] was divided into nine intervals (Figure 2); that is, m = 9. The following values were chosen for the dimensionless frequency $x = \Delta\lambda/\Delta\lambda_D$: 0.0, 0.3, 0.6, 1.0, 1.3, 1.6, 1.9, 2.2, 2.6. Multiplying the square AS matrix by column I, we obtain the unknown energy sources at optical depths r (in t_0 units), respectively equal to 0.01, 0.05, 0.14, 0.30, 0.50, 0.70, 0.86, 0.95, 0.99. The Doppler halfwidth of the H_α line was assumed to be constant at all heights, and equal to 0.460 Å. /37

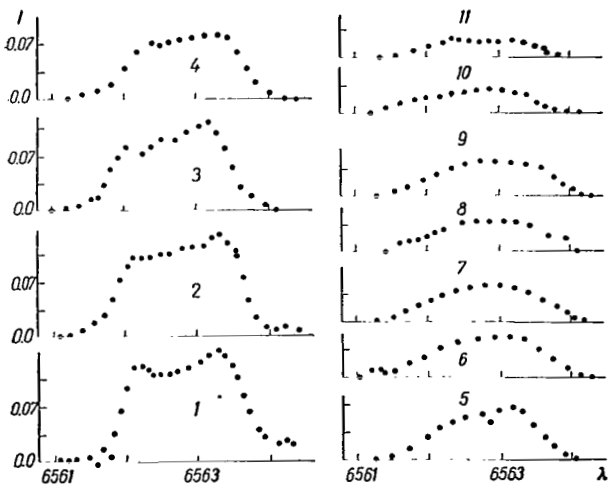

Figure 1.

The distribution of the excitation sources, g(t), along the line of sight at various heights above the photosphere level is shown in Figure 3 (the optical depth in t_0 units is plotted on the

TABLE 1.

h, km	t_0	
	$\tau_0=1$	$\tau_0=3$
2000	7.2	22.2
2500	4.2	12.6
3000	2.4	7.2
3500	1.4	4.2
4000	0.8	2.4
4500	0.47	1.4
5000	0.27	0.81
5500	0.16	0.48
6000	0.09	0.28
6500	0.05	0.15

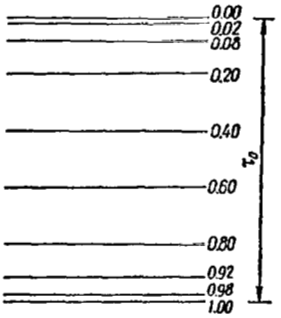

Figure 2.

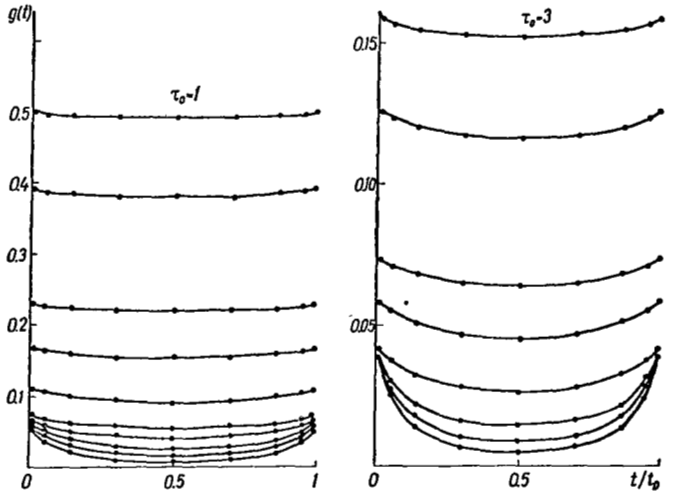

Figure 3.

X-axis, and the values of g(t) in units of the continuous spectrum of the photosphere are plotted on the Y-axis). /38

The values of g(t) are the sum of own sources of energy and sources attributable to photospheric radiation. The distribution of excitation sources in the chromosphere caused by photospheric radiation can be described by the formula [8]

$$g(\tau_0-\tau) = \frac{\lambda\omega}{2\sqrt{\pi}}\int_{-\infty}^{+\infty} I_0(x)\,\alpha(x)\,E_2[\alpha(x)(\tau_0-\tau)]\,dx,$$

where

ω is the dilution factor;

$I_0(x)$ is the absorption contour of the H_α line in the spectrum of the photosphere.

It is obvious that $g(\tau_0 - \tau)$ must be computed for those values of $\tau_0 - \tau$ (Figure 4),

corresponding to depth t along the line of sight, and linked by the following relationships [3]

$$t = \frac{1}{2} t_0(h)\left[1 - \frac{2}{\sqrt{\pi}}\int_0^{\sqrt{\frac{\beta}{2R}}} e^{-y^2}dy\right],$$

$$\tau = \frac{1}{\sqrt{2\pi R\beta}} t_0(h)\, e^{-\frac{\beta s^2}{2R}}.$$

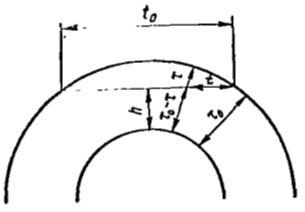

Figure 4.

The following table was compiled for convenience in finding τ in terms of known values of t:

t/t_0	0.01	0.05	0.14	0.30	0.50	0.70
τ/t_0	0.0010	0.0039	0.0087	0.0132	0.0152	0.0132
		0.86	0.95	0.99		
		0.0087	0.0039	0.0010		

Computing the values of $g(\tau_0 - \tau)$ from g(t), we obtain own excitation sources (Table 2).

Table 3 lists the relative share of own excitation sources (averaged along the line of sight). Table 3 shows that up to a height of about 3500 km the basic source of chromospheric excitation in the H_α line is resonance scattering of photospheric radiation. Beginning at h = 5000 km, emission from the H_α line /39 is almost totally attributable to internal excitation sources.

TABLE 2.

t/t_0	$\frac{g_{tot}-g_{phot}}{g_{tot}}$, $\tau_0=1$						
	$t_0=2.4$	$t_0=1.4$	$t_0=0.8$	$t_0=0.47$	$t_0=0.27$	$t_0=0.16$	$t_0=0.09$
0.01	0.036	0.040	0.051	0.087	0.145	0.208	0.369
0.05	0.027	0.034	0.047	0.084	0.142	0.205	0.365
0.14	0.016	0.026	0.042	0.079	0.138	0.203	0.364
0.30	0.007	0.019	0.037	0.075	0.134	0.201	0.362
0.50	0.004	0.017	0.035	0.072	0.133	0.199	0.361
0.70	0.007	0.019	0.037	0.075	0.134	0.201	0.362
0.86	0.016	0.026	0.042	0.079	0.138	0.203	0.364
0.95	0.027	0.034	0.047	0.084	0.142	0.205	0.365
0.99	0.036	0.040	0.051	0.087	0.145	0.208	0.369

t/t_0	$\frac{g_{tot}-g_{phot}}{g_{tot}}$, $\tau_0=3$							
	$t_0=0.05$	$t_0=4.2$	$t_0=2.4$	$t_0=1.4$	$t_0=0.81$	$t_0=0.48$	$t_0=0.28$	$t_0=0.15$
0.01	0.479	0.026	0.025	0.033	0.050	0.065	0.117	0.150
0.05	0.476	0.018	0.020	0.030	0.047	0.063	0.115	0.149
0.14	0.475	0.009	0.013	0.024	0.042	0.062	0.112	0.147
0.30	0.473	0.002	0.008	0.020	0.039	0.057	0.109	0.145
0.51	0.472	0.001	0.006	0.018	0.037	0.056	0.108	0.144
0.70	0.473	0.002	0.008	0.020	0.039	0.057	0.109	0.145
0.86	0.475	0.009	0.013	0.024	0.042	0.062	0.112	0.147
0.95	0.476	0.018	0.020	0.030	0.047	0.063	0.115	0.149
0.99	0.479	0.026	0.025	0.033	0.050	0.065	0.117	0.150

TABLE 3.

h, km	$\frac{g_{tot}-g_{phot}}{g_{tot}}\cdot 100$		h, km	$\frac{g_{tot}-g_{phot}}{g_{tot}}\cdot 100$	
	$\tau_0=1$	$\tau_0=3$		$\tau_0=1$	$\tau_0=3$
2500	16	—	4500	79	74
3000	40	21	5000	87	83
3500	56	46	5500	91	88
4000	66	61	6000	94	93
			6500	95	95

REFERENCES

1. Ivanov, V. V., Astron. Zhurnal, Vol. 37, 1960, p. 1021. /40

2. Matveyeva, M. V., Izv. GAO in Pulkovo, 1962, p. 170.

3. Kostik, R. I., IN: Voprosy astrofiziki [Problems of Astrophysics], "Nauka Dumka" Press, Kiev, 1966, p. 79.

4. Sobolev, V. V., Perenos luchistoy energii v atmosferakh zvezd i planet [Radiant Energy Transport in the Atmospheres of Stars and Planets], Gostekhizdat, Moscow, 1956.

5. Yakovkin, N. A., Kostik, R. I., Astrofizika, Vol. 2, 1966, p. 379.

6. Kostik, R. I., Astrofizika, Vol. 3, 1967, p. 155.

7. Krat, V. A., Krat, T. V., Izv. GAO in Pulkovo, 1955, p. 153.

8. Yakovkin, N. A., Zel'dina, M. Yu., Astron. Zhurn., Vol. 41, 1964, p. 914.

9. Bugayenko, L. A., Skorik, K. Ye., IN: Voprosy astrofiziki [Problems of Astrophysics], "Nauka Dumka" Press, Kiev, 1966, p. 121.

A SPECTRAL STUDY OF ACTIVE PROMINENCES

E. A. Gurtovenko, N. N. Morozhenko,
and A. S. Rakhubovskiy

ABSTRACT: The spectra of the active prominences of July 9 and 11, 1966 are analyzed. The physical conditions in these prominences are the same as in quiescent prominences, but their turbulent velocities are very high and are of the same order of magnitude as in limb flares. This "microturbulence" does not correspond to a normal velocity distribution.

In July 1966, the Main Astronomical Observatory of the Academy of Sciences /41
of the Ukrainian SSR observed active region No. 21034, as part of the International Proton Flare Program (PFP). A coordinated group (the Medon Observatory) proposed that we process and analyze the spectra of the active prominences of July 9 and 11.

Observations of the prominences were made with an H_α filter and on a spectrograph with a dispersion of 1.2 Å/mm (II order) and 0.8 Å/mm (III order) [1].

The coordinates of the prominences of July 9 and 11 (we will designate them A and B, respectively) were identical: $\varphi = +40°$, $\lambda = +90°$. We will now present the results of our observations for each prominence.

The prominence of July 9, 1966. Motion pictures were taken between 0632 and 1402 UT*. During this period the prominence changed brightness and shape so drastically that one would do well to speak of a set of phenomena of the prominence surge type in the same place on the limb.

The characteristic anomalies of the development of the prominence, and which can be traced on an H_α-filtrogram, are its compactness and brightness in the initial stage near the brightness maximum (Figure 1a), the subsequent formation of bright point coronal condensations and finger-shaped surges (Figure 1b) which lasted for a rather long time.

Table 1 lists prominence brightness values, I, expressed in units of disk

---

* Translator's Note: UT - universal time, or Greenwich mean time (GMT).

brightness near the limb, for certain times in the initial phase of development. These data were obtained from H_α-filtrogram measurements and refer to the brightest parts of the prominence. If the optical thickness of the prominence, τ_0, is small, then its emission in a projection on the disk will practically be added to disk emission (backing). During the observations with our filter [2], the disk brightness in the H_α line was about 0.35 units of disk brightness when observed with the same filter in the continuous spectrum near the H_α line. Table 1 lists the corresponding prominence brightness values, I_s, in units of the brightness of the continuous spectrum for the condition that the prominence is observed in a projection on the disk near the limb. These values exceed the

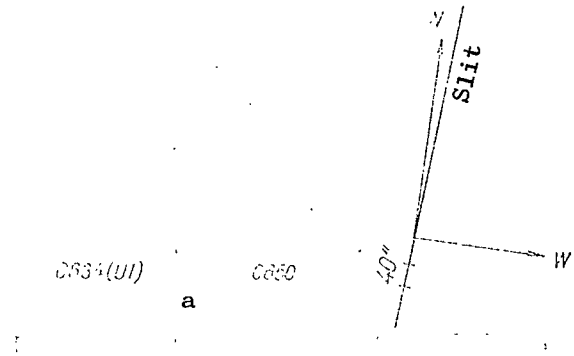

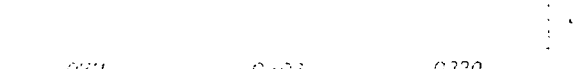

Figure 1. H_α-filtrogram of the prominence of July 9, 1966.

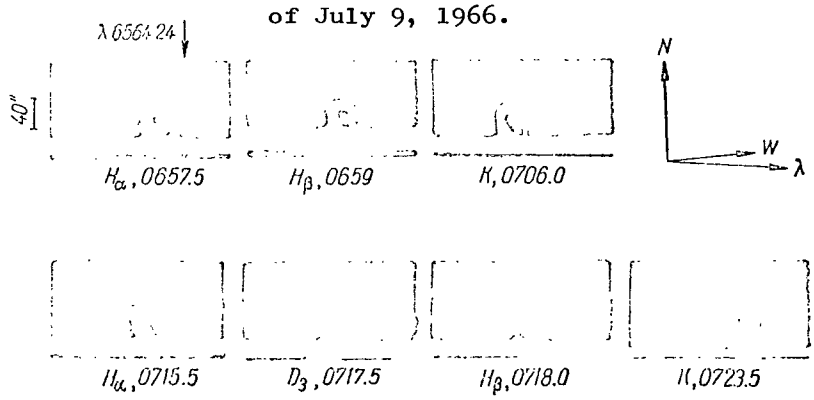

Figure 2. Spectrograms of certain lines of the prominence of July 9, 1966.

maximum of brightness magnitude, $I_s \approx 0.45$, used as the criterion for classification as a flare. In this case the brightest of the prominence nodes in the initial stage of prominence development would be recorded during disk observation in the form of weak flares or bright points. /43

Phenomena of the flare-prominence type are observed frequently. Unclear is whether or not they can be given some intermediate classification between flares and prominences. It seems to us that it is generally impossible to establish a sharp dividing line between flares and active prominences on a limb.

TABLE 1.

Observation time UT	I	I_s
0632	0.88	0.66
0639	1.15	0.75
0644	0.88	0.66
0651	0.72	0.60
0711	0.81	0.63

Spectral observations were made between 0655 and 0727 UT in the H_α - H_{12}, K, H Ca^+, and D_3 He lines. Emission in the D_1, D_2, and Na I lines was not detected visually, so no spectrography of these metallic lines was attempted.

Emission was observed in the H, K, D_3, H_α - H_8 lines on the obtained spectrograms, with only a very bright node traced in the H_8 line.

As we know, in the case of flares [3, 4] the maximum metallic emission is delayed with respect to the maximum hydrogen emission by several minutes. According to the data from our observations, the period of spectrography occurs precisely at the post-maximum phase of the prominence-flare; in this case what is observed is a purely "nonmetallic" flare (if it is considered a flare). On the other hand, the presence, or absence, of metallic luminescence is noted as well in prominences, including quiescent ones. Therefore, an anomaly in the spectrum of the observed prominence is the absence of emission in the metallic lines.

Figure 2 shows the spectrograms of the prominence in the different lines for certain times, and Figure 3 shows drawings from the H_α filtrograms for short time intervals for the entire interval of spectrography. Some of the drawings

show the position of the slit at the time of spectrography.

An outstanding feature of the spectrograms in all the lines is the unique emission contour, indicating the presence in the prominence of complex macroscopic motions. The shape of the line is reminiscent of a loop with a wide, left-hand, short-wave branch, which, in the upper part, becomes a "cap" extended along the dispersion, and a right-hand, long-wave branch, adjacent to the "cap" in the upper part of the prominence. One of the first spectrograms in the H_α line was obtained at 0657. At this time the slit intersected two bright nodes, a and b, as seen on the H_α filtrogram (see Figures 1, 3). Node a has a slight negative velocity. Higher above the node the emission in the left-hand branch of the profile remains bright, but, its negative radial velocity increases with increase in height, so it becomes barely visible on an H_α filtrogram. Node b pertains to the "cap," has almost no radial velocity, but does have a significant dispersion of radial velocities between approximately +60 and -40 km/sec as limits. /44

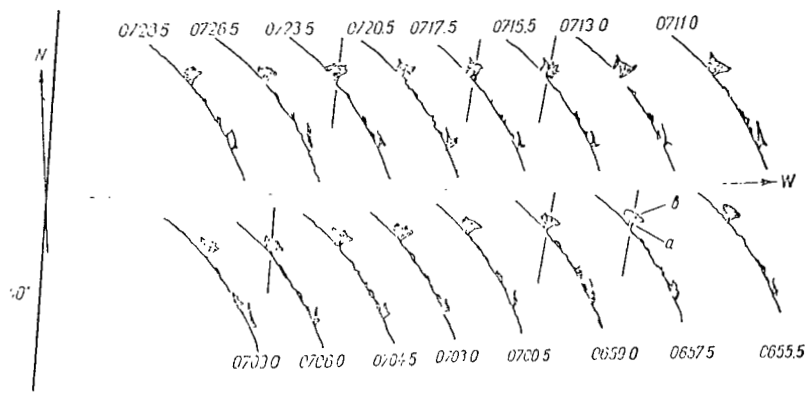

Figure 3. The appearance of the prominence of July 9, 1966, during the period of spectrography (drawings from the H_α filtrograms).

The right-hand, long-wave branch (component) of the H_α line has a constant radial velocity of +60 km/sec along the entire height of the prominence. This branch blends with the telluric line λ 6564.24 Å, which is clearly visible in

the emission background. Characteristic anomalies of the long-wave component also include its comparatively low brightness and small width. It is possible that it forms in a uniform, isolated cloud, or stream of matter moving at a constant velocity.

The shapes of the other spectral lines of the prominence are similar to the H_α line. Moreover, the nature of the motion of the matter described (see Figure 2) remained quite stable for the time spectrography was in progress (about 25 minutes). The spectrogram of the H_α line shows a slight decrease in brightness and a widening of the right-hand branch of the loop. /45

The prominence of July 11, 1966. This prominence was observed with an H_α filter from 1108 to the time of decay (about 1230). The prominence arose between 1058 and 1108. The prominence was not observed at this time, but other, small, formations were noticed in the same place on the limb at 1058.

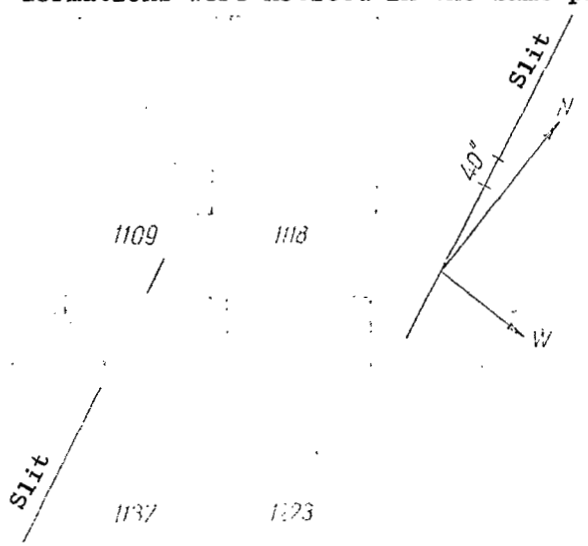

Figure 4. H_α filtrograms of the prominence of July 11, 1966.

The characteristic anomalies of the development that can be observed on H_α filtrograms, are drastic changes resembling eruptions in the initial stage of development, and the formation of bright coronal condensations linked to the photosphere by weak streams of matter. Several replicas of the H_α filtrograms are shown in Figure 4.

Spectrography of the H_α - H_8, H, K, and D_3 lines was begun at 1125, at the end of the initial eruptive phase, and continued until 1215, when the prominence had almost completely decayed. The brightness /46 of the H_α and H, K Ca^+ lines was low. No emission in the H_α line was seen. There was no emission in the metallic lines.

An anomaly of the spectrum in the initial period of observation is the difference in the radial velocities of the individual clusters of matter (Figure 5), something that confirms the eruptive nature of the first stage of development. This is why the lines are not compact in form (the K 1140 line, Figure 5, for example). Essentially, the photometric section of emission in the line can

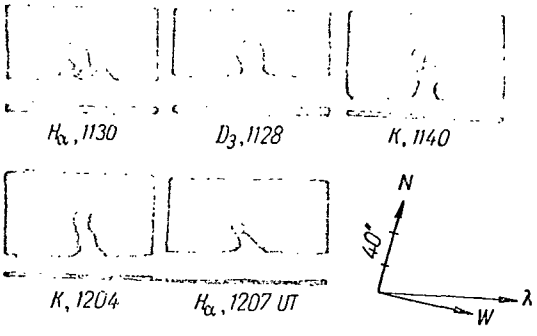

Figure 5. Spectrograms of certain lines of the prominence of July 11, 1966.

be obtained only for individual nodes, displayed by height (along the line) and in the direction of dispersion. Motion of matter during this period is very confused.

The nature of the eruption is less well defined in the second stage of development (1200 to 1215). The lines are more compact and stable. The narrow, right-hand component, dimly visible in the H_α line because of its low brightness, is clearly seen in the H and K lines (see Figure 5) in this period. It is shifted to the red by a magnitude corresponding to a radial velocity of about 40 km/sec. It is surprising that in the period after the eruption of the prominence the shape of its spectral lines is very similar to the "spectral loop" in prominence A, the only difference being that the magnitude of the radial velocity components is somewhat less, and the right-hand branch is extended to a great height and does not separate at "cap" height.

It seems to us that this similarity in the shapes of the lines in prominences A and B is not coincidental. It points to the presence in the active region of a stable magnetic field, regulating the nature of the motion of the matter in active prominences. The loop-shaped appearance of the spectral lines /47 allows us to include these prominences in the system of loop prominences (SLP) formed during the development of large flares. The investigation made by V. Banin [5] of a large flare near the limb can be cited to confirm this. An active prominence of the SLP type, with exactlythese same loop-shaped spectral lines, arose from this flare.

Spectrophotometric Investigations

Since the design of the telescope used for the observations [1] is such that simultaneous photographs of different parts of the spectrum cannot be taken, all the lines were photographed at different times with an interval of from 1 to 5 minutes. Repeated photographs of the same lines show that prominence A developed

relatively slowly during this period, and that no noticeable changes took place in the contours of the lines during the photography. Therefore, the data obtained for the same line at different times were averaged during processing. Five photometric sections (Figure 6) were made in the observed lines in order to cover the picture of the development of the prominence more completely.

The pattern of development of prominence B is more complex. The location and shape of the nodes varied from photograph to photograph, so in this case it was impossible to average the data, or to draw general conclusions about the various lines. Three photometric sections were used in the lines, obtained during the stabilization phase of the prominence (1204, 1206, 1207). /48

Figure 6. Diagram of the photometric sections of the emission lines for the prominence of July 9, 1966.

Observation data. The contours of the lines of prominence A have a complex shape because of the partial blending of the blue and red components of the loop (Figure 7) in all sections except the first. The components are rather widely separated in sections 3-5, and it is quite easy to isolate them in pure form. In section 2, where the blue and red components almost flow together, we were unable to isolate the contours unequivocally, so here large errors are possible. /49

The contours of the lines of the different nodes were constructed for prominence B. The contours of the nodes deviating toward the blue (node I) and the red node (II), also overlapped, as a rule, and it was necessary to isolate the respective components during processing.

The contours obtained were used to determine the equivalent widths, A, the optical thicknesses, τ_0, and the Doppler halfwidths, $\Delta\lambda_D$ (Tables 2, 3). The optical thicknesses of the H_α and H, K lines were determined from the dependence of the central intensity, I_0, on τ_0, obtained from the tables compiled by N. A. Yakovkin and R. I. Kostik [6] for resonance lines. We chose the Yakovkin-

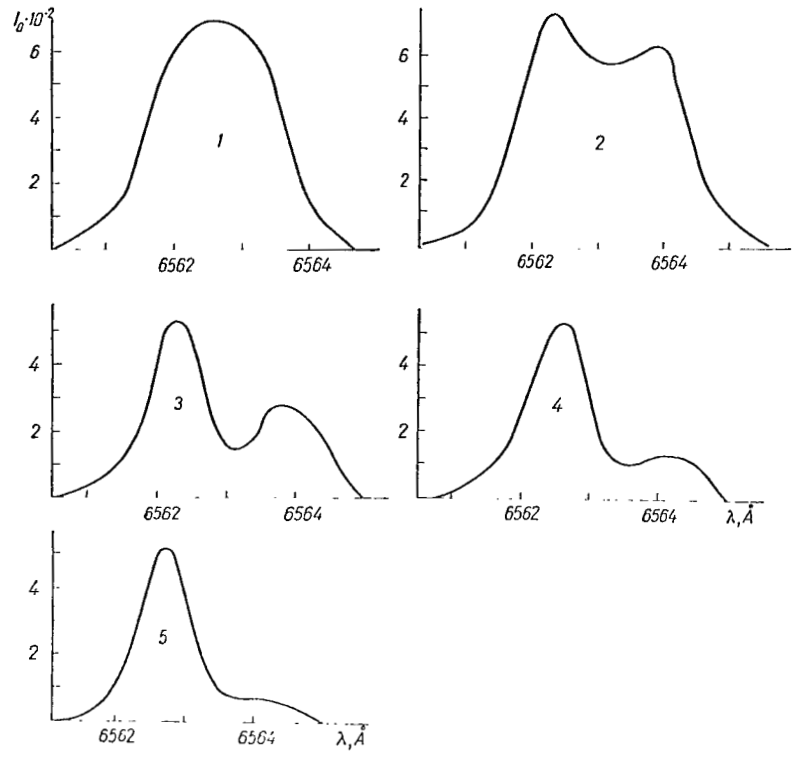

Figure 7. The contours of the H_α line of the prominence of July 9, at 0716 UT at the different sections.

Kostik method because it does not limit the behavior of the function of the source with depth, and by comparing the theoretical contour with the observed contour, it allows us to make more precise the preliminary value of τ_0 found from the graph. In this case we were unable to refine τ_0 because of the anomalous shape of the contours (the shape of the contours will be discussed in more detail below). For this reason, the use of the Yakovkin-Kostik method is not correct enough, and the τ_0 value obtained can be considered an approximation only.

This method can be applied only to resonance lines, or to lines of the resonance type (H_α, or lines with low metastable levels, for example). Therefore, the optical thicknesses in the H_β - H_ϵ lines were not established. However, it can be asserted that they are not great because the optical thickness in the H_α line is not in excess of three for denser prominences.

The optical thicknesses of prominence A in the D_3 line was estimated by comparison with the same lines in quiescent prominences. The values of τ_0 in the D_3 lines, as is also true for weak quiescent prominences, turned out to be very small, within limits of from 0.1 to 0.01.

We attempted to estimate the Doppler halfwidths of the H_α lines, the optical thicknesses of which were greater than unity, in terms of the wings of the contours. Since the optical thicknesses are small in the wings of lines expanded by the Maxwellian thermal velocities of the atoms, and since their shape can be defined as Gaussian, we can write

$$I_\lambda = \frac{I_0}{I_0} e^{-\tau_0 F_0 v^2}, \qquad (1)$$

where

$F_0 = \frac{1 - e^{-\tau_0}}{\tau_0}$ is the self-absorption factor for the center of the line; /51

$v = \Delta\lambda/\Delta\lambda_D$.

Using the different values of $\Delta\lambda$, we can obtain a sufficiently reliable $\Delta\lambda_D$. In the process of finding $\Delta\lambda_D$ it became clear that the shape of the contours of the H_α lines in the wings could not be described as Gaussian, and the entire contour on the whole could not be described by a Maxwell velocity distribution. The Doppler widths found for the different values of $\Delta\lambda$ using Eq. (1), decrease with approach to the nucleus of the line. This effect was also detected in other lines. Therefore, the values of $\Delta\lambda_D$ listed in Tables 2 and 3, must be understood to be simply parameters defining the mean values of the characteristic velocities. The magnitudes of $\Delta\lambda_D$ were estimated in terms of the halfwidths of the contours for the optically thin lines H_β - H_ϵ, H, K, D_3. The values of the

TABLE 2.

Section	$\Delta\lambda_S \cdot 10^3$	$\Delta\lambda_k \cdot 10^3$	τ_{0S}	τ_{0k}	$\Delta\lambda_{DS}$	$\Delta\lambda_{Dk}$	$I_{0S} \cdot 10$	$I_{0k} \cdot 10$
				H_α				
1	7.76	--	1.91	-	0.957	--	0.650	--
2	6.41	3.020	2.62	1.35	0.713	0.584	0.709	0.536
3	2.52	0.767	1.33	0.30	0.530	0.742	0.537	0.218
4	3.24	0.347	1.65	0.13	0.548	0.693	0.591	0.118
5	2.92	0.214	1.56	0.09	0.518	0.677	0.578	0.087
				H_β				
1	0.670	—	—	--	0.615	—	0.139	--
2	1.140	0.118	—	—	0.700	0.361	0.223	0.016
3	0.354	0.215	—	—	0.354	0.450	0.120	0.070
4	0.361	0.079	—	—	0.363	0.313	0.125	0.037
5	0.431	0.084	—	—	0.414	0.217	0.160	0.040
				H_γ				
1	0.166	--	—	—	0.505	—	0.042	—
2	0.350	0.088	-	—	0.488	0.391	0.096	0.031
3	0.076	0.171	--	—	0.304	0.332	0.019	0.055
4	0.059	0.037	-	—	0.202	0.132	0.032	0.036
5	0.161	0.024	---	--	0.287	0.169	0.065	0.019
				H_δ				
1	0.082	--	--	—	0.446	---	0.026	—
2	0.024	-	---	-	0.330	--	0.095	—
3	0.025	0.010	--	--	0.108	0.326	0.035	0.013
4	—	---	—	—	—	--	—	-
5	--	---	—	--	—	—	--	--
				H_ϵ				
1	0.130	—	---	--	0.379	--	0.043	—
2	0.170	—	—	—	0.456	—	0.055	—
3	--	—	--	—	—	—	—	--
				K				
1	0.498	—	0.43	—	0.470	—	0.132	—
2	1.073	0.417	0.95	0.44	0.431	0.362	0.290	0.132
3	0.510	0.200	0.71	0.30	0.265	0.304	0.225	0.090
4	0.418	0.155	0.79	0.35	0.226	0.160	0.241	0.110
5	0.605	0.159	0.79	0.37	0.307	0.132	0.253	0.117
				D_3				
1	0.512	--	0.075	—	0.586	--	0.120	--
2	0.615	0.361	0.085	0.045	0.586	0.533	0.117	0.086
3	0.305	0.192	0.044	0.030	0.566	0.497	0.086	0.063
4	0.230	0.073	0.052	0.025	0.364	0.337	0.089	0.051
5	0.166	0.031	0.039	0.010	0.475	0.331	0.057	0.019

TABLE 3.

Line	Time of photo-graph	Sec-tion	Node I (blue)				Node II (red)			
			$A \cdot 10^{-5}$	τ_0	$\Delta\lambda_D$	$I_0 \cdot 10$	$A \cdot 10^{-5}$	$\tilde{v}_0$	$\Delta\lambda_D$	$I_0 \cdot 10$
H_α	1125	2	4.44	1.6	0.66	0.590	1.78	0.74	0.825	0.360
		1	3.00	0.67	1.23	0.340	0.74	0.27	1.14	0.150
	1129	2	1.27	0.65	0.56	0.330	3.10	0.88	0.89	0.420
		1	5.04	1.83	0.79	0.630	0.52	0.30	0.62	0.170
	1130	2	—	—	—	—	4.44	1.66	0.65	0.600
		1	1.76	0.83	0.49	0.400	1.02	0.58	0.68	0.290
		3	1.70	0.30	1.04	0.310	—	—	—	—
	1207	2	1.44	0.60	0.77	0.312	—	—	—	—
		1	1.12	0.59	0.70	0.298	0.314	0.23	0.49	0.145
H_β	1127	2	0.575	—	0.82	0.098	0.190	—	0.56	0.019
	1127	—	0.420	—	0.53	0.105	0.142	—	0.62	0.030
K	1134	2	0.324	0.28	0.45	0.085	0.300	0.28	0.74	0.085
		1	0.690	0.46	0.65	0.140	—	—	—	—
	1140	2	0.300	0.28	0.34	0.085	0.330	0.25	0.66	0.075
		1	0.700	0.37	0.69	0.116	—	—	—	—
	1204	2	0.270	0.31	0.36	0.098	0.087	0.17	0.28	0.052
		1	0.308	0.29	0.41	0.088	0.138	0.16	0.42	0.050
		3	—	—	—	—	0.166	0.14	0.43	0.045
	1216	2	0.470	0.40	0.46	0.120	—	—	—	—
		1	0.308	0.26	0.48	0.080	0.101	0.11	0.38	0.035
		3	—	—	—	—	0.690	0.10	0.30	0.032
D_3	1126	2	0.415	—	0.93	0.080	0.085	—	0.64	0.025
	1128	—	0.238	—	0.52	0.075	0.051	—	0.38	0.025

TABLE 4.

Section	Hydrogen						Ionized Calcium			Helium
	$N_2 \cdot 10^{-13}$	$N_3 \cdot 10^{-10}$	$N_4 \cdot 10^{-10}$	$N_5 \cdot 10^{-10}$	$N_6 \cdot 10^{-10}$	$N_7 \cdot 10^{-10}$	$N_1 \cdot 10^{-12}$	$N_2 \cdot 10^{-9}$	$\frac{N_2}{N_1} \cdot 10^4$	$N \cdot 10^{-9}$
					Blue Components					
1	1.34	7.32	2.45	1.82	2.19	6.35	4.05	0.84	2.06	2.81
2	1.35	6.05	4.20	3.60	5.73	1.52	8.10	1.80	2.22	3.20
3	0.50	2.38	1.29	0.84	0.70	—	3.77	0.90	2.39	1.58
4	0.66	3.05	1.33	0.64	—	—	3.49	0.75	2.15	1.19
5	0.60	2.75	1.60	1.75	—	—	4.83	1.01	2.09	0.86
					Red Components					
1	—	—	—	—	—	—	—	—	—	—
2	0.573	2.86	1.55	0.960	—	—	3.16	0.744	2.35	1.87
3	0.160	0.72	0.80	0.614	0.296	—	1.80	0.332	1.85	1.00
4	0.065	0.36	0.29	0.404	—	—	1.11	0.259	2.33	0.38
5	0.043	0.20	0.41	0.262	—	—	0.98	0.232	2.37	0.18

equivalent widths of A (expressed in ergs) for H_α were corrected for self-absorption.

Tables 2 and 3 list the initial data for evaluating the physcial conditions in prominences. The formula

$$A = \frac{N_m A_{mi} h\nu}{4\pi}$$

was used to find the N_m populations of the corresponding upper levels of the atoms of hydrogen, ionized calcium and helium through the equivalent widths. The N_i populations of the lower levels of the H_α, H, and K lines were found through τ_0, so their values are not sufficiently reliable. Tables 4 and 6 list the population data. Turbulent velocities (Tables 4, 5, and 6) were computed through the Doppler halfwidths.

Determination of electron temperatures. Electron temperatures at the sites of hydrogen glow were determined from the populations for the excited hydrogen levels. The Saha-Boltzmann formula, written in the following form, was used

$$b_m N^+ n_e = \frac{N_m}{m^2} K_0 T_e^{3/2} e^{\frac{\chi_m}{kT_e}}, \qquad (2)$$

where

$$K_0 = \frac{(2\pi mk)^{3/2}}{h^2} = 2.42 \cdot 10^{15};$$

N^+, N_m are the ion and atom content in the excited state m on the line of sight;

χ_m is the ionization potential of level m;

n_e is the electron density;

b_m is a parameter characterizing the degree of deviation from thermodynamic equilibrium.

Investigations show [7] that for the lower levels $b_m \gg 1$. With increase in m, the value of b_m tends to unity, and when $\chi_m = 0$, $b_m = 1$. This property of b_m was used to determine the electron temperature.

The right-hand side of Eq. (2) can be computed for known N_m, and a given T_e, and represented graphically. Extrapolating the graphic obtained to the point $\chi_m = 0$, we find the corresponding values of $b_m N^+ n_e$, for which $b_m = 1$ at the point of intersection with the axis. In other words, we find the magnitude

of N^+n_e for a given T_e which we substitute in the equation of ionization equilibrium

$$N_1\Phi_1 + N_2\Phi_2 = N^+n_e\Sigma R_m, \tag{3}$$

where

Φ_1, Φ_2 are the photoionization factors; and

R_m is the recombination coefficient at the m level.

The values of Φ were found through the formula

$$\Phi_m = W\frac{8\pi}{c^2}k_m\nu_m^3 Ei\left(\frac{h\nu_m}{kT_m}\right), \qquad \text{54}$$

where

W is the dilution factor (in our case W = 0.3);

k_m, T_m are the coefficient of absorption and the Planckian temperature at the limit of the corresponding series (in our case T_1 = 6900°, according to the data in reference [8], and T_2 = 6000°).

Individual values of R_m were computed using Cilie's formula [9] up to m = 30, to determine ΣR_m. Eq. (3) takes into account only radiation processes, since they play the dominant role in prominences. Ionization with a level $m \geq 3$ was not taken into account because the product $N_2\Phi_2$ is several orders of magnitude greater than $N_m\Phi_m$.

The value of N_1 can be found through Eq. (3), and then the ratio N_2/N_1 can be found. The population of the second level, N_2, is established by L_α solar radiation, the temperature of which proves to be very close to the electron temperature because of the large optical thickness of the L_α line [10]. Therefore, the ratio N_2/N_1 can be found through the Boltzmann formula with $T = T_e$. If the value of T_e obtained through the Boltzmann formula does not coincide with that used earlier, a second approximation must be made, and continued until the value of T_e used to compute N^+n_e, and the value obtained through the Boltzmann formula agree with the proper degree of accuracy. Table 5 lists the electron temperatures found using this method for each section of prominence A.

TABLE 5.

Section	v_T (H), km/sec	v_T (Ca II), km/sec	v_T (D_3), km/sec	v_r(H), km/sec	v_r(Ca II), km/sec	v_r(D_3) km/sec	T_e
			Blue Components				
1	35.2	36.0	28.5	0.0	0.0	0.0	7800
2	32.3	33.0	28.5	10.6	8.4	15.6	7500
3	19.5	20.2	27.5	25.0	28 2	23.4	7800
4	20.5	17.2	16.2	18.8	23.6	10 3	7900
5	20.0	23.4	22.5	12.7	16.0	7.7	7300
			Red Components				
1	—	—	—	—	—	—	—
2	22.8	27.6	25.7	50.4	38.7	37.5	7600
3	21.2	23.2	23.9	45.4	54.0	53.0	7000
4	23.1	12.2	14.6	40.1	55.5	58.5	7300
5	22.1	10.1	14.3	49.8	59.3	63.5	—

TABLE 6.

Line	Time of Photo-graph	Sec-tion	Node I (blue)				Node II (red)			
			$N_l \cdot 10^{-11}$	$N_m \cdot 10^{-10}$	v_T, km/sec	v_r, km/sec	$N_l \cdot 10^{-11}$	$N_m \cdot 10^{-10}$	v_T, km/sec	v_r, km/sec
H_α	1125	2	7.70	4.20	30.2	16.0	4.40	1.70	37.7	13.7
		1	6.00	2 80	56 2	8.8	2.20	0.70	52.1	20.0
	1129	2	2.70	1.20	25 7	19.8	5.70	3.20	40.4	14.3
		1	10.50	4.75	36.0	10.8	1.30	0.49	28.4	16.6
	1130	2	—	—	—	—	7.80	4.18	29.2	10.0
		1	3.00	1.66	22.4	16.0	2.90	0.96	30.7	11.7
		3	2.30	1.60	48.0	6.7	—	—	—	—
	1207	2	3.40	1.36	35.1	11.7	—	—	—	—
		1	3.00	1.06	31 8	8.1	0.82	0.30	22.4	11.5
H_β	1127	—	—	2.11	51.0	6.1	—	0.70	34.5	14.4
	1127,5	—	—	1.56	33 0	10.2	—	0.52	37.8	13.0
K	1134	2	3.10	0.054	34.2	19.5	2.91	0.050	34.2	6.4
		1	7.30	0.115	50.4	8.7	—	—	—	—
	1140	2	2.70	0.050	25.9	21.5	4.10	0.055	50.1	7.1
		1	6.60	0.116	52.5	11.3	—	—	—	—
	1204	2	2.50	0.045	27.1	3.9	1.00	0.014	21.3	11.2
		1	2.90	0.051	31.2	11.9	1.50	0.023	31.8	8.5
		3	—	—	—	—	1.40	0.028	33.0	10.5
	1216	2	4.10	0.078	35.1	1.3	—	—	—	—
		1	3.50	0.051	36.6	10.0	1.40	0.017	29.0	8.9
		3	—	—	—	—	0.77	0.011	22.9	11.5
D_3	1126	—	—	0.230	49.8	3.2	—	0.044	32.1	20.7
	1128	—	—	0.123	26.5	—	—	0.026	19.3	—

The accuracy with which T_e is found is very much dependent on the accuracy with which N_m is found. In this particular case the error is about ±1000°. The electron temperature at the sites of hydrogen glow on the prominences investigated is between 7000 and 8000°. /56

Turbulent and radial velocities. Excitation sources. Turbulent velocities were found through the formula

$$c^2\left(\frac{\Delta\lambda_D}{\lambda}\right)^2 = \frac{2RT_e}{\mu} + v_T^2.$$

It should be pointed out that for the observed width of the lines, the contribution of the first term of the right-hand side of this equation is negligibly small when T_e = 8000°. The lines are expanded mainly by turbulent velocities. The $\Delta\lambda_D$ values listed in Tables 2 and 3 were used to determine v_T. The radial velocities were estimated from the magnitude of the shift of the emission lines relative to the corresponding Fraunhofer line. The v_T and v_r obtained are listed in Tables 5 and 6.

We used the solution of the inverse problem of the theory of radiation diffusion, obtained by R. I. Kostik [11], to determine the excitation sources. Table 7 lists the values of the function $g(\tau)$, describing the source distribution in the case of atoms excited only by photospheric radiation, and the source $G(\tau)$, found according to the line contour using the tables from R. I. Kostik's work [11], for the H_α and K lines.

TABLE 7.

H_α			K Ca II		
τ	$G(\tau)\cdot10^2$	$g(\tau)\cdot10^2$	τ	$G(\tau)\cdot10^2$	$g(\tau)\cdot10^2$
1.900	4.36	4.07	0.430	2.85	3.30
1.730	3.83	3.28	0.393	2.78	3.19
1.330	3.20	2.47	0.300	2.68	3.02
0.700	2.62	2.36	0.158	2.58	3.00
0.352	2.52	2.77	0.079	2.53	3.13
0.147	2.62	3.34	0.033	2.58	3.17
0.052	3.20	3.77	0.012	2.68	3.27
0.015	3.83	3.99	0.003	2.78	3.29
0.002	4.36	4.07	0.001	2.85	3.30

We can find the function g(τ) through the approximate formulas [12] /57

$$g(\tau) = g^1(\tau) + g^1(\tau_0 - \tau),$$

$$g^1(\tau) = \frac{W}{2\sqrt{\pi}} \int_{-\infty}^{+\infty} I(v)\, e^{-v^2} E_2(\tau_e^{-v^2})\, dv,$$

where

I(v) is the intensity at the corresponding points on the Fraunhofer contour;

$E_2(\tau e^{-v^2})$ is a second order integral exponential function.

Discussion of the Results

Motion of matter. If we digress from the expansion of emission lines attributable to temperature, turbulence, and possibly other physical effects, the contour of the "spectral loop" in prominences A and B at the stabilization stage can be assumed to be a unique envelope of the velocity vector of the matter in the plane containing the line of sight. It is difficult to establish whether the loop characterizes the velocity of the matter moving continuously in a closed trajectory, or whether it reflects the overlapping of the velocities of several individual streams. However, the predominant motion of the matter took place in the plane containing the line of sight. This we can understand from a comparison of the "spectral loop" and the H_α filtrogram. In this case, the three-dimensional trajectory of the motion of the main mass of the matter can be represented by an arc. Two streams of matter, moving with acceleration in opposite directions toward definite centers in the photosphere, form at the top of the arc in a stationary coronal condensation.

Also possible is the fact that the "spectral loop" is the result of the overlap of the emission from individual, independent, streams of matter with different mean velocities, as well as different velocity gradients inside the streams. In this case the red component (the right-hand branch of the loop) can be equated to a comparatively uniform cloud, or stream, with a stable velocity. The possibility that this stable flow is corpuscular cannot be excluded. Its spatial velocity can exceed significantly the observed radial velocity, especially if the direction of its motion is close to the radial.

Before discussing the results of the spectrophotometry, it should be pointed out again that the accuracy of the construction of the contours is not very high /58

because of the partial blending of the blue and red components. Moreover, processing included all the spectral material including some mediocre quality photographs.

Based on an analysis of Tables 2 and 3, the conclusion is that both prominences were optically thin in all lines except H_α. At the same time, the lines were very wide, so their total intensities were quite substantial. For example, in cross section 1 (see Table 2) the observed total intensity is about $0.45 \cdot 10^6$ erg $\cdot$ cm^{-2} $\cdot$ sec^{-1}, or 0.75 units of the energy passed by the H_α filter in the Main Astronomical Observatory of the Academy of Sciences of the Ukrainian SSR [2] near the limb of the disk in the continuous spectrum near the H_α line. This magnitude is close to the intensity of the brightest nodes (see Table 1), measured on the H_α filtrogram in the initial phase of development of the prominence.

The populations of the ground and excited levels for hydrogen, as well as for ionized calcium, and helium are the same as they are in quiescent prominences of average brightness [13, 14]. Table 4 lists the values of the population ratio, N_2/N_1, for CaII, and they are very close to analogous magnitudes in quiescent prominences [15].

The values of the functions of $G(\tau)$ (Table 7) describing the true source distribution in the medium for the H_α and K lines are close to the values of $g(\tau)$, found on the assumption that the excitation mechanism is scattering of photospheric radiation.

These data indicate that the principal mechanism in line excitation in the prominences of July 9 and 11, 1966, is scattering of photospheric radiation. In this respect, the prominences are no different than quiescent prominences. However, their optical thicknesses are somewhat less than the mean for quiescent prominences. It should be pointed out that in the case of small optical thicknesses in active prominences with high velocities, a unique effect of abnormally increased line emission is possible, even if excitation by photospheric radiation is all that is acting. When radial velocities are high, the prominences can absorb radiation from the continuous spectrum near the H_α line [12]. The fact that a prominence such as this, or its individual parts, will be recorded by an H_α filter as bright formations when observed on the disk near the limb

cannot be excluded. This, apparently, explains the great brightness of certain active prominences, loop prominences in particular.

As will be seen from Tables 5 and 6, the turbulent velocities of the prominences investigated were very high. In loop prominence A they reached a maximum in the upper part of the loop (cap), and decreased as they approached the photosphere. In ionized calcium and helium the turbulent velocities behave identically in the red and blue components, while in hydrogen the turbulent velocities are almost constant. /59

In the eruptive stage of prominence B, the turbulent velocities in the sections closer to the photosphere (section 1), decrease and in the loop stage (1204, 1206, 1207) stabilize within the limits of error and are virtually independent of the height of the section above the photosphere.

The non-Doppler nature of the line contours indicates that the turbulent velocities in different parts of the prominence along the line of sight are different, and increase from the center to the surface layers.

The radial velocities of the individual parts of the prominence are rather high. In prominence A, the radial velocities of the blue component increase from 0 to 36 km/sec as they approach the photosphere, and then decrease to 20 km/sec. The radial velocities of the red component of hydrogen change very little, and reach about 60 km/sec. However, v_r for the red component of ionized calcium and of helium increases from 38 to 63 km/sec as it approaches the photosphere.

When prominence B was in its eruptive stage, the radial velocities of the nodes displaced toward the blue, increased near the photosphere (section 1), and the radial velocities of the nodes displaced toward the red, decreased. In its loop stage, as in prominence A, the radial velocities decreased with approach to the photosphere. However, only two photometric sections were made through the loop of prominence B, so it is difficult to draw any certain conclusions in this case.

Conclusions

1. The observed prominences are, apparently, only a link in a series of active limb formations, which arose and developed in the same location of the active region over an extended period of time. Their development can be characterized by rapid changes in shape. The period of decay in the shape of /60

one type is of the order of a few score minutes (from 20 minutes to 1 hour).

2. In the more quiescent stage the shape of the spectral lines has a complex loop-shaped structure, indicating the presence of a special motion trajectory, or of several individual streams of matter.

3. Apparently, in the quiescent stage of development, the motion of the matter in the prominences, observed on different days, is similar in nature, indicating the presence of a stable magnetic field regulating the nature of movements of the matter in the formations of a type of active prominences.

4. By type of spectrum, the prominences can be included among the "non-metallic" type with a moderate number of hydrogen lines.

5. Temperatures, total populations of levels, densities of matter, and the excitation mechanism for the emission lines in these prominences were the same as in common quiescent prominences.

6. The prominences differ sharply from quiescent ones in the high magnitudes of the turbulent velocities, which are not described by normal distributions.

REFERENCES

1. Gurtovenko, E. A., Didychenko, Ye. I., Izv. GAO AN UKSSR, No. 3, 1960, p. 2.

2. Gurtovenko, E. A., IN: Nablyudeniya solntsa. MGG. [Observations of the Sun. IGY], Academy of Sciences SSSR Press, Moscow, 1959, pp. 25-35.

3. Stepanyan, N. N., Izv. KrAO, No. 46, 1961, p. 41.

4. Alikayeva, K. V., IN: Spektrofotometricheskiye issledovaniya aktivnikh obrazovaniy na Solntse [Spectrophotometric Investigations of Active Solar Formations], "Naukova Dumka" Press, Kiev, 1964, pp. 73-80.

5. Banin, V. G., Izv. KrAO, Vol. 35, 1966, p. 190.

6. Yakovkin, N. A., Kostik, R. I., Astrofizika, Vol. 2, 1966, p. 379.

7. Tomas, R., Atey, R., Fizika solnechnoy khromosfery [Physics of the Solar Chromosphere], "Mir" Press, 1965.

8. Hirayama, T., Publ. Astr. Soc., Vol. 15, No. 2, Japan, 1963, pp. 104-132.

9. Cilie, G. G., Monthly Notices, Vol. 92, 1932, p. 82.

10. Yakovkin, N. A., Solnechnyye dannyye, Vol. 8, 1963, p. 167.

11. Kostik, R. I., Astrofizika, Vol. 3, No. 1, 1967, p. 17.

12. Yakovkin, N. A., Zel'dina, M. Yu., Solnechnyye dannyye, Vol. 9, 1964, p. 62.

13. Morozhenko, N. N., IN: Voprosy astrofiziki [Questions of Astrophysics], "Naukova Dumka" Press, Kiev, 1966, pp. 21-36.

14. Gurtovenko, E. A., Semenova, N. N., Izv. GAO AN UKSSR, Vol. 4, 1961, p. 31.

15. Morozhenko, N. N., Byull. Solnechnyye dannyye, Vol. 5, 1964, p. 63.

INVESTIGATION OF RR LYRAE TYPE VARIABLE STARS IN THE GLOBULAR CLUSTER M3

E. S. Kheylo

ABSTRACT. RR Lyrae variables in M3 are studied. Seasonal moments of maxima and O-C diagrams of 12 RR Lyrae stars are given.

The problem of period variation in RR Lyrae type stars in general is a rather complex one, but the complexity is worse in the case of stars that are members of glubular clusters because of the observation difficulties. Quite a long series of uniform observations [5] are investigated in order to analyze the behavior of the RR Lyrae galactic field. There is no such series for globular clusters. The interpretation of this quite long series, although composed of different types of observations, cannot yield sufficiently reliable results. The following example is typical. In determining the O-C magnitude (deviations of a particular point on the light curve from the ephemeresis) the "mean" of the ascending branch is often used as a reference point. But it is perfectly clear that the difference between the photometric systems used by the various authors can result in our actually referring to different points on the curve, rather than to one. What follows from Figure 1 is that the "mean" of the ascending branch occurs in different phases. /62

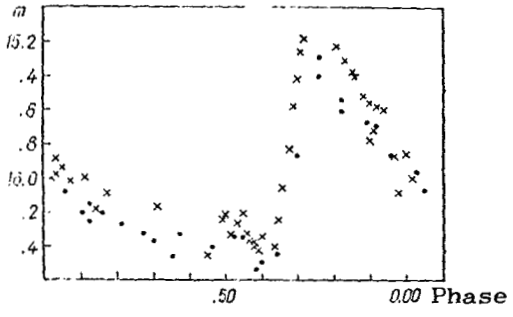

Figure 1. Observation of the variable star 40 in M3 according to Sandage (●) and Hett (+), reduced to a single period.

Consequently, before the investigation of a particular star can be started, all observations used must be reduced to a single photometric system. This was done for this article. /63

The objects of the study were variables 21, 37, 40, 55, 64, 65, 81, 93, 94, 107, 108, and 119, all belonging to the globular cluster M3, one of the most abundant in RR Lyrae type stars. The numbers of the variables were brought into agreement with the Sawyer Catalog [16]. The choice of stars was governed by the

following considerations: (1) the data on their observations were published, beginning with JD 2413372; (2) all the variables have stable light curves; (3) N.P. Kukarkina has revised all the observations of a great many variables in M3, but she did not study the above-mentioned stars.

Observation material used. The author established the stellar magnitudes of the variables from photographs in the glass slide library in the Shternberg State Astronomical Institute. Of these, 72 photographs were obtained from a 40 centimeter astrograph for the period from JD 2436633 to JD 2437791, and 48 were obtained from a 70 centimeter Cassegrainian reflector (f = 10.5 m) from JD 2437779 to JD 2438898. Visual estimates of the brightness of the variables were made using the Neiland-Blazhko method. Each plate was processed twice, turning 180° to eliminate parallax errors. Stars AH, AM, AV, I-1, I-2, I-7, I-39, I-46, I-47, II-15, III-25, 167 and 179 from Sandage's paper [15] were used for purposes of comparison.

The observations listed in Table 1 were used, along with our own observations.

B.V. Kukarkin very kindly placed at our disposal the observations of the M3 variables made on the 52 centimeter Schmidt telescope in the Byurakan Observatory. Thus, processing involved the use of almost one thousand observations of each star, distributed very unevenly over the period between 1895 and 1965. The observations made by B.V. Kukarkin and by the author are listed in the appendix.

Reduction of the observations to a single photometric system. We took as a basis the system used in the P_k catalog compiled by B.V. Kukarkin and N.P. Kukarkina[2], because it is, in our opinion, the most reliable. However, it is impossible to use the reduction formulas given in reference [2] for variable stars because the color indicator for each star varies over its cycle, and generally speaking, is unknown for a given moment in time.

In this case the reduction of all the observations to a single system was facilitated by the fact that almost all the authors used the same comparison stars (Nos. 218, 227, 250, 258, 263, 609, 740, 1055, 1131, 1327 [21]). Plotting the magnitudes of the comparison stars in the system of each author along one axis, and the magnitudes in the P_k system on the other, we can obtain a function for reducing a given, individual series. /64

TABLE 1. LIST OF THE OBSERVATIONS OF M3 VARIABLES

Author	Number of Pictures	Time Interval in Julian Days
		Short Series from
Bailey [6]	50	2413372 to 2415161
Hett [10]	8	2419479 — 2419534
	17	2420625 — 2420656
	44	2429367 — 2429431
Rybka [14]	4	2421316 — 2421358
Larink [11]	1	2422455
	135	2422729 — 2422840
Müller [12]	1	2423858
	91	2424283 — 2424317
Slavenas [19]	21	2424564 — 2424565
	75	2424619 — 2424622
Greenstein [9]	75	2424647 — 2424684
Schwarzschild [17]	4	2428964 - 2428983
Belserene [8]	28	2431965 - 2431995
	10	2422682 - 2432700
Roberts, Sandage [13]	24	2434447 - 2434508
R. Baker, H. Baker [7]	6	2434509
	38	2434833 - 2434835
Szeidl [20]	231	13 Series of various lengths
		2428963 - 2436791

Note: Hett [10] explained that Bailey must have been mistaken and gave the times of the beginnings of the exposures instead of their mean exposure times for the observations of 1897. In this article the corresponding corrections were made when Bailey's observations were processed.

Transition curves were used to reduce to the P_k system the stellar magnitudes of the variables obtained in the observations made by Bailey, Hett, Rybka, Müller Schwarzschild, Belserene, Roberts and Sandage, R. Baker and H. Baker, Szeidl, Kukarkin and ourselves. Slavenas gave the luminosity of the variables in a power scale, and the formulas for converting from his system to the Shapley-Davis system of stellar magnitudes [18]. Using these formulas, we constructed a transition curve for reducing Slavenas's observations. The conversion from the Greenstein system to the P_k system was made using another method, one utilizing the mean /65 light curve, because Greenstein failed to publish stellar comparison scales. This was also done for Larink's observations.

Determination of seasonal moments of maxima of the variables. All observations made of each of the stars were divided into groups by seasons (years). Belserene's periods, and an arbitrary initial moment equal to JD_{hel} 2430000.000, were used to construct the seasonal light curve.

Naturally enough, the light curve can be rather clearly "drawn" and the seasonal moment of maximum determined reliably from the observations made by Müller, Larink, and others; i.e., from those authors whose observations were numerous. The observations made by Rybka, Schwarzschild, and others, provide just a few points on the curve. But these points can be used to determine the seasonal moment of maximum (if with considerably less reliability).

Since all observations were reduced to a single system, it can be assumed that we have a uniform series for each star. From this series we choose several seasons in which the observations fill the entire light curve uniformly, and rather densely (for example, for variable 21 the observations made by Hett, Müller, Belserene, Roberts and Sandage, Kukarkin and myself), and we construct a mean light curve corresponding to each season. We shift these curves along the abscissa so that their maxima coincide. Averaging the brightness values for the variable through the same identical phase on all the mean curves, and assigning a definite weight to each value, we obtain a "weighted" mean light curve for each of the variables examined. Superimposing this curve on the individual curves, and shifting it along the abscissa so that the "weighted" curve best fits the individual points, we determine the phase of the seasonal maximum. This method is a somewhat modified method of superimposition of a mean curve [1].

A few remarks are in order. First of all, using the "weighted" curve, we can add to our photometric system any observations for which we can construct a more or less reliable mean curve, that adequately depicts graphically the relationship between the values of the stellar magnitudes on the particular mean curve, and the magnitudes on the "weighted" curve for the same phases. This is how the Greenstein and Larink series were added to the P_k system. Second, the proposed method is applicable only to variables with stable light curves. If the /66 shape of the light curve varies (the Blazhko effect), only investigation of really long, uniform series of observations can yield reliable results. The stability or instability, of a light curve obviously can be established by

several months of observations. Third, because of various, and often unaccountable errors even mean curves constructed in a single system using the observations made by different authors, yield few, but none the less differing, values of such stellar characteristics as brightness at maximum, amplitude, location of the minimum, etc. These values, when taken from the "weighted" curve, will undoubtedly be more reliable.

The moments of seasonal maxima, found by using the method described, were used to derive conventional equations, and to improve the elements of the light curves for the variables by the method of least squares. The deviation of O-C from the improved elements also provides us with an opportunity to evaluate the nature of the change of period for each star.

Results. Table 2 lists summaries of the moments of seasonal maxima of brightness of the stars studied, and their deviations from the ephemeris. The behavior of the O-C diagram for each star is shown in Figure 2, and the "weighted" mean light curves are shown in Figure 3. Summarized information on the variables is listed in Table 3. Figure 4 shows the period-amplitude relationship. As usual, asymmetry "by period" (Figure 5) is characterized by the magnitude

$$\varepsilon = p^{-1}(t_{max} - t_{min}),$$

and asymmetry "by stellar magnitude" (Figure 6) by the magnitude

$$\xi = m_{\frac{1}{2}} - \frac{1}{2}(m_{max} + m_{min}),$$

where $m_{1/2}$ is the stellar magnitude at that section of the light curve where the time distance between the ascending and descending branches is one-half the period.

Analysis of results, and conclusions. We have already noted [3, 4] the unquestioned reality of the changes in the period values in M92. As will be seen from Figure 2, in this particular case the periods of all the variable stars studied did not remain constant. However, in contrast to previous conclusions [8, 20] not one of the O-C diagrams obtained can be accurately described by a parabolic formula, that is, the change in the period cannot be considered secular.

TABLE 2. Summary of the Moments of Seasonal Maxima.

Author	Max JD_{hel}	E	O–C
$Max_{I,II}$ = JD2430000.415 + 0^d.5157336 · E; $1/P$ = 1.9389856			
Variable *21*			
Bailey	2413380.101:	−32226	0^d.233:
	680.248:	−31644	.223:
	4177.410	−30680	.218
	840.646:	−29394	.220:
	5161.402:	−28772	.190:
Hett	9500.623	−20358	.029
	20637.789	−18153	.002
Larink	2751.211	−14055	−.052
Müller	3858.470:	−11908	−.073:
	4296.325	−11059	−.076
Greenstein	667.139	−10340	−.075
Szeidl	8986.392	− 1965	−.090
	9346.364:	− 1267	−.100:
Hett	412.390	− 1139	−.088
Szeidl	755.353	− 474	−.088
	30070.459	137	−.095
Belserene	1977.669	3835	−.068
	2686.812	5210	−.059
Szeidl	3415.543:	6623	−.060:
	763.672:	7298	−.051:
	4120.586	7990	−.024
Roberts, Sandage	487.783	8702	−.030
Szeidl	91.393:	8709	−.030:
R. Baker,	509.970	8745	−.019
H. Baker	834.881	9375	−.021
Szeidl	5224.245:	10130	−.035:
	601.275	10861	−.007
Kukarkin	3.343	10865	−.001
Szeidl	928.258	11495	.001
Kheylo	6669.382	12932	.016
Szeidl	7024.214	13620	.023
Kheylo	8.335:	13628	.017:
	762.234:	15051	.029:
Szeidl	89.042	15103	.018
Variable *37*			
Max_{hel} = JD2430000.2[illegible] + 0^d.3266384 · E; $1/P$ = 3.0614891			
Bailey	2413380.201:	−50881	−0 .024:
	680.389:	−49962	− .017:
	4073.653	−48758	− .024
	420.863:	−47695	− .033:
	840.606:	−46410	−0^d.020:
	5161.685	−45497	− .025
Hett	9500.754	−32143	− .022
	20637.790	−28059	− .014
Rybka	1340.728:	−26510	−− .002:
Larink	2752.813	−22199	.005
Müller	3858.792:	−18891	.007:
	4296.816	−17469	.008
Slavenas	564.981	−16639	.003
	627.693	−16147	.001
Greenstein	67.867	−16324	− .002
Szeidl	8986.354:	− 3103	− .001:
	9346.311:	− 2001	.001:
Hett	412.950	− 1797	.005
Szeidl	755.265:	− 749	.003:
	30070.473:	216	.005:
Belserene	1977.725	6055	.015
	2686.862	8226	.021
Szeidl	3415.583	10457	.011
	763.428	11522	− .014
	4120.454	12615	− .003
Roberts, Sandage	487.927	13740	.001
Szeidl	91.515	13751	− .004
R. Baker,	509.809	13807	− .001
H. Baker	834.816	14892	.006
Szeidl	5224.500	15905	.005
	601.435	17149	− .001
Kukarkin	3.300	17155	− .006
Szeidl	928.402:	18150	.001:
Kheylo	6669.519	20419	.006
Szeidl	7024.200	21505	.007
Kheylo	8.526	21518	.007
	762.487	23765	.011
Szeidl	89.268	23847	.008
Kheylo	8864.594	27136	.020
Variable *40*			
Max_{hel} = JD 2430000.397 + 0^d.5315416 · E; $1/P$ = 1.8130993			
Bailey	2413380.247:	−30133	.003:
	680.284	−29529	.003
	4073.533	−28[illegible]6	.002
	420.461	−28217	.010
	840.737	−27[illegible]5	.011
	5161.7[illegible]	−26[illegible]3	.006
Hett	9500.70[illegible]	−19[illegible]5	.005
	20637.931	−16[illegible]4	.001

Author	Max JD_{hel}	E	O—C
Rybka	1340.646:	—15700	0^d.003:
Larink	2751.494	—13142	.007
Müller	3958.983:	—11134	.001:
	4296.907	—10340	.001
Slavenas	564.961	— 9854	.005
	627.833:	— 9740	.001:
Greenstein	67.548:	— 9668	.005:
Schwarzschild	8970.668:	— 1866	.006:
Szeidl	86.669	— 1837	.002
	9346.285:	— 1185	.000:
Hett	412.456:	— 1065	.009:
Szeidl	755.514	— 443	.004
	30070.453	128	.001
Belserene	1977.678	3586	.007
	2686.958:	4872	— .004:
Szeidl	3415.550	6193	— .001
	763.562	6824	— .004
	4120.413	7471	.002
Roberts, Sandage	487.736	8137	.002
Szeidl	91.603	8144	.002
R. Baker, H. Baker	509.804	8177	— .007
	834.662	8766	— .008
Szeidl	5224.593	9473	— .010
	601.294:	10156	— .003:
Kukarkin	3.500	10160	— .006
Szeidl	928.365	10749	— .008
Kheylo	6669.634:	12093	— .005:
Szeidl	7024.272	12736	— .001
Kheylo	8.141:	12743	— .005:
	762.241:	14074	— .001:
Szeidl	89.257	14123	— .012
Kheylo	8863.656	16071	— .015

Variable *55*

$\mathrm{Max}_{hel} = \mathrm{JD}\ 2430000.032 + 0^d.5298136 \cdot E$; $1/P = 1.8874563$

Bailey	2413380.892	—31368	.053
	680.760	—30802	.047
	4073.869	—30060	.031
	420.909:	—29405	.046:
	840.503	—28513	.028
	5161.577	—28007	.035
Hett	9500.739	—19817	.022
	20637.705	—17671	.012
Rybka	1340.211:	—16345	— .018:
Larink	2751.65[illegible]	—13681	— .032
Müller	3853.92[illegible]	—11591	— .038:

Author	Max JD_{hel}	E	O—C
	4296.549	—10765	-0^d.039
Slavenas	627.604	—10159	— .029
Greenstein	67.954	—10004	— .034:
Schwarzschild	8970.582:	— 1943	— .022:
Szeidl	86.503:	— 1913	— .005
	9346.255:	— 1234	— .013:
Hett	412.441	— 1109	— .025
Szeidl	755.238	— 462	— .020
	30070.484	133	— .013
Belserene	1977.813	3733	— .013
	2686.705	5071	— .012
Szeidl	3415.204	6446	— .006
	763.304	7103	.006
	4120.383	7777	— .009
Roberts, Sandage	487.542	8470	— .011
Szeidl	91.251:	8177	— .011:
R. Baker, H. Baker	509.808	8512	.003
	834.593	9125	.012
Szeidl	5224.523	9851	— .001
	601.227	10572	.006
Kukarkin	3.346	10576	.005
Szeidl	928.134	11169	.018
Kheylo	6669.327:	12578	.001:
Szeidl	7024.311	13255	.010
Kheylo	8.539:	13265	.000:
	762.328:	14651	— .003:
Szeidl	89.358	14702	.006
Kheylo	8863.279	16729	— .004

Variable *64*

$\mathrm{Max}_{hel} = \mathrm{JD}\ 2430000.382 + 0^d.6054590 \cdot E$; $1/P = 1.6516395$

Bailey	2413380.546:	—27449	.013:
	680.846:	—26953	.006:
	4073.789	—26304	.005
	420.711	—25731	.000
	840.910:	—25037	.010:
	5161.794	—24507	.001
Hett	9500.521	—17341	.009
	20637.561	—15453	— .003
Larink	2751.228	—11972	.006
Müller	3858.598:	—10143	— .003:
	4296.950	— 9419	— .000
Greenstein	667.491	— 8827	— .002
Schwarzschild	8970.489:	— 1760	— .002:
Szeidl	9346.476:	— 1079	— .001:
Hett	412.473	— 970	— .001

Author	Max JD$_{hel}$	E	O—C
Szeidl	755.146:	— 401	—0^d.026:
	30070.093	116	— .007
Belserene	1977.811	3267	— .001
	2686.804	4438	.000
Szeidl	3415.177	5641	.006
	763.320	6216	.010:
	4120.534	6806	.003
Roberts, Sandage	487.423	7412	— .011
Szeidl	91.069	7418	— .003
R. Baker, H. Baker	509.829	7449	— .012
	834.961	7986	— .011
Szeidl	5224.299	8629	.016
	601.490:	9252	.006:
Kukarkin	3.293	9255	— .002
Szeidl	923.129	9792	— .003
	7024.326	11602	.014
	709.614	12986	.002

Variable *65*

Max_{hel} = JD 2430089.332 + 0^d.6633094 · E; $1/P$ = 1.4962458

Bailey	2413380.728:	—21967	— .008:
	629.769:	—24418	— .031:
	4073.766:	—23830	— .038:
	420.833:	—23311	— .039:
	5161.790	—22202	— .071
Hett	9500.704:	—15710	— .016:
	20337.540:	—14009	— .025:
Larink	2751.522	—10846	— .001
Müller	3358.306:	— 9190	.013:
	4296.068	— 8535	.013
Greenstein	667.665	— 7979	.013
Schwarzschild	8970.430:	— 1511	.009:
Szeidl	86.463:	— 1517	.002:
	9346.030:	— 979	.002:
Hett	412.857	— 879	— .005
Szeidl	755.054	— 367	.003
	30070.500	105	— .008
Belserene	1977.256	2953	— .024
	2686.293	4019	— .020
Szeidl	3415.547	5110	.001
	763.021	5690	— .002
	4120.642	6165	— .002
Roberts, Sandage	487.555	6711	— .003
Szeidl	91.567	6740	— .006
R. Baker, H. Baker	509.522:	6747	.004:
	833.622	6747	.004

Author	Max JD$_{hel}$	E	O—C
	831.436	7233	0^d.005
Szeidl	5221.067	7816	— .006
	601.013	8350	.002
Kukarkin	3.019	8383	— .002
Szeidl	928.511	8870	.009
	7024.598	10510	.019
	789.165	11651	.006
Kheylo	8563.124	13261	— .051

Variable *81*

Max_{hel} = JD 2430090.461 + 0^d.5201108 · E; $1/P$ = 1.8899633

Bailey	2413380.619:	—31410	.057:
	630.625:	—30843	.057:
	4073.725:	—30100	.028:
	420.824:	—29444	.010:
	810.928	—28650	.020
	5161.565:	—28014	.006:
Hett	9500.769	—19213	— .017
	20337.824	—17691	— .022
Rybka	1340.480:	—16366	— .025:
Larink	2751.621	—13699	— .022
Müller	3358.524:	—11607	— .019:
	4296.627	—10779	— .020
Greenstein	667.531	—10078	— .022
Schwarzschild	8970.793:	— 1945	— .018:
Szeidl	86.674	— 1915	— .011
	9346.453:	— 1235	— .027:
Hett	412.610	— 1110	— .009
Szeidl	755.466:	— 462	— .017:
	30070.300	133	— .004
Belserene	1977.742	3738	— .006
	2686.753	5078	— .004
Szeidl	3415.317	6455	.005
	763.491	7113	— .006
	4120.117	7787	— .001
Roberts, Sandage	487.845	8482	— .002
Szeidl	91.029	8498	.005
R. Baker,	509.543:	8523	.000:
	834.944	9138	— .002
Szeidl H. Baker	5224.377	9374	.006
	691.114	10586	— .005
Kukarkin	3.215	10590	.000
Szeidl	928.105	11204	.016
Kheylo	8560.304:	12605	.020:

Author	Max JD_{hel}	E	O—C
Szeidl	7024.417	13276	$0^d.010$
Kheylo	8.112:	13283	.001:
	762.517:	14071	.001:
Szeidl	89.511:	14722	.010:
Kheylo	8863.074	16751	.007

Variable 93

$Max_{hel} = JD\ 2430000.420 + 0^d.6023007 \cdot E;\ 1/P = 1.6603002$

Bailey	2413380.515:	—27593	—.020:
	4073.767	—26442	—.016
	420.703:	—25866	—.005:
	840.489	—25169	—.023
	5161.498	—24636	—.040
Hett	9500.470	—17432	—.042
	20637.617	—15544	—.039
Larink	2751.139	—12035	.010
Müller	3858.781:	—10196	.021:
	4296.656	— 9469	.023
Slavenas	564.690	— 9024	.034
	627.930	— 8919	.032
Greenstein	67.676	— 8853	.026
Schwarzschild	8970.510:	— 1709	.024:
Szeidl	86.160	— 1683	.016
	9346.338	— 1085	.016
Hett	412.591	— 975	.016
Szeidl	755.302	— 406	.018
	30070.301	117	.014
Belserene	1977.774	3284	.001
	2686.680	4461	.001
Szeidl	3415.468:	5671	.003:
	763.600:	6249	.005:
	4120.158	6841	.001
Roberts, Sandage	487.551	7451	.009
Szeidl	91.171:	7457	.003:
R. Baker,	834.472	8027	.014
Szeidl H. Baker	5224.169	8674	.005
	601.205:	9300	.009:
Kukarkin	3.017	9303	.004
Szeidl	928.256	9843	.008
Kheylo	6669.072	11073	.022
	7024.432	11663	.019
Szeidl	8.010:	11669	.025:
Kheylo	762.248:	12668	.021:
Szeidl	89.357:	12933	.016:
Kheylo	8863.251	14716	.024

Author	Max JD_{hel}	E	O—C

Variable 94

$Max_{hel} = JD\ 2430000.394 + 0^d.5236036 \cdot E;\ 1/P = 1.9095135$

Bailey	2413380.904:	—31735	—$0^d.016$:
	680.450:	—31163	.010:
	4073.743	—30112	.009
	420.956	—29749	.013
	840.945:	—28947	.000:
	5161.968:	—28334	— .002:
Hett	9500.754:	—20049	— .017:
	20637.695	—17878	— .015
Rybka	1340.495:	—16536	— .012:
Larink	2751.321	—13912	— .016
Müller	3858.943:	—11727	— .006:
	4296.750	—10901	— .007
Slavenas	564.888	—10279	.000
	627.726	—10259	— .005
Greenstein	67.537	—10183	.005
Schwarzschild	8970.701	— 1966	— .018:
Szeidl	86.423:	— 1936	— .010:
	9346.197:	— 1249	— .014:
Hett	412.711	— 1122	— .000
Szeidl	755.190:	— 468	— .025:
	30070.472	134	— .007
Belserene	1977.773	3776	.002
	2686.855	5130	.003
Szeidl	3415.317:	6521	.005:
	763.573	7183	.007:
	4120.216	7867	.014
Roberts, Sandage	487.839	8569	.005
Szeidl	91.510:	8576	.010:
	5224.151:	9975	.003:
	601.212	10595	.005
Kukarkin	3.304	10699	.002
Szeidl	928.519:	11320	.003:
Kheylo	6669.554	12735	.002
Szeidl	7024.038:	13412	.006:
Kheylo	8.273:	13420	.001:
	762.505:	14822	.016:
Szeidl	89.218	14873	.019
Kheylo	8863.305	16924	.011

Author	Max JD_{hel}	E	O—C

Variable *107*

Max_{hel} = JD 2430000.039 + $0^d.3090348 \cdot E$; $1/P = 3.2358815$

Bailey	2413380.751	—53778	—0^d.012:
	680.827	—52807	— .011
	4073.926	—51535	— .004
	5161.732	—48015	— .001
Hett	9500.592	—33975	— .010
	20637.519	—30296	— .002
Rybka	1340.246	—28022	— .020:
Larink	2751.328	—23456	.009
Müller	3858.602	—19873	.012:
	4296.806	—18455	.001
Slavenas	564.743	—17588	.008:
	627.774	—17384	— .004
Greenstein	67.952	—17254	.000
Schwarzschild	8970.959	— 3330	.006:
Szeidl	86.401	— 3280	— .004
	9346.420	— 2115	— .010
Hett	412.869	— 1900	— .004
Szeidl	755.276	— 792	— .007
	30070.179	227	— .011
Belserene	1977.553	6399	.000
	2686.478	8693	.000
Szeidl	3415.170	11051	— .012
	763.143	12177	— .013
	4120.082	13332	— .008
Roberts, Sandage	487.532	14521	— .001
Szeidl	91.243	14533	— .001
R. Baker,	509.476	14592	.001
H. Baker	834.891	15645	.003
Szeidl	5224.273	16905	.001
	601.297	18125	.002
Kukarkin	3.157	18131	.008
Szeidl	928.256	19183	.002
Kheylo	6669.329	21581	.010
Szeidl	7024.099	22729	.008
Kheylo	8.427	22743	.010:
	762.383	25118	.008:
Szeidl	89.268	25205	.007
Kheylo	8863.468	28681	.002

Author	Max JD_{hel}	E	O—C

Variable *108*

Max_{hel} = JD 2430000.979 + $0^d.5193917 \cdot E$; $1/P = 1.9245810$

Bailey	2413380.716	—31955	0^d.022
	690.515:	—31408	.009:
	4073.854:	—30651	.008:
	420.954:	—29383	.006:
	840.795:	—29175	.012:
	5161.838	—28557	.000
Hett	9500.574	—20207	— .024
	20637.906	—18018	— .026
Larink	2751.221	—13951	— .024
Müller	3858.495	—11820	— .027:
	4296.522	—10977	— .027
Slavenas	627.511	—10340	— .026
Greenstein	67.520	—10203	— .026
Schwarzschild	8970.913:	— 1931	.000:
Szeidl	86.506	— 1951	.005
	9346.072	— 1259	.004
Hett	412.560	— 1131	— .0[illegible]
Szeidl	755.512	— 471	— .0[illegible]
	30070.393	135	— .00[illegible]
Belserene	1977.655	3803	.007
	2686.[illegible]	5170	.000
Szeidl	3415.099	6572	— .003
	7763.227	7242	.000
	4120.198	7929	.003
Roberts, Sandage	487.556	8636	.000
Szeidl	91.188	8643	— .005
R. Baker,	509.899:	8679	.000:
H. Baker	831.659	9301	.007
Szeidl	5224.371	10054	.015
	601.079	10779	.010
Kukarkin	3.150	10783	.003
Szeidl	928.430	11409	.010
Kheylo	6669.359	12835	.013
Szeidl	7024.282	13518	.016
Kheylo	8.436	13526	.013
	762.118	14683	.013
Szeidl	89.145	14[illegible]	.021
Kheylo	8833.176	17057	.029

Author	Max JD_{hel}	E	O—C

Variable *119*

$Max_{hel} = JD\ 2430000.192 + 0^d.5177411 \cdot E$; $1/P = 1.9314673$

Bailey	2413380.605:	—32099	—0^d.007:
	680.988:	—31519	— .004:
	4073.980	—30760	.032
	420.875:	—30090	.031:
	810.769:	—29279	.037:
	5161.790	—28659	.058
Hett	9500.942:	—20278	.022
	20637.868:	—18082	— .011:
Rybka	1340.428:	—16725	— .026:
Larink	2751.274	—14000	— .025
Müller	3858.725:	—11861	— .022:
	4296.742	—11015	— .014
Greenstein	667.970	—10298	— .006
Schwarzschild	8970.929:	— 1987	.007:
Szeidl	86.451:	— 1957	— .004:
	9346.283:	— 1262	— .002:
Hett	412.565	— 1134	.009
Szeidl	755.301	— 472	.001
	30070.070:	136	— .017:
Belserene	1977.956	3821	— .007
	2686.739	5190	— .011
Szeidl	3415.215	6597	.003
	763.144:	7269	.010:
	4120.381	7959	.006
Roberts, Sandage	487.971	8669	.005
Szeidl	91.086	8675	.008
R. Baker,	509.725:	8711	.008:
Szeidl H. Baker	834.857	9339	— .001
	5224.207:	10091	.008:
	601.113	10819	— .002
Kukarkin	3.180	10823	— .006
Szeidl	928.326	11451	— .001
Kheylo	6660.207	12882	— .008
Szeidl	7024.377	13568	— .008
Kheylo	8.527	13576	.000
	762.180	14093	.014
Szeidl	89.109:	15045	.020:
Kheylo	8863.402	17120	.000

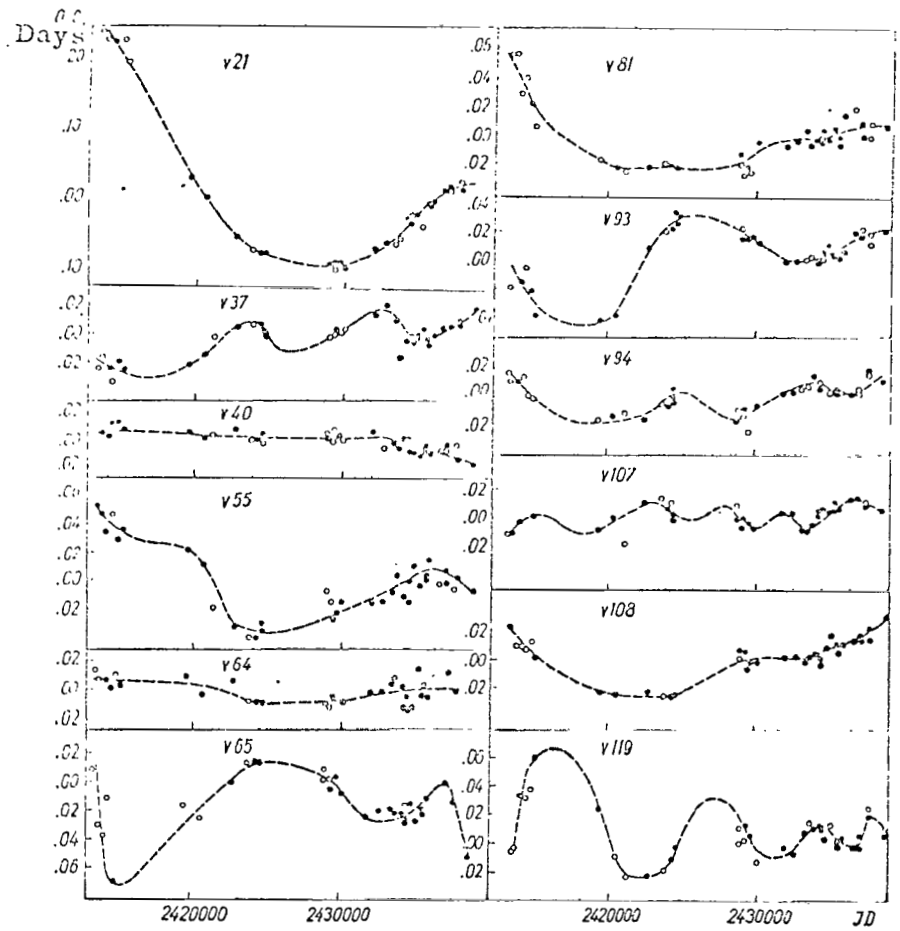

Figure 2. Changes in periods of stars studied (the circles correspond to the less reliably established moments of seasonal maxima).

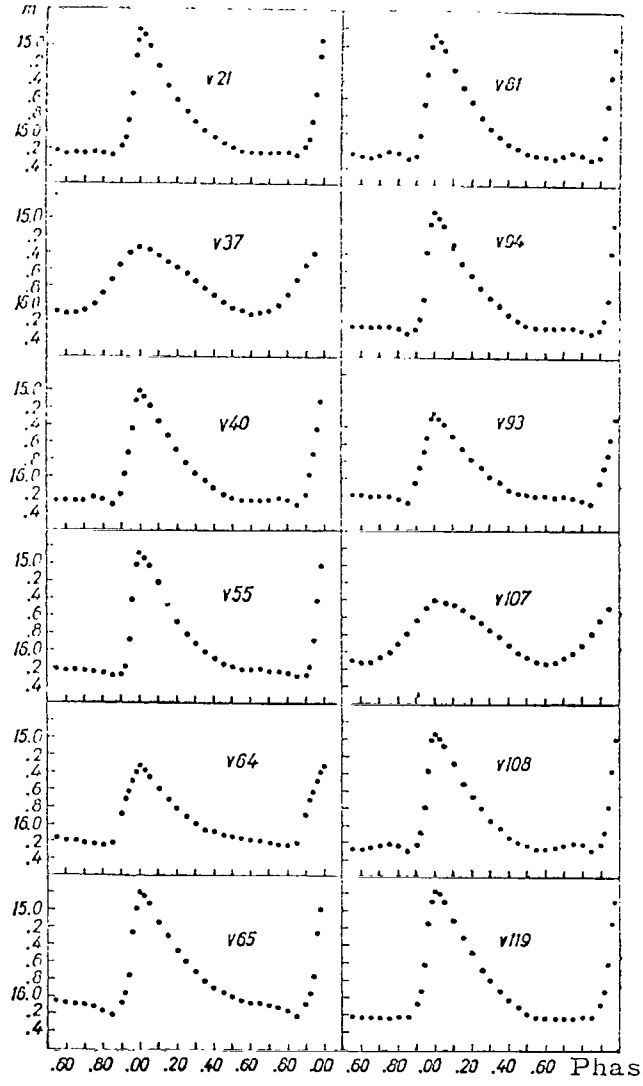

Figure 3. "Weighted" mean light curves for 12 RR Lyrae type variables in M3.

Yet, individual sections of the diagrams are parabolas. It is entirely possible that all the changes in the periods of RR Lyrae type stars in globular clusters, treated as secular up to this point, simply are the result of unjustifiably bold extrapolation. There, observation material must be assembled in order to answer the question of whether or not changes in the periods of RR Lyrae type stars are evolutionary. /80

It is interesting to note that the O-C diagrams for stars 37 and 107 (both belong to subtype RR_c) have definite waves with almost identical amplitudes. This creates the impression that the period, while remaining constant on the whole, changes within small limits. The O-C diagram for the variable 119, has the form of a curve with a decreasing amplitude, indicating damping of period oscillations. This conclusion will be valid if the curve we have drawn corresponds to reality, but we cannot be absolutely certain about this for points other than those beginning with JD 24290000.

Star	Period	m_{max}	A	m_{med}	ε	ξ	Subtype
21	$0^d.5157336$	$14^m.81$	$1^m.46$	$15^m.54$	0.150	$0^m.56$	*a*
37	.3966381	15 .31	0 .78	15 .73	.390	.05	*c*
40	.5515416	15 .01	1 .31	15 .66	.140	.48	*a*
55	.5298136	14 .88	1 .43	15 .60	.125	.53	*a*
64	.6051590	15 .32	0 .91	15 .78	.180	.30	*b*
65	.6683304	14 .79	1 .43	15 .50	.140	.43	*a*
81	.5291108	14 .86	1 .41	15 .58	.130	.55	*a*
93	.6023007	15 .24	1 .03	15 .76	.150	.32	*b*
94	.5236946	14 .90	1 .43	15 .62	.130	.51	*a*
107	.3090348	15 .40	0 .74	15 .77	.400	.03	*c*
108	.5196047	14 .94	1 .36	15 .62	.140	.53	*a*
119	.5177411	14 .76	1 .49	15 .50	.170	.53	*a*

The light curves for all stars investigated are typical for RR Lyrae type variables. Stars v 37 and v 107 belong to the RR_c subtype, v 64 and v 93 to the RR_b subtype, and the rest to the RR_a subtype. There is a slight increase in brightness before the minimum on the light curves for RR_a stars. The exception is v 65. Based on period magnitude, v 65 should belong to the RR_b subtype, but /81 based on the amplitude value, should belong to the RR_a subtype. Nor can the possibility that it is different in its other characteristics from RR_a stars in M3 be ignored.

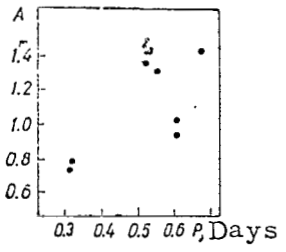

Figure 4. The period-amplitude function in M3.

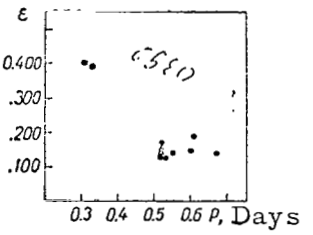

Figure 5. The period-asymmetry "by period" function in M3.

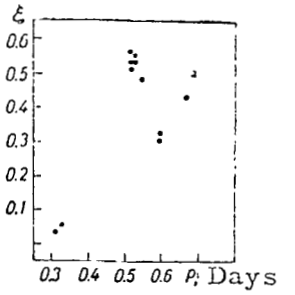

Figure 6. The period-asymmetry "by stellar magnitude" function in M3.

According to the data listed in Table 3, the mean apparent median magnitude of RR_a stars is $15^m.58$, for RR_b it is $15^m.77$ and for RR_c it is $15^m.76$. Thus, the conclusion with respect to different absolute magnitudes for different subtypes of RR Lyrae type stars is confirmed once again.

Taking the value of the absolute stellar magnitude of RR Lyrae type stars to be equal to $0^m.0$, and ignoring the difference between the P_k and the international photographic system, we obtain the apparent modulus of the distance to M3 as

$$m-M = 15^m.64$$

APPENDIX

Observations by V. V. Kukarkin

JD_{hel}	v21	v37	v40	v55	v64	v65	v81	v93	v94	v107	v108	v119
	m	m	m	m	m	m	m	m	m	m	m	m
2435577.540	15.16	15.54	15.63	15.81	16.08	16.31	16.18	16.16	15.97	15.64	16.12	16.10
8.280	16.18	.52	.88	16.09	.15	15.24	.22	15.72	.62	16.09	15.32	.02
.337	.26	.74	16.04	.12	.12	.01	14.82	.36	.79	.12	.68	14.87
.448	.26	16.00	.13	14.64	15.43	.56	15.61	.92	16.11	15.38	16.10	15.52
.496	.26	15.80	.11	15.14	.36	.68	.78	.97	.08	.62	.15	.74
9.290	15.92	.56	15.22	16.02	16.03	16.10	16.28	16.18	15.23	.91	14.79	16.13
.313	16.12	.64	.44	.00	15.88	.10	.35	.16	.60	.77	15.26	15.90
.333	.19	.84	.44	.02	16.08	.12	.21	.27	.73	.29	.62	.40
95.294	.20	.54	.49	.07	.08	15.90	14.97	15.81	.97	16.04	16.12	16.10
.337	.23	.76	.54	.00	.15	16.10	15.43	.94	16.02	15.84	15.08	.19
.360	.02	.86	.70	15.84	15.84	.04	.52	.94	15.94	.86	14.66	.13
.380	.17	.83	.92	14.90	.68	.08	.68	.90	16.06	.66	.96	15.75
.420	.16	.98	16.06	.63	.46	.08	.74	16.15	15.49	.42	15.08	14.72
6.233	15.68	.27	.20	16.12	16.08	.21	16.15	.25	.88	16.10	16.07	16.22
.265	.91	.24	.26	.13	.02	.05	.34	.20	16.00	16.04	.09	.24
7.286	.83	.77	.16	.14	15.54	.04	.24	.10	.06	15.64	.04	.11
8.293	.72	.75	.10	.12	16.10	15.97	.16	15.74	.00	.92	.16	.30
.308	.84	.88	.18	15.98	.08	.50	.26	.64	.07	.83	.03	.16
601.373	.76	.64	15.50	.92	.10	.84	.27	.71	15.78	.76	.11	.18
.388	.80	.64	.60	.88	.12	16.04	.19	.92	.90	.79	.12	.20
.403	.84	.49	.78	.92	15.94	.00	.21	.81	.90	.82	.14	.14
.419	.82	.50	.80	16.10	.80	.04	.20	16.06	16.11	.82	.16	.27
.434	.84	.34	.77	.04	.78	.02	.23	15.97	.02	.95	.14	.20
.450	.96	.37	.78	.09	.46	15.94	.21	16.11	.08	16.06	.13	.26
.496	.94	.37	16.00	.15	.27	16.13	.21	.11	.08	.06	.16	.24
.526	16.06	.67	.02	.14	.68	.06	.20	.11	.13	.16	.16	.19
2.235	.20	.96	.19	.02	.83	.08	15.58	—	—	15.26	15.78	15.34
.250	.22	16.02	.16	15.58	.97	.10	.52	—	—	.26	.71	.54
.266	.02	15.78	.13	.01	16.04	.21	.74	—	—	.35	.90	.56
.310	14.75	.91	.19	14.67	.00	15.94	.76	—	—	.77	16.03	.94
.341	.96	.92	.03	15.06	.14	.24	.72	—	—	.92	.01	.82
.356	15.10	.76	.03	.30	.09	14.78	.86	—	—	.92	—	16.00
.372	.18	.56	15.66	.53	.06	.82	.87	—	—	16.02	.07	.12

JD_{hel}	v21	v37	v40	v55	v64	v65	v81	v93	v94	v107	v108	v119
.387	.45	.38	14.92	.58	.14	.97	16.03	—	—	.09	.10	.05
.401	.41	.59	15.04	.68	.12	.98	15.94	—	—	.16	15.96	.13
.430	.76	.22	.09	.86	.03	15.28	16.15	—	—	.06	16.16	.19
.444	.80	.42	.09	.93	15.89	.40	.15	—	—	.10	.07	.18
.458	15.84	.56	15.16	15.97	16.00	15.34	16.24	—	—	.02	.13	.34
.473	.95	.50	.52	16.00	.17	.59	.14	—	—	15.97	.16	.34
.488	.90	.53	.52	15.92	15.85	.52	.24	—	—	.72	.16	.37
6.391	16.16	.24	.32	.96	.30	.42	.29	15.96	.04	.74	15.17	14.80
.392	.23	.18	.45	16.04	.36	.26	15.73	16.06	.05	.94	.18	.96
.370	.12	.50	.55	.10	.43	14.83	.00	.00	.08	16.04	.21	15.16
.437	14.82	.80	.91	.11	.74	15.39	.38	.10	14.86	.06	.40	.82
.456	.89	.92	16.01	.13	.71	.36	.44	.16	.76	.06	.84	.90
.478	15.04	.89	.06	.00	.80	.43	.58	.16	.89	.08	.85	.96
.495	.18	.86	.12	15.44	.80	.48	.68	.11	.96	.05	.91	16.06
14.243	—	.58	15.99	—	.65	16.15	—	.13	16.30	—	16.02	—
.308	—	16.06	16.12	—	.88	.00	—	.10	14.82	—	—	—
.337	—	.04	.15	—	16.04	.02	—	.07	.92	—	—	—
.357	—	.05	.14	—	.08	15.10	—	.28	15.04	—	—	—
.393	—	15.90	.13	—	.16	14.91	—	.10	.20	—	—	—
.410	—	.70	.22	—	.20	15.04	—	15.65	.42	—	—	—
.468	—	.62	.20	—	.15	.28	—	14.80	.89	—	—	—
.491	—	.46	.02	—	.08	.59	—	15.11	16.00	—	—	—
5.243	—	.78	15.98	—	15.84	.68	—	16.10	.20	—	—	—
.253	—	.80	.99	—	16.17	.62	—	.20	.23	—	—	—
.276	—	.74	.99	—	—	—	—	.00	.15	—	—	—
.287	—	.74	16.06	—	15.98	—	—	.10	.15	—	—	—
.302	—	.69	15.90	—	—	—	—	.05	.15	—	—	—
.315	—	.80	16.06	—	.89	.97	—	.24	15.94	—	—	—
.340	—	16.04	.00	—	.95	.88	—	.27	14.84	—	—	—
.352	—	.06	.14	—	.78	.82	—	.14	.82	—	—	—
.365	—	15.99	—	—	.22	16.04	—	.24	.92	—	—	—
.379	—	.88	.08	—	.71	15.88	—	.19	15.08	—	—	—
.393	—	—	—	—	—	.90	—	.27	.14	—	—	—
.418	—	.81	.09	—	.40	.86	—	.27	.22	—	—	—
.432	—	.78	.14	—	.50	.98	—	.27	.45	—	—	—
.445	—	.38	.17	—	.62	.98	—	.28	.66	—	—	—
.457	—	.84	.06	—	.45	.90	—	.27	.66	—	—	—
.470	—	.62	.06	—	.60	.95	—	.27	.76	—	—	—
.483	—	.02	.20	—	.65	16.15	—	.32	.83	—	—	—
.496	—	.14	—	—	.74	.04	—	.02	.94	—	—	—

Observations by E.S. Kheylo
40-centimeter astrograph

JD_{24}	v21	v37	v40	v55	v81	v93	v91	v107	v108	v115
	m	m	m	m	m	m	m	m	m	m
2430633.594	16.34	15.62	16.32	16.50	16.04	15.24	15.83	15.96	15.15	17.05
9.590	—	.49	15.87	.13	.59	16.25	16.14	.72	.87	16.15
.592	.33	.66	16.20	.02	.02	15.30	.07	.78	16.02	.15
.594	.56	.54	.10	.22	.15	—	.20	.78	.07	.62
46.514	16.14	.83	15.51	15.74	.00	16.04	14.56	.65	14.86	15.61
.559	.17	—	.41	.60	.22	—	15.09	.78	.95	—
.569	.22	.83	.64	.58	15.52	.01	.63	16.04	15.58	16.91
7.573	.22	.96	—	.71	16.11	15.65	14.56	.11	14.78	15.65
57.574	.11	16.07	16.20	.78	15.52	16.07	16.14	15.31	16.22	14.60
.579	.15	.07	.28	16.00	.78	.07	.32	.52	15.96	15.65
.610	.30	15.59	.27	.30	16.04	.07	.20	96	.70	.78
8.283	15.93	16.20	.44	15.62	14.95	15.13	.32	.68	16.22	16.07
.320	16.22	.32	.32	.70	15.52	.42	.20	.68	.22	14.86
.373	.22	15.97	.20	.70	.69	.67	.20	.74	15.74	15.6
.419	.22	.58	.48	.87	.78	.83	.32	.87	16.13	.69
.463	.26	.44	.21	16.17	16.11	.85	.18	.70	.22	.78
60.291	.22	.63	.12	15.78	15.74	.98	.27	.96	15.96	.37
.336	.30	.63	.18	16.04	.96	16.27	.26	16.04	.31	.61
1.359	.14	.54	15.16	15.26	.99	15.56	15.83	15.69	16.22	16.04
.404	.30	.33	.42	14.93	.63	.63	16.30	.78	.22	15.70
.421	.22	.44	.54	15.61	14.85	.84	.27	16.04	.04	14.78
.467	.30	.83	.65	.61	15.21	16.07	.32	15.78	.00	.93
.512	.13	.98	16.00	16.00	.68	.00	.41	.74	.22	15.26
.578	.15	16.36	.12	15.78	.93	.01	.56	.63	15.52	16.00
4.505	15.96	.32	.32	16.22	16.04	.07	.07	.70	16.22	15.67
6.327	.06	15.44	14.94	15.78	15.62	.14	.32	.78	15.37	.96
.372	.30	.73	15.24	.87	.70	.16	15.65	.87	.70	16.13
.422	.68	16.08	.58	16.39	16.07	—	14.73	16.07	.74	.07
.468	.78	.20	.91	15.86	.22	15.99	15.01	15.78	.78	.04
.514	.88	.14	.83	16.22	.39	16.07	.48	.61	16.14	.06
.565	.93	15.84	16.20	.14	.07	.13	.83	.67	.30	.00
8.342	.13	.63	.32	15.45	14.93	.09	16.07	.74	14.85	15.67

JD_{hel}	v21	v37	v40	v55	v64	v65	v81	v93	v94	v107	v108	v119
.386	.01	16.32	.20	.52	15.32	.21	.32	.30	15.15	.74		
.433	.37	.25	.35	.70	.52	15.63	15.32	.52	.60	16.04		
.477	.78	.14	.25	16.04	.78	.04	.10	.67	.72	.09		
.529	.68	15.49	15.41	.22	16.04	.10	14.63	.70	16.00	.04		
.570	—	.44	.10	.22	.22	.24	15.17	.86	.14	.05		
9.336	.78	.83	16.32	14.85	15.74	.98	16.32	.67	.30	15.68		
.380	14.78	16.25	.45	15.00	14.82	16.07	.07	.65	14.93	.96		
.425	.96	.21	.32	.59	15.15	.19	.21	.71	.85	.96		
.469	15.39	.07	.32	.78	.67	15.96	.20	16.04	15.59	16.04		
.560	.78	15.44	.32	.87	.74	16.20	14.49	15.96	.87	.22		
85.349	.40	.66	.27	.70	.45	15.11	15.17	.67	16.22	15.52		
7.279	16.22	.59	14.97	16.15	16.15	.59	16.44	.67	.00	16.07		
.324	.15	.95	15.17	15.65	15.93	.83	15.34	.65	.22	15.00		
.369	.22	16.20	.63	14.78	14.66	16.07	14.80	.74	.22	14.78		
.415	15.26	.29	.75	15.65	15.00	.07	15.41	16.22	.22	15.32		
92.291	16.07	.14	.26	.93	.78	.14	16.14	15.74	15.37	16.00		
.336	.14	.04	.49	16.07	.93	15.96	.35	.78	.40	.15		
.382	.22	15.40	.83	.22	16.22	16.07	.18	16.09	.72	16.39		
.520	.25	16.14	16.32	.13	.22	15.56	.07	15.62	16.22	14.85		
9.322	14.81	15.49	.21	.13	.13	.58	.07	.67	.13	.93		
.367	15.13	.74	15.83	15.96	.22	.66	15.49	.67	.04	15.39		
.412	.68	16.32	.10	.96	15.96	.85	14.63	.71	.04	.74		
.458	.71	.32	.39	16.22	16.00	16.00	15.46	16.00	.11	.89		
700.401	.37	15.95	16.20	.00	.22	15.04	16.07	15.89	.00	.68		
2.398	14.92	16.25	.35	15.96	15.96	.95	.32	.45	15.96	14.78		
6.311	—	.06	.35	16.30	16.30	16.30	15.73	.98	14.96	16.11		
702.284	15.29	15.44	15.04	15.13	.13	.20	16.07	16.04	.78	.22		
.329	.72	.61	.46	14.71	.07	.20	.07	15.93	.78	15.65		
.376	.91	.61	.46	15.52	15.72	.14	.35	.78	.65	14.85		
.423	.88	.76	.76	.68	14.71	.18	14.97	.23	.72	15.00		
.528	16.22	.93	16.25	16.15	15.68	15.19	16.25	16.07	16.22	16.00		
47.395	15.37	.46	15.49	.04	16.13	.75	.25	.13	.04	.22		
735.452	14.96	.54	16.32	15.72	.04	.98	15.83	15.68	.22	.04		
.496	15.35	.74	.21	16.07	.07	16.07	.95	.68	15.78	.07		
.540	.62	.86	.10	.04	14.71	.21	16.32	.65	16.22	.13		
57.532	16.07	.58	.18	.00	16.22	15.34	.07	.70	15.62	14.85		
9.408	.07	16.13	.27	.22	.13	.54	14.98	.87	.87	16.15		
91.321	.00	15.65	.21	.22	.04	.63	.86	16.13	.87	15.71		
.364	—	16.10	—	.42	.04	—	15.00	.18	—	16.12		
.407	.05	.26	.36	.14	.04	.83	.66	15.62	.70	.22		

Menicus telescope AZT-2

JD$_{sel}$	v21	v37	v40	v55	v64	v65	v81	v93	v94	v107	v108	v119
2437779.389	^{m}15.78	^{m}15.73	^{m}15.37	^{m}15.70	^{m}15.04	^{m}16.24	^{m}16.07	^{m}16.19	^{m}15.83	^{m}15.83	^{m}15.90	^{m}15.73
87.370	16.21	.44	16.25	.72	16.07	.04	15.36	.10	16.35	.65	16.36	16.31
.418	.31	.60	.29	.70	.09	.03	.00	.19	.28	.41	.08	.36
.478	15.87	16.03	.04	.97	.07	15.63	.36	.19	.38	.59	.03	15.94
.507	.03	16.25	15.83	15.93	—	—	.67	15.57	.19	.59	.22	.36
90.391	16.00	15.61	.00	.66	.09	14.89	16.09	16.28	15.70	.97	15.84	16.21
4.419	15.87	—	—	.78	15.31	15.26	15.70	—	—	.70	.42	15.87
823.387	.90	16.14	16.25	.05	14.64	16.00	14.84	.19	.68	16.00	16.24	.71
.415	16.20	.01	15.66	16.16	.66	15.76	.80	.19	16.01	.00	15.05	.81
8303.358	15.81	15.46	.54	15.76	.98	.74	15.58	15.70	15.24	15.48	16.00	16.10
.393	.85	.63	.70	.82	15.16	16.16	16.22	16.02	.06	.56	.00	.00
.435	.80	.61	16.01	—	.16	15.84	14.87	.01	.37	.18	—	.10
848.362	.90	.81	15.54	16.40	16.32	16.48	15.60	15.72	16.15	.40	.48	15.40
.412	.46	16.07	16.15	15.46	15.30	15.13	16.07	—	.40	.84	.48	.03
.548	.87	15.24	.32	.30	.90	.28	.15	16.28	.28	16.32	.56	.78
52.543	14.89	.59	.38	16.32	16.16	.24	15.35	15.70	.20	.00	.40	14.87
4.400	16.10	.59	15.65	15.53	15.84	16.00	16.29	16.01	15.08	.00	15.30	16.00
5.432	.00	.57	.12	.58	.86	15.75	.36	15.13	.50	15.51	.44	.05
.493	15.90	.46	.61	.77	16.40	16.00	.22	.54	.20	.76	.54	.16
.546	.90	.83	16.01	16.00	.48	.16	.49	.86	.63	.74	.85	.27
6.436	16.26	.60	15.63	15.09	.32	14.97	.09	16.16	16.01	.69	.18	.16
.507	.31	.63	14.94	.61	.32	15.10	.42	.34	15.08	.84	.69	.21
9.373	15.89	.44	15.70	16.40	.48	.62	15.02	.23	16.10	.32	16.24	15.78

JD_{hel}	v21	v37	v40	v55	v64	v65	v81	v93	v94	v107	v108	v119
.416	.91	.70	16.15	.24	.40	.90	.14	.46	.35	.70	.32	.82
.458	16.10	.59	.08	.32	.40	.76	.50	.25	.35	.61	.40	.85
60.377	15.80	.32	15.15	.40	.48	16.32	16.09	—	—	.38	.40	.66
.415	.80	.57	.13	.40	.32	15.22	15.34	.19	—	.61	.48	.85
.456	16.00	.85	.57	.40	.24	.13	.08	.56	.24	.61	.32	16.16
.505	.00	16.20	—	.38	14.72	.22	.30	.30	.38	16.10	.48	.18
1.400	15.76	15.65	.83	.40	16.48	.98	16.07	15.77	.01	15.70	.48	15.80
.440	.80	.90	.10	.32	.24	16.08	.00	.41	.15	16.00	.32	.00
.498	16.10	.93	.48	.38	.01	.20	14.95	.48	.29	.00	.48	16.05
.533	.21	.94	.60	.40	15.13	.32	15.15	.63	.27	15.92	.48	.15
3.352	15.12	.65	16.01	15.07	16.40	15.44	16.22	.70	15.39	16.32	.40	.15
.388	.93	16.05	.15	.45	15.09	.66	.36	.64	.57	15.92	.24	15.16
7.303	16.26	15.77	.24	16.24	.07	.35	14.97	16.19	16.28	16.08	15.84	.31
71.284	15.85	16.19	.20	15.11	16.00	.46	16.27	.10	15.83	15.82	16.40	.80
.322	16.23	.21	.31	.46	15.18	.40	.36	.28	16.10	.81	.40	.81
.364	.26	.13	14.98	.69	—	.61	.32	—	.10	16.14	.48	16.14
.401	.26	15.44	.98	.72	16.40	.83	.42	.28	.28	15.84	.24	.16
.440	.00	.39	15.37	16.00	.00	.87	.34	.24	.30	16.08	.37	.26
.475	.10	.55	.53	.11	.00	.87	.28	.36	.34	15.56	.02	.21
2.292	15.90	16.09	16.29	14.90	.00	16.26	.08	15.08	15.57	16.18	.27	15.76
.330	.96	15.90	.33	15.01	.00	.37	.16	.23	.19	.23	.38	.88
.409	16.20	.53	15.44	16.00	.00	15.19	.34	.89	16.14	15.47	.25	16.24
.512	.15	.71	.08	.00	.00	.10	.22	16.20	.34	.76	15.22	—
3.491	.20	.60	16.27	15.61	.00	.85	.30	15.60	.01	.60	16.35	15.96
.709	.15	.83	.28	.01	.00	16.08	.31	.23	.18	.25	.31	16.18
98.119	—	16.03	15.19	16.02	.00	.28	.18	16.30	15.13	.26	.27	.17

REFERENCES

1. Zverev, M. S., et al., "Variable Stars", Gostekhizdat, No. 3, 1947, P. 157.
2. Kukarkin, B. V. and Kukarkina, N.P., Pereminnyye zvezdy, No. 13, 1961, p. 239.
3. Kheylo, E. S., IBVS., 1964, p. 43.
4. Kheylo, E. S., IBVS., 1965, p. 104.
5. Tsesevich, V. P., Zvezdy tipa RR Liry, [RR Lyrae Type Variable Stars], Naukova Dumka Press, Kiev, 1966.
6. Bailey, S., HA, Vol. 78, 1913, p. 5.
7. Baker, R. and Baker, H., AJ, Vol. 61, 1956, p. 283.
8. Belserene, E., AJ, Vol. 57, 1952, p. 237.
9. Greenstein, J., AN, Vol. 257, 1935, p. 301.
10. Hett, J., AJ, Vol. 50, 1942, p. 15.
11. Larink, J., Berg. Abb., Vol. 2, 1922, p. 6.
12. Müller, Th., Berl. Bab. Veröff, Vol. 11, 1933, p. 1.
13. Roberts, M. and Sandage, A., AJ, Vol. 65, 1955, p. 185.
14. Rybka, E., BAN, Vol. 5, 1930, p. 257.
15. Sandage, A., AJ, Vol. 58, 1953, p. 61.
16. Sawyer, H., DDO Publ., 1955, p. 259.
17. Schwarzschild, M., HC, 1940, p. 437.
18. Shapley, H. and Davis, H., AJ, Vol. 51, 1920, p. 140.
19. Slavenas, P., AN, Vol. 24, 1929, p. 169.
20. Szeidl, B., Mit. Sternw., Budapest., 1965, p. 48.
21. Von Zeipel, M., Ann. de l'Obs. de Paris, Vol. 25, 1908, p. 1.

STELLAR ROTATION THEORY

V.V. Porfir'yev

ABSTRACT. Modern theory of the structure of rotating stars is reviewed. A hypothesis for noncircular stellar rotations is discussed.

Once stellar rotation was discovered by G.A. Shein and O. Struv, attempts /89 were begun to account for the possible effects on the theory of the internal structure and evolution of stars. The great interest aroused by this problem is quite understandable because rotation is the only dynamic element that can be introduced into the theory.

The development of the theory of the internal structure of stars has resulted in defining three problems of particular attention for researchers. The first of these is clarification of the question to what degree rotation can change the physical conditions in the center of the star. The fact of the matter is that rotation leads to the appearance of a field of centrifugal accelerations and stellar equilibrium is possible with a lower central pressure than is the case for nonrotating stars. On the other hand, rotation disrupts the central symmetry of the star. Therefore, we cannot state a priori that when the star is observed "from the equator" and "from the pole", the same luminosity will be established (for a specified mass). This effect can distort the mass-luminosity ratio obtained from observations.

The second problem is that of the meridianal circulation that occurs in rotating stars. Today it is quite clear that only this kind of circulation could provide the intermixing of stellar material in the process of evolution. Since the question of the intermixing of material is a cardinal one in the theory of the internal structure of stars, the importance of this problem requires no substantiation.

The third basic problem of stellar rotation theory is that of establishing the relationship between angular velocity and the coordinates in the body of the star. Related to this is the problem of explaining the basic observational data on stellar rotation. What follows will point out that many of the effects ob-

served in the rotation of stars have a simple explanation if difference in rotation laws is taken into consideration. It should be pointed out that the majority of the authors to date have paid very little attention to this problem, taking it that stellar rotation is similar to the rotation of a solid body. However, this assumption is valid only as a first approximation, because observations of the /90
sun, and of the large planets, indicate that stellar rotation is not rigid.

We should also note the close connection between the problem of stellar magnetism and stellar rotation. At the present time, this problem cannot be solved because of great mathematical difficulties, and an obvious inadequacy of observational data.

There are a number of mathematical difficulties involved in changing to an examination of rotating stars. The most fundamental of these is the conversion to equations in partial derivatives. In addition, there are more equations describing the stellar model. At the present time there are practically no methods for solving and investigating these sets of equations. Even their solution by numerical methods on modern electronic digital computers requires hundreds of hours of machine time, and is impractical. Therefore, investigations of rotational effects are limited to cases of quite low angular velocities. Then these equations can be linearized by expanding the unknown functions into small parameter series and taking into account only first order terms.

The solution of the linearized equations is found by expansion of the unknown functions into a Legendre polynomial series. The rather complex system of ordinary differential equations obtained in this way can be solved by conventional numerical analysis methods. We note that the calculation of one model of a rotating star, even assuming a rather slow rotation, requires about 30 minutes on an M-20 computer.

Until recently, scientists felt that the assumption concerning slow rotation was rather artificial. However, J.J. Monachan and J. Roxburg [1] demonstrated that in the case of real models, the ratio of centrifugal acceleration at the equator of the star to the acceleration of the force of gravity decreases with approach to the center so quickly that rotation can be assumed to be slow, even if this ratio is near unity on the surface of the star. The rather simple methodology they proposed provides results, even for rapid rotation in the limit,

integrating the initial system of equations. Comparison of the results obtained by R.D. James with those obtained by the Monachan and Roxburg method, showed that /91 the latter yields highly satisfactory results.

We note that observations show an almost total absence of stars rotating at maximum velocities.

Only in spectral class B does one find stars that rotate at velocities near maximum (Be stars). In all other spectral classes the rotation rates were below maximum by several orders of magnitude. These considerations show that an approximation of slow rotation is good enough, and that the results obtained are quite adequate for practical purposes. Let us examine some of the results of calculations made of models of rotating stars.

Unfortunately, all models were built on the assumption of rigid rotation. Apparently, however, it can be assumed that in fact the effects of rotation have an identical order of magnitude for any rotation law possible in real stars.

The most complete calculation of rotational effects was made by P. Sweet and A. Roy [3] for the Cowling model. According to their results, a rotating star has a somewhat lesser central density, and a somewhat higher central temperature. The difference between rotating and nonrotating stars is not in excess of 10-15%, even for very high rotation rates. An analogous result was obtained by this author [4] for a star with a constant absorption coefficient in the shell. Thus we can assume that taking rotation into account does not change our ideas as to the physical conditions in the centers of stars.

A rotating star has a somewhat higher luminosity than a nonrotating one for given mass and chemical composition. At the same time, because the conditions for radiation transfer in the equatorial plane and in the direction of the polar axis are different for a rotating star, the polar regions of the star are hotter than the equatorial regions (the so-called gravitational darkening). This results in the observed luminosity of a star being greater if its axis of rotation is parallel to the line of sight than if the line of sight lies in the equatorial plane. The difference in observed absolute stellar magnitudes can be $0^m.5$ in the case of slow rotation [1], and even $1^m.0$ in the case of very rapid rotation [3].

The difference in the temperatures of the polar and equatorial regions in-

dicates that the spectral class of the star is a function of the orientation of its axis of rotation. The nature of the latter's shift on the spectrum-luminosity diagram is clear from the figure. /92

This effect is substantial even for low rotation rates, although its magnitude is proportional to the square of the angular velocity. It is absolutely essential that gravitational darkening be taken into account when constructing the spectrum-luminosity diagram, especially for early spectral classes. Unfortunately, the difficulties involved in determining rotation rates have resulted in most of the papers devoted to investigation of the spectrum-luminosity diagram completely ignoring these effects.

Thus, the conclusion is that taking rotation into account is unimportant when knowledge of the physical conditions in the center of the star is definite. Specifically, consideration of rotation can scarcely change the computed periods of evolution to any significant extent. On the other hand, comparison of evolutionary tracks with the observed distribution of stars in the main sequence undoubtedly requires consideration of gravitational darkening.

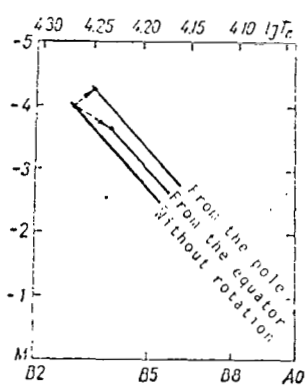

At the present time it is considered that meridianal circulation cannot ensure intermixing of the material in a rotating star because this circulation takes place extremely slowly. This conclusion is based on the fact that the theory of evolution, which was developed on the assumption of an absence of intermixing, is in good concordance with observations, and on the fact that calculations show an exceptional slowness of meridianal circulation.

The very existence of meridianal circulation in rotating stars was postulated by A. Eddington after it was proven that the equations of radiative transfer cannot be satisfied in a rigidly, or barotropically, rotating star [5]. The first attempts to determine the rate of meridianal circulation were made by A. Eddington [6], and yielded a very high value for the meridianal flow rate. However, a more precise and detailed examination of the question, made by P. Sweet [7], revealed that the value of the meridianal circulation rate in a rotating star is much lower than the value obtained by A. Eddington. It was shown that the meridianal circulation rate can be found through the expression /93

$$V_z = (1 - {}^3/_2 \sin^2\vartheta)\, p(z)\, ML^{-3} R^5 \left(\frac{\Omega}{\Omega_\odot}\right)^2 [\text{cm/sec}], \qquad (1)$$

where the mass, luminosity, and radius of the star are expressed in solar units; p(z) is some coordinate function that can be tabulated for any model.

Calculation revealed that for the Cowling model the meridianal circulation rate for the most rapidly rotating stars does not exceed 10^{-3} cm/sec. This author [8] computed the circulation rates for a model with a constant absorption coefficient for several rotation laws. Estimates yielded values of the meridianal circulation rate of the order of 10^{-3} to 10^{-1} cm/sec, and this is in good concordance with Sweet's results.

The meridianal circulation rate, even for submaximum rotation rates, is sufficient to provide intermixing of the material for a period of the order of 10^6 to 10^7 years, and one that is very short when compared with stellar evolution periods.

However, when there is meridianal circulation, material enriched with helium is carried away from the energy-releasing nucleus of the star. As L. Mestel [9] has pointed out, this results in the occurrence of a nonsymmetrical distribution of the molecular weight, and this, in turn, results in the formation of a meridianal circulation (μ-flows) in the shell that is opposite in direction to the Sweet-Eddington circulation (Ω-flows), and completely cancel the latter. In other words, the carry out of material with a high molecular weight from the nucleus results in "blocking" the exchange of material.

The assumption of rigid rotation raises objections to the Sweet-Mestel theory. Actually, as this author himself has pointed out [10], if we substitute the value of the meridianal flow rate in the Euler equation for the φ velocity component, it is easy to prove that rigid rotation can be sustained over a time interval significantly shorter than 10^6 to 10^8 years. When meridianal flow is present in a star, there must be established a rotation law, characteristic of which is equal distribution of the rotational moment along the line of flow and equatorial deceleration, in contrast to that observed for the sun. The action of Mestel's μ-flows causes the meridianal circulation to take place beyond some radius r_μ. It is only in this zone that the rotation law /94

holds. Thus, some additional mechanism is needed to sustain rigid rotation in the star. The mechanism could be a magnetic field, for example. However, what is not clear is the effect a magnetic field has on meridianal circulation and how valid are the results of P. Sweet and L. Mestel.

The Sweet-Mestel theory produces a number of unavoidable discrepancies for models different from the Cowling model. The meridianal flow rate is infinitely high on the boundary of the convective nucleus, or near the μ-barrier [11].

R.S. Smith [12] tried to take non-zero boundary conditions into account in the meridianal circulation problem. However, the meridianal flow rates he obtained at the boundary of the star were very high (of the order of $10^6\alpha$, where α is the ratio of centrifugal acceleration to the acceleration of gravity). Moreover, the radian component of the meridianal flow rate does not tend to zero with approach to the surface of the star, and this contradicts the condition of stationarity. Finally, no assumptions can remove the discrepancy in the meridianal flow with approach to the boundary of the external convective zone. All of which leads to the conclusion that the problem of meridianal circulation in rotating stars is far from solved at the present time.

In recent years it has become clear that central to the theory of the internal structure of rotating stars is the rotation law question. Although taking nonrigidity of rotation into consideration does not change our conceptions of the effect of rotation on physical conditions in the central regions of the star, and although our conclusions as to the role of gravitational darkening remain, knowledge of the true rotation law for stars will enable us to answer many important and interesting questions dealing with theory and to once again pose the problem of meridianal circulation in rotating stars.

The law of stellar rotation is defined by the conditions prevailing for the transfer of angular momentum. The rotation law for a standard model was examined in detail when the transfer of momentum is by a radiation equilibrium flux [13, 14]. The results are of great interest in connection with the investigation of giants and supergiants. A rotation law, attributed to the effect of a magnetic field, was calculated by V. Ferraro, and was in good concordance with Fay's law /95 [15]. J. Wasiutinski [18], L. Bierman [16], and K. Elsasser [17] have recently made detailed investigations of a rotation law defined by the effect of turbulent

friction. In particular, L. Bierman and K. Elsasser showed that equilibrium rotation is not rigid in the case of nonisotropic friction. The rotation law then is defined only by a field of turbulent velocities.

These results are exceptionally important in the investigations of the rotation of convective zones and nuclei. Unfortunately, our present knowledge of the true distribution of the velocity field in convective zones and nuclei does not permit us to make a concrete calculation of the rotation law that takes nonisotropic internal friction into account.

This author has pointed out [10] that stationary rotation of stars is possible, generally speaking, only in two cases. The first, already discussed earlier, corresponds to an equal distribution of the rotational momentum along the line of flow. In the second case the absence of meridianal circulation is postulated. The rotation law for the sun was computed by M. Schwarzschild [19] and J. Roxburg [20] for this latter case. This author computed the rotation law for stars with large mass [22]. The following examination of the theory of the internal structure of rotating stars for the case when the rotation law is defined by absence of meridianal circulation will result in an explanation of practically all the observed facts.

The rotation law when there is no meridianal circulation is defined by the condition of the compatibility of the hydrostatic equilibrium equations. It appears that the j-th component of the expansion of the square of the angular velocity into a Legendre polynomial can be represented in the form [21]

$$z_j = \delta_0^j - \frac{(2j+1)(2j+3)}{j+1} nA_j \xi^j \int_0^{\xi} \frac{Q_{j+2}}{x^{j+2}} dx, \qquad (2)$$

where

δ_0^j is the Kronecker delta;

ξ is the Emden radius;

n is the pseudopolytropic indicator;

A_j is a coefficient defined by the boundary conditions;

Q_j is a known function of density, temperature, and their derivatives.

Physically the function Q_j is defined as the corresponding component of the expansion of the vector product of the density and temperature gradients as a Legendre polynomial. For a polytropic gas sphere, and also for the case when /96 the pressure is a function only of density, all $Q_j \equiv 0$. Rotation in this case

should be rigid. In all the other cases Eq. (2) describes baroclinic rotation.

It is completely obvious that the function Q_j cannot change signs throughout the star, although it is not monotonic. This makes possible the evaluation of the behavior of the angular velocity as a function of the radius without making the complete calculation of the model. Actually, the function Q_j equals zero at the boundary of the convective nucleus, and does not change sign elsewhere in the star. Therefore, the sign of Q_j is determined by the sign of its derivative on the boundary of the convective nucleus.

Using the boundary conditions for a model with a constant coefficient of absorption in the shell, it is not difficult to obtain the expression

$$\operatorname{sign}\{Q_j\} = \operatorname{sign}\left\{\left(\frac{1}{\theta}\cdot\frac{d\theta}{dn}\right)^2 - \theta^n\right\}; \qquad (3)$$

the sign of the magnitude enclosed by the brackets determined the sign of the derivative of Q on the boundary of the convective nucleus and, as a result, the sign of Q.

The angular velocity decreases toward the surface, or increases, depending on the sign of Q. Since the behavior of the angular velocity is determined primarily by the magnitude z_0, and since the coefficient A_2 is essentially negative, we find that if Q is positive, the angular velocity will increase from the center to the surface.

Readily seen is that the magnitude of Eq. (3) will depend on the radius of the convective nucleus. Numerical estimates show that if the convective nucleus occupies less than 30% to 35% of the radius of the star, Q will be negative, and this corresponds to a decrease in the angular velocity outward. When the radius of the convective nucleus is large, Q is positive, and in the equilibrium case the angular velocity should increase toward the surface. Comparisons of these results with known models of stars show that the sign of Q should change in the region of the spectral class BO-B2. A more precise evaluation is impossible. This qualitative result leads to a number of conclusions that can be significant for stellar evolution.

Let us now examine stellar rotation in terms of different stages of development.

At present, the formation of stars is thought to be accompanied by some rotational moment, characterized by macroturbulence in a protostellar cloud. The entrapped rotational moment can be less than the maximum possible because the very rapid compression of the star results in the development of maximum rotation rate. /97

Further compression of the star must be accompanied by loss of rotational moment, and, consequently, loss of mass. This creates the impression that the loss of mass takes place at a rate that provides for loss of a significant part of the mass of the star for the time of its evolution in the stage of gravitational compression. However, a detailed calculation (the details of the calculation will be published separately) shows that this conclusion is incorrect. It appears that if the loss of mass occurs from the entire surface of the star, and if the terminal rotation rate is less than the maximum by a factor of 10 (determined in the terminal state), and the radius of the star decreases by a factor of 64 during compression, the loss of mass will be 47% of the initial mass. In a real case, when compression is less, and the terminal velocity is 30% to 40% of the maximum, the loss of mass will probably be but a few percent.

A more probable rotation law for the gravitational compression stage is rigid rotation attributed to the high value of turbulent friction. According to references [16, 17, 18] it can be anticipated that the rotation law will differ from a rigid law, but qualitative considerations lead to the conclusion that the difference is significant only in the outer layers of the star.

The star experiences substantial reconstruction with transition to the main sequence stage. The star's internal layers are compressed, and the new rotation law can be characterized by a decrease in angular velocity toward the surface. Preliminary estimates provide a basis for the assumption that a noncirculating rotation law is automatically established for stars later than B5-B7. The distribution of rotation rates in terms of spectral classes is determined exclusively by losses of mass during the process of evolution at the gravitational compression stage. The assumption that the rate of loss of mass has little to do with the mass of the star is quite acceptable. In other words, a star with less mass, in general, loses more of its rotational moment during the process of gravitational compression, than does a star with large mass, because its evolution time is longer.

The automatic establishment of nonturbulent rotation is impossible in the case of stars of early spectral classes because this would require greater compression of the outer layers. In other words, we would have to expect a decrease in the effective polytropic indicator with transition to the main sequence stage, and this is impossible. /98

Thus, rather strong circulation can be expected in the case of stars of early spectral classes. There is a good deal of observation data in favor of this assumption. First of all, when circulation is strong, the rotation law is characterized by the equal distribution of the specific angular momentum, and the observed linear rotation rate should decrease. Since the meridianal circulation rate in this case is determined exclusively by the deviation of the true rotation law from the nonturbulent law, the decrease in the observed rotation rate should be greater for the earlier stars, and this is in good concordance with observations [23]. In addition, an increase in the meridianal flow rate should result in an increase in the macroturbulence in the outer layers of the star, and this is well substantiated by observations.

The transition to the main sequence stage in all cases is accompanied by a sharp increase in the angular velocity of the central regions of the star. However, it is difficult to accept the assumption that this increase can break down the stability of the star, as J. Roxburg suggests [24]. The corresponding calculations show that restructuring the star from a polytrope ($n = 1.5$) to a real model with a radiative shell does not upset stability. These calculations will be published separately.

Stability should be provided automatically for the rotation law without circulation, right up to the point of exhaustion of the hydrogen in the nucleus during the evolutionary process at the main sequence stage. The star begins to undergo reconstruction at this time, and strong circulation results. It is probable that this effect, one that is similar to the Mestel μ-flows, hinders the intermixing of material between nucleus and shell. No detailed calculations have as yet been made of this circulation in an inhomogeneous star, and it is unlikely that they can be made successfully, given the present state of computer technology. All that can be said is that a linearized system of equations cannot be used in this case.

The formation of meridianal circulation should lead to the establishment /99
of another rotation law and, consequently, to a reduction in the observed rotation rate. This effect, according to I.M. Kopylov [25], is observed in all stars of class III luminosity within the main sequence. In addition, we know that all stars on the upper edge of the main sequence are either variable, or peculiar. Qualitatively, this is in good concordance with the theory developed above. It is entirely probable that the occurrence of meridianal circulation upsets the oscillating stability of the star and that rotational oscillations develop in the star [26]. Given certain assumptions, we can compute the contours of the lines forming in stars in which radial oscillations are complicated by a variable meridianal circulation [27]. The results of the calculation are very preliminary in nature, but show that changes in the contours of the lines for βCMa type stars can be explained similarly.

It is interesting to consider the fact that when there is variable circulation without any radial pulsations, the change in the spectral lines is such that it will be interpreted as ordinary pulsations. It should be pointed out that no one has yet taken this fact into consideration.

More reliable information on the rotation laws for stars can be obtained by examining the radial velocity curves for eclipsing-binary stars. Unfortunately, the difficulties involved in observing and interpreting the spectra, and the presence of gaseous flows in binary systems complicate the problem so much that obtaining unambiguous information is extremely difficult. On the other hand, a rotation law with equatorial deceleration can be expected for eclipsing-binary stars. References [28, 29] have pointed out that the observations do not, at the very least, contradict this assumption.

A theoretical determination of the rotation law for the sun would be most interesting because it could be verified directly by observations. Unfortunately, the problem is made extraordinarly complicated because of the sun's powerful exterior convective zone. A complicating factor is the effect of turbulent friction which, as a practical matter, cannot be taken into consideration, given the present state of our knowledge of motions in a convective zone. However, if it is assumed that the coefficient of internal friction is extremely anisotropic, but that its horizontal components are small, the observed rotation /100
law should agree with the rotation law for the lower boundary of the convective zone.

Thus, the assumption that the rotation law for a star at the main sequence stage is determined by the condition of absence of circulation, allows us to explain practically all the facts now known about stellar rotation, and to reduce them to a single system.

The particular importance of considering rotation during critical reconstruction of a star should be pointed out. Meridianal circulation can develop, and rotational oscillations can occur, at the moment of reconstruction in a star. The possibility that this will lead to "feeding" hydrogen to the energy-releasing zone, to the intermixing of material, and to other, similar effects, cannot be overlooked. It is quite possible that rotation can stabilize a collapsing star. Unfortunately, at the present time it is difficult even to formulate these questions precisely. But there is no basis for saying they are a long way from solution. Investigation of stellar rotation is of special significance for the development of a complete theory of stellar evolution.

REFERENCES

1. Monachan, J.J. and Roxburg, J., MN, Vol. 131, 1965, p. 13.
2. James, R. D., Ap. J., Vol. 140, 1964, p. 552.
3. Sweet, P. and Roy, A., MN, Vol. 113, 1953, p. 701.
4. Porfir'yev, V.V., Tsirk. LAO, No. 25, 1960, pp. 35-36.
5. Zeipel, H., MN, Vol. 84, 1929, pp. 665, 684, 702.
6. Eddington, A., MN, Vol. 90, 1929, p. 59.
7. Sweet, P., MN, Vol. 110, 1950, p. 548.
8. Porfir'yev, V.V., AZh., No. 33, 1956, p. 690.
9. Mestel, L., MN, Vol. 113, 1953, p. 716.
10. Porfir'yev, V.V., AZh., No. 39, 1962, p. 710.
11. Mestel, L., Star and Stellar Structure, Chicago, 1965, p. 465.
12. Smith, R. S., Z.f. Aph., Vol. 63, 1966, p. 166.
13. Kippenhan, R., Ibid., Vol. 46, 1948, p. 26.
14. Kippenhan, R., Ibid., Vol. 48, 1949, pp. 109, 203.
15. Ferraro, V.C.A., MN, Vol. 97, 1937, p. 458.
16. Bierman, L., A.f. Aph., Vol. 28, 1951, p. 304.
17. Elsasser, K., Ibid, Vol. 63, 1966, p. 65.
18. Wasiutinski, J., Astroph. Norv., Vol. 4, 1946.
19. Schwarzschild, M., Ap. J., Vol. 106, 1947, p. 427.
20. Roxburg, J., MN, Vol. 128, 1964, p. 395.
21. Porfir'yev, V.V., IN: Voprosy astrofiziki [Problems of Astrophysics], Naukova Dumka Press, Kiev, 1966, p. 86.
22. Porfir'yev, V. V., Model d'étoiles et évolution stéllaire, [Star Models and Stellar Evolution], Liege, 1960, p. 222.
23. Walker, N., Observatory, Vol. 86, 1965, p. 245.
24. Roxburg, J., Ap. J., Vol. 143, 1965, p. 111.
25. Kopylov, I.M., Izv. KpAO, Vol. 37, 1966, p. 454.
26. Porfir'yev, V.V. and Oliynik, G.A., AZh., Vol. 41, 1963, p. 878.
27. Porfir'yev, V.V., AZh., Vol. 40 , 1963, p. 579.
28. Porfir'yev, V.V. and Kalenichenko, V.V., AZh., Vol. 41, 1963, p. 878.
29. Porfir'yev, V.V. and Kalenichenko, V.V., AZh., Vol. 43, 1966, p. 560.

INVESTIGATION OF INTERSTELLAR ABSORPTION AND DISTRIBUTION OF STARS IN THE REGION $\alpha_{1950.0} = 19^h22^m$, $\delta_{1950.0} = +17°$

V. I. Kuznetsov

ABSTRACT: Absorption and distribution of stars is investigated in the $\alpha_{1950.0} = 19^h22^m$, $\delta_{1950.0} = +17°$ region. Interstellar absorption is calculated for $\gamma_{pg} = 4.0$. The line of sight is shown as passing through the arm of Sagittarius and that the maximum stellar density appears near the sun at distances of 100-300 parsecs. The luminosity function for this region is shown to agree with the luminosity function obtained by S. McCuskey.

The $\alpha_{1950.0} = 19^h22^m$, $\delta_{1950.0} = +17°$ region is located near the galactic /102 equator at a "fork" in the Milky Way. It is characterized by an absence of type O-B2 stars. It is included in P. P. Parenago's plan [1]. The boundaries of the region are 19^h16^m to 19^h28^m along α, and 16° to 18° along δ.

Interstellar Light Absorption

The catalog of photographic, photovisual magnitudes, and the spectral classes of stars in this region [2] was the basis for the investigation of light absorption by the color excess method.

Spectral classification was made by a colleague at the Abastuman Astrophysical Observatory, S. P. Apriamashvili. The classification was made from three photographs taken with the Abastuman 70-centimeter meniscus telescope with a 8-degree objective prism (dispersion was 166 Å/mm near H_γ), using the MKK atlas [3] and the Abastuman system of criteria [4].

The normal color indicators, CI_0, were determined by the Elvius method [5]. Table 1 compares the values of CI_0 obtained with the CI'_0 values taken from the Allen tables. $CI'_0 - CI_0$ was assumed equal to zero for stars of spectral class earlier than B8.

The entire region was broken down into twelve sectors in order to establish the boundaries of areas with identical absorptions. The color excess, CE, for each sector was constructed as a function of the uncorrected distance modulus m - M. Sectors with the same CE behavior were combined, and the region was broken down into five sectors with identical absorption (Figure 1).

The graphs of the relationships between CE and m - M corresponding to these sectors are shown in Figure 2.

The relationship between total photographic absorption and distance was found from Table 2 [$(m - M)_0$ is the true distance modulus; A is the value of the total photographic absorption; R is the distances in parsecs]. Figure 3 shows the absorption curves for each of the five sectors of the region.

TABLE 1. /103

Sp	A0	A7	F0	F2	F5	F6	F8	G0	G2	G3	G5	G8	K0	K2	K5
CI_0	—0.18	0.10	0.18	0.22	0.27	0.29	0.35	0.35	0 42	0.49	0 54	0.72	0.87	1.01	1.26
CI_e	—0.18	0.09	0.19	0.23	0.29	0.31	0.34	0.40	0.48	0.53	0.62	0.78	0.91	1.09	1.34

The value of the coefficient γ (when conversion is from selective absorption to total) was taken as 4.0, computed using the empirical relationship between absorption and the Whitford wavelength [6].

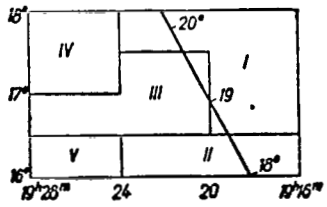

Figure 1.

Heaviest absorption was observed in sectors I and IV. Absorption in these sectors begins at distances of 100 and 170 parsecs respectively, then increases sharply, and at a distance of 1 kiloparsec from the sun takes the value $2^m.0$. The mean dimensions of the most heavily absorbing clouds are 90 and 140 parsecs.

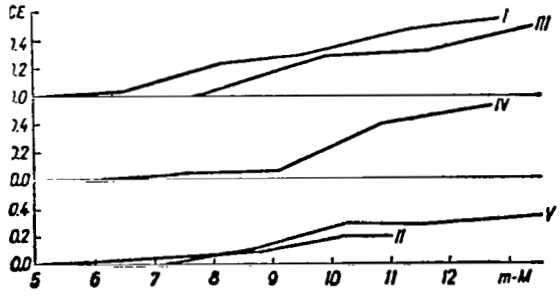

Figure 2.

Sectors II and V are characterized by relatively light absorption. Here absorption gradually increases with distance, reaching $1^m.0$ at 1 kiloparsec. In sector V the distance interval 700- /104
2750 parsecs is almost free of absorbing matter.

In sector III absorption began at a distance of 380 parsecs from the sun, increased sharply to $1^m.2$ at a distance of 560 parsecs, then increased slowly to $2^m.0$ at a distance of 2 kiloparsecs.

The mean magnitude of the coefficient of light absorption near the galactic

TABLE 2.

$m-M$	CE	A	$(m-M)_0$	R
		Sector I		
5.00	0.00	0.00	5.00	100
5.75	0.01	0.04	5.71	138
6.50	0.02	0.08	6.42	201
7.35	0.12	0.48	6.87	230
7.75	0.17	0.68	7.07	259
8.25	0.23	0.92	7.33	292
9.00	0.26	1.04	7.96	391
9.62	0.30	1.20	8.42	483
10.50	0.38	1.52	8.98	625
11.35	0.46	1.84	9.51	798
12.00	0.50	2.00	10.00	1000
12.85	0.55	2.20	10.65	1349
		Sector II		
5.00	0.00	0.00	5.00	100
6.15	0.01	0.04	6.11	167
7.00	0.04	0.16	6.84	233
8.00	0.06	0.24	7.76	357
8.81	0.09	0.36	8.45	490
9.50	0.14	0.56	8.94	614
10.00	0.18	0.72	9.28	718
10.50	0.20	0.80	9.70	871
11.00	0.22	0.88	10.12	1057
		Sector III		
5.00	0.00	0.00	5.00	100
7.90	0.00	0.00	7.90	380
8.50	0.08	0.32	8.18	432
9.00	0.15	0.60	8.40	479
9.50	0.22	0.88	8.62	530
9.95	0.29	1.16	8.79	561
10.75	0.31	1.24	9.51	828
11.62	0.32	1.28	10.34	1170
12.50	0.41	1.64	10.86	1486
13.45	0.50	2.00	11.45	1950
		Sector IV		
5.00	0.00	0.00	5.00	100
6.00	0.00	0.00	6.00	158
7.00	0.02	0.08	6.92	242
7.56	0.01	0.16	7.40	302
8.50	0.06	0.24	8.26	449
9.00	0.07	0.28	8.72	555
9.50	0.15	0.60	8.90	603
10.00	0.21	0.96	9.04	643
10.50	0.33	1.32	9.18	686
10.85	0.40	1.60	9.25	708
11.50	0.44	1.76	9.74	886
12.00	0.48	1.92	10.08	1038
12.75	0.53	2.12	10.63	1337
		Sector V		
5.00	0.00	0.00	5.00	100
7.02	0.00	0.00	7.02	253
8.00	0.06	0.24	7.76	357
8.50	0.10	0.40	8.10	417
9.00	0.14	0.56	8.44	488
9.52	0.20	0.80	8.72	555
10.30	0.28	1.12	9.18	686
11.40	0.28	1.12	10.28	1138
12.00	0.30	1.20	10.80	1445
12.50	0.32	1.28	11.22	1804
13.60	0.35	1.40	12.20	2754

plane, computed by S. McCuskey [7], is equal to $0^m.9$ at 1 kiloparsec. The investigated direction is characterized by heavy absorption, reaching $2^m.0$ at 1 kiloparsec in certain sectors of this region. However, a comparison with the results of the investigations made by colleagues at the Main Astronomical Observatory of the Academy of Sciences of the Ukrainian SSR in adjacent regions, and in lesser longitudes of the constellation Aquila, shows that absorption in the region under investigation (the region is located in the northern part of the constellation Aquila) is significantly less. /105

Comparison of the absorption curves obtained with the results for adjacent regions investigated by G. L. Fedorchenko [8, 9], shows concordance.

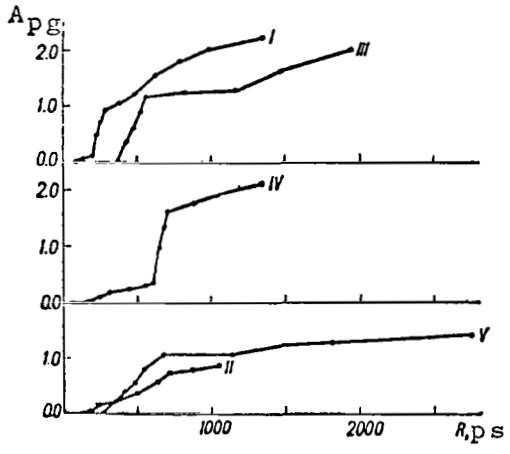

Figure 3.

Spatial Distribution of Stars. The densities of stars in various spectral classes at different distances from the sun were computed for the region as a whole according to the true distances of the stars, and their spectra. In computing the stellar densities, the list of stars [2] was supplemented with bright stars from the AGK_2 catalog. The value of the maximum stellar magnitude is $m_{pg} = 12.5$.

Stellar densities, computed for 10^3 parsecs^3 are listed in Table 3 (n is the number of stars in a given spectral interval; δ is the stellar density).

TABLE 3. ∠106

Sp / R	O-B2		B5		B8-A0		A2-A5		F0-F5		dF8-G2		dG5		gF8-K	
	n	δ	n	δ	n	δ	n	δ	n	δ	n	δ	n	δ	n	δ
0— 100	—	—	—	—	—	—	—	—	3	4.93	10	16.42	4	6.57	—	—
100— 200	—	—	—	—	3	0.70	3	0.70	14	3.27	25	5.83	13	3.03	—	—
200— 300	—	—	—	—	2	0.17	9	0.78	19	1.64	36	3.11			—	—
300— 400	—	—	—	—	3	0.13	6	0.27	18	0.80					—	—
400— 500	—	—	1	0.03	2	0.05	6	0.16							3	0.08
500— 600	—	—	—	—	3	0.05	9	0.16							3	0.05
600— 700	—	—	—	—	2	0.03	11	0.14							8	0.10
700— 800	—	—	1	0.01	4	0.04									6	0.06
800— 900	1	0.01	—	—	5	0.04										
900—1000	1	0.01	—	—	4	0.02										
1000—1100	—	—	—	—	3	0.02										
1100—1200	—	—	1	0.00	7	0.03										
1200—1300	—	—	—	—	6	0.02										
1300—1400	—	—	—	—												
1400—1500	—	—	—	—												
Mean δ			3	0.003	44	0.033	44	0.21	54	1.385	71	4.32	17	3.49	20	0.07

The region is characterized by the absence of early type stars (O-B2). This ∠107 fact, obviously, indicates that the line of sight in the given direction passes to the north of the Sagittarius arm without intersecting it. The densities of

stars B8-A0, A2-A5, as will be seen from Figure 4, reach their highest values in the immediate vicinity of the sun: at distances of 100 to 300 parsecs. In general, the densities of the stars in the various spectral classes decrease gradually in the direction investigated with distance from the sun.

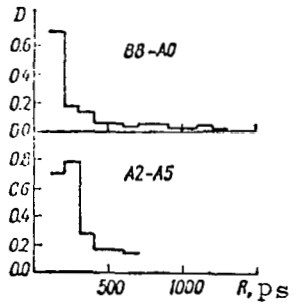

Figure 4.

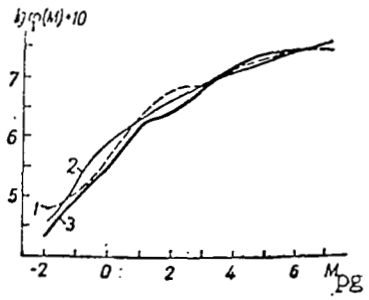

Figure 5.

The luminosity function was computed through the formula

$$\Phi = \Sigma \frac{e^{\frac{-(M-M_s)^2}{2\sigma_s^2}}}{\sqrt{2\pi}\sigma_s} D(r),$$

where

M is in absolute magnitudes;

M_s and σ_s are the mean value of the absolute magnitudes and their dispersion in a given spectral interval;

D(r) is the stellar density for the given interval.

Table 4 lists the values of the function M_s, σ_s and D.

TABLE 4.

Sp	M_s	σ_s	D
B5	−1.0	±0.7	0.003
B8-A0	+0.1	0.8	0 033
A2-A5	1.6	0.8	0.21
F0-F5	3.6	0.8	1.385
dF8-G2	5.0	0.8	4.32
dG5	6.2	0.8	3.49
gF8-K	1.3	0.8	0.07

Figure 5 compares the computed luminosity function (curve 3) with the Van Rhijn (curve 1) [10] and McCuskey (curve 2) [7] functions. /108

REFERENCES

1. Parenago, P. P., AZh., Vol. 33, No. 5, 1956, p. 749.

2. Apriamashvili, S. P., Kuznetsov, V. I., Byull. Abastumanskoy observatorii, Vol. 35, 1967.

3. Morgan, W. W., Keenan, P. C., Kellman, E., An Atlas of Stellar Spectra, Chicago, 1942.

4. Kharadze, Ye. K., Bartaya, R. A., Byull. Abastumanskoy observatorii, Vol. 25, 1960, p. 139.

5. Elvius, T., Stockh. Obs. Ann., Vol. 16, No. 5, 1951, p. 3.

6. Whitford, A. E., Ap. J., Vol. 107, 1948, p. 102.

7. McCuskey, S. W., Ap. J., Vol. 123, 1956, p. 458.

8. Fedorchenko, G. L., Izv. GAO AN UKSSR, Vol. 4, No. 2, 1963, p. 118.

9. Fedorchenko, G. L., Izv. GAO AN UKSSR, Vol. 5, No. 1, 1963, p. 128.

10. Rhijn, P. J., van, Groningen. Pub., Vol. 47, 1936.

STRUCTURAL ANOMALIES OF THE MILKY WAY IN LONGITUDES 338-22°

V. I. Kuznetsov

ABSTRACT: The results of the investigations of references [1-20] are generalized. The existence of a dust bridge between the spiral arms of Sagittarius and Carina-Cygnus is confirmed by data on the distribution of absorbing matter. The stellar arm of Sagittarius and hydrogen are compared, as is the spatial density of B8-A0 and A2-A5 stars with the density of the absorbing clouds. In general, an increase, or decrease in the density of the absorbing matter between the spiral arms of Sagittarius and Carina-Cygnus corresponds to the stellar density of B8-A0 and A2-A5 type stars.

This article generalizes the results of investigations [1-20] of, and draws /109 conclusions about, the structure of the Milky Way in longitudes l^I = 338-22°.

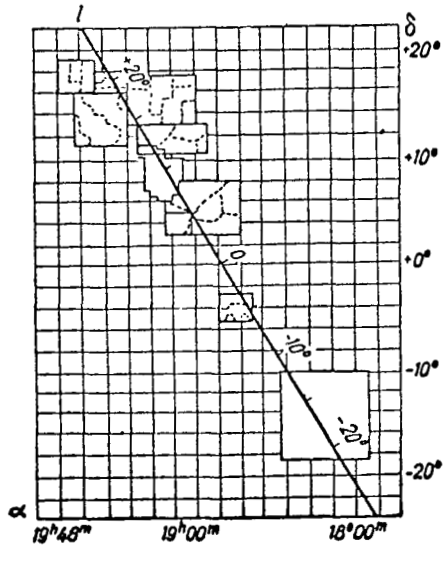

Figure 1.

Figure 1 shows the arrangement of the areas within the selected longitude region. The coordinates α and δ are equated to the era 1950.0.

The Dust Bridge Between the Sagittarius and Carina-Cygnus Spirals

References [1-20] contain the different values of the coefficient γ, used in converting from differential to total absorption. One value must be used to insure uniformity of the data on the distribution /110 of absorbing matter, and of stars in space.

The values of γ_{pg} most probable for the international system, 4.0, was used. The results obtained by Whitford [21], and by Blanko [22], served as guidance in selecting γ_{pg}.

The absorption-distance functions cited in references [1, 8, 13], were recomputed using γ_{pg} = 4.0.

The distribution of the absorbing matter within the limits of the longi- /112 tudes and distances studied can be investigated in detail by using the absorption

curves for all areas examined.

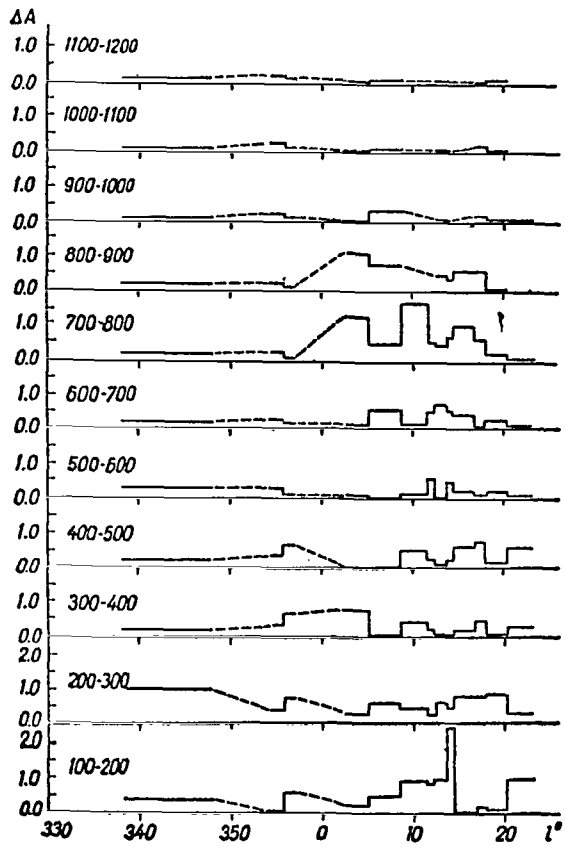

Figure 2.

Figure 2 shows the change in absorption, $\Delta A = A_N - A_{N-100}$, as a function of the galactic longitude at different distance intervals from the sun, taken every 100 parsecs. The magnitude A_N denoted absorption at distance N, where N = 200, 300, ..., 1200 parsecs. At distances greater than 1200 parsecs from the sun, ΔA changes in the limits 0.00 to $0^m.10$.

The bulk of the absorbing matter (see Figure 2) is located up to 1 kiloparsec from the sun in the longitudinal limits 0 to 18°. Between longitudes 338 and 0°, where the spiral arm of Sagittarius passes closer to the sun, there is less dust matter. The dashed line shows those places where no data are available on absorption.

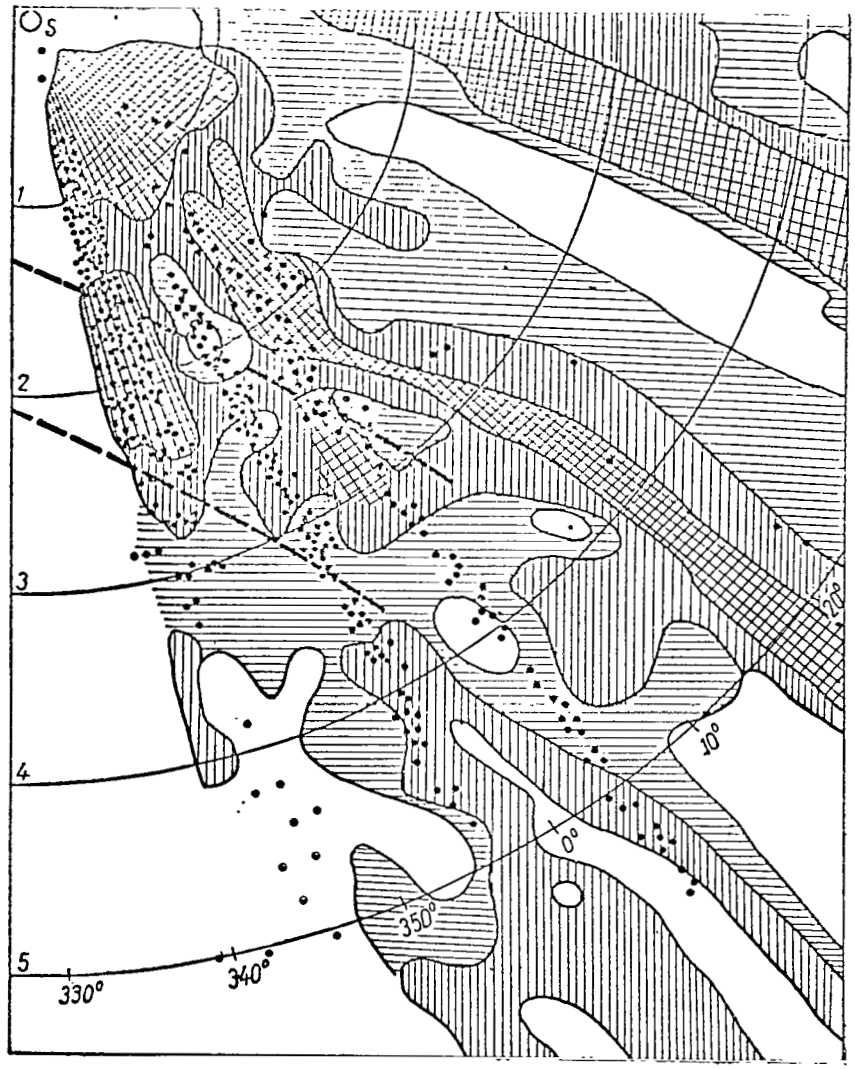

∠111

Figure 4.

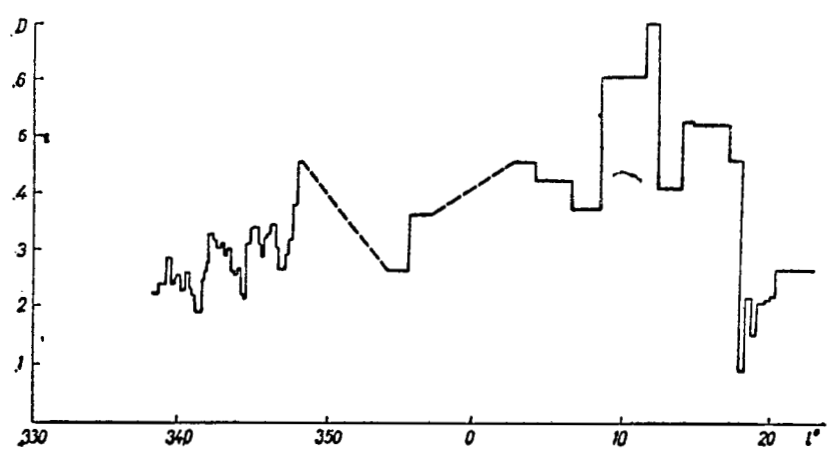

∠112

Figure 3.

The mean absorption coefficient D, expressed in stellar magnitudes per kiloparsec, as a function of the longitude l is shown in Figure 3.

The density of the dust matter increases with distance from the arm of Sagittarius in the direction of higher longitudes. The maximum value of the magnitude of D is between longitudes 9° and 12°. The density of the dust matter decreases sharply between longitudes 18° and 22°.

Only those areas comprising a dust layer bounded by latitudes ±1.5° were used in plotting ΔA and D in terms of l. /113

The values of ΔA were taken from the total absorption curve [10] between longitudes 338 and 348° when plotting ΔA in terms of l. The values of D were taken for those areas lying directly on the galactic equator [11] when plotting D in terms of l.

Thus, the interval of longitudes investigated can be characterized by very heavy interstellar absorption of light.

The data obtained on the distribution of absorbing matter confirm the existence of the dust bridge between the Sagittarius and Carina-Cygnus spirals already pointed out by I. I. Pronik [24]. Another result obtained is that the dust bridge ends in longitudes 18° to 22°.

The Position of the Sagittarius Arm

Comparing the position of O-B3 stars with the distribution of neutral hydrogen, it can be noted that in general, the hydrogen arm of Sagittarius is shifted somewhat relative to the stellar arm and is adjacent to it on the outer side relative to the center of the galaxy (Figure 4, the dots are plots of O-B3 stars in the plane of the galactic equator; the dashed lines are the axes of two parts of the Sagittarius arm and the direction of the arm, as determined by I. M. Kopylov [23]).

Early O-B3 stars in the region, investigated by V. I. Voroshilov [3-7] are located at distances of from 1200 to 3000 parsecs. By using the converted absorption curves in the two regions investigated by S. P. Apriamashvili [1, 2], and the catalog of stellar magnitudes and spectra he compiled, we can obtain the values of l and R for the O-B3 stars in the given directions. The regions

investigated by S. P. Apriamashvili were studied at relatively long distances from the sun, thanks to the presence of photometric and spectral material on the weak stars. Since the region investigated by S. P. Apriamashvili in the constellation Aquila overlaps the region investigated by V. I. Voroshilov, the l and R values for the O-B3 stars are plotted in Figure 4 at distances greater than 3 kiloparsecs.

The Spatial Distribution of B8-A0, A2-A5 Stars

The density, δ, of B8-A0 and A2-A5 stars as a function of distance is shown in Figure 5 (the hatched rectangles show the disposition of the dust clouds). /114
The height of the hatched area is proportional to the mean absorption coefficient in the individual clouds, d, expressed in stellar magnitudes per kiloparsec. The graphs are disposed from bottom to top in order of increasing longitude. The longitude interval 338°-348° corresponds to the investigations of I. I. Pronik [9-12]; 354°-357° to S. P. Apriamashvili [1, 2]; 2°30'-4°00'-6°30'-8°30' to V. I. Voroshilov [3-7]; 11°24'-12°14'-13°48'-14°-36' to V. I. Voroshilov and E. P. Polishchuk [8]; 14°36'-17°00'-18°00' to G. L. Fedorchenko [14-17]; 18°00'-20°16' to the author [19-20]; 20°16'-22°00' to G. L. Fedorchenko [18].

To be noted here is that beginning at longitude 338°, corresponding to the shortest distance of the Sagittarius spiral from the sun, the stellar density of B8-A0 stars, and the density of the absorbing matter are insignificant. The spatial density of B8-A0 stars begins to increase in the direction of higher longitudes with distance from the Sagittarius arm. The density and amount of absorbing matter also increase. The maximum stellar density of B8-A0 stars is in the longitude limits 11°24' to 14°36'. Between longitude limits 14°24' and 22°00' there is a gradual reduction in the density of the absorbing matter with reduction in the stellar density.

Analogously, there is a gradual increase in the density of A2-A5 stars, and of the absorbing matter, with distance from the Sagittarius arm. It should be noted that the increase in the density of A2-A5 stars takes place over a wider longitude interval than it does in the case of B8-A0 stars.

Comparison between the maximum stellar densities of B8-A0 and A2-A5 stars with the density of the absorbing matter shows that the correlation of the maxima

becomes more apparent with distance from the Sagittarius arm.

/115

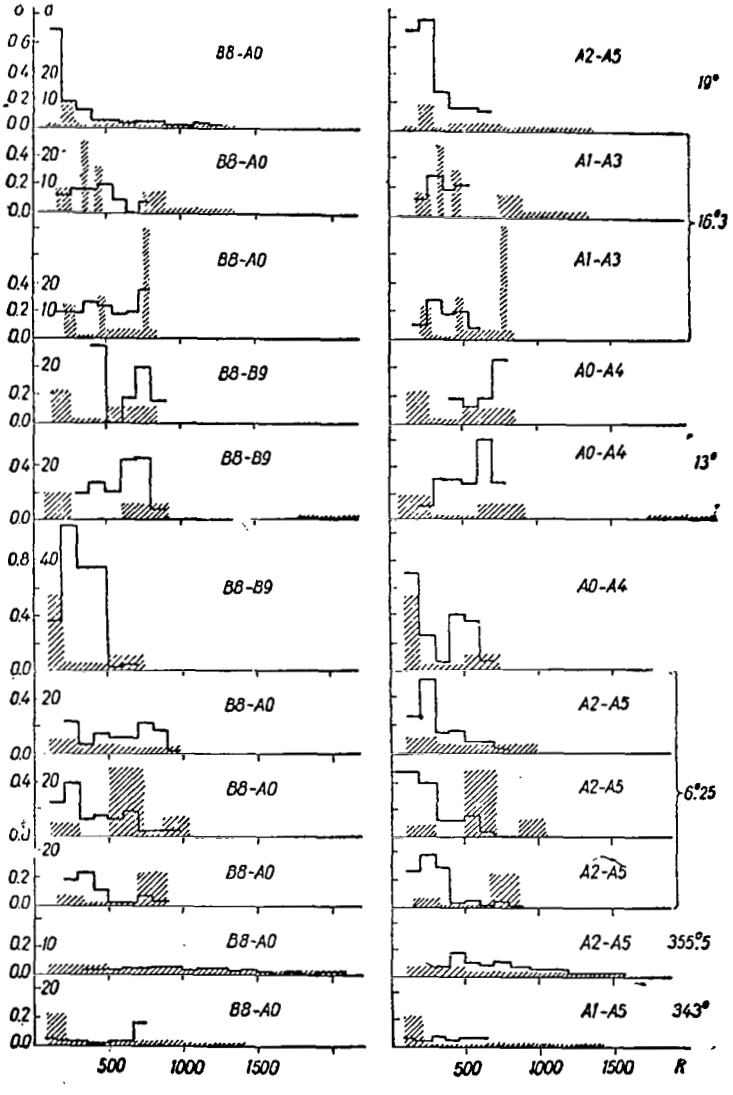

Figure 5.

The stellar densities of B8-A0 and A2-A5 stars were computed using S. P. Apriamashvili's data [1, 2]. The spatial density of B8-A0 stars is roughly uniform to 1500 parsecs, but in the interval between 1500 and 2100 parsecs it decreased in bounds by a factor of three. The stellar density of A2-A5 stars fluctuates somewhat to 800 parsecs, then gradually decreases with distance from 800 to 1500 parsecs.

It can be said that the sites of increased stellar density correspond to /116
the heaviest concentration of dust matter. The increase, or decrease in the density of the absorbing matter in the dust bridge between the Sagittarius and Carina-Cygnus spirals correspond to an increase, or decrease in the stellar density of B8-A0, A2-A5.

REFERENCES

1. Apriamashvili, S. P., Byull. Abastumanskoy observatorii, No. 30, 1964, p. 49.

2. Apriamashvili, S. P., Byull. Abastumanskoy observatorii, No. 31, 1964, p. 27.

3. Voroshilov, V. I., et al., Katalog fotograficheskikh, fotovisual'nykh velichin 22,000 zvezd [Catalog of the Photographic and Photovisual Magnitudes of 22,000 Stars], Academy of Sciences of the Ukr. SSR Press, Kiev, 1962.

4. Voroshilov, V. I., Izv. GAO AN UKSSR, Vol. 4, No. 2, 1962.

5. Voroshilov, V. I., Izv. GAO AN UKSSR, Vol. 5, No. 1, 1964.

6. Voroshilov, V. I., IN: Voprosy astrofiziki [Problems of Astrophysics], "Naukova Dumka" Press, Kiev, 1966, p. 156.

7. Voroshilov, V. I., IN: Voprosy astrofiziki [Problems of Astrophysics], "Naukova Dumka" Press, Kiev, 1966, p. 136.

8. Voroshilov, V. I., Polishchuk, E. P., IN: Voprosy astrofiziki [Problems of Astrophysics], "Naukova Dumka" Press, Kiev, 1967.

9. Pronik, I. I., Izv. KrAO, No. 20, 1958, p. 208.

10. Pronik, I. I., Izv. KrAO, No. 21, 1959, p. 268.

11. Pronik, I. I., Izv. KrAO, No. 22, 1960, p. 152.

12. Pronik, I. I., Izv. KrAO, No. 23, 1960, p. 46.

13. Weaver, H., Aph. J., Vol. 110, No. 2, 1949, p. 190.

14. Fedorchenko, G. L., Izv. GAO AN UKSSR, Vol. 4, No. 2, 1963, p. 113.

15. Fedorchenko, G. L., Izv. GAO AN UKSSR, Vol. 4, No. 2, 1963, p. 134.

16. Fedorchenko, G. L., Izv. GAO AN UKSSR, Vol. 5, No. 1, 1963, p. 128.

17. Fedorchenko, G. L., IN: Issledovaniye po fizike zvezd i diffuznoy materii [Research on the Physics of Stars and Diffuse Matter], Academy of Sciences of the Ukr. SSR Press, Kiev, 1964, p. 63.

18. Fedorchenko, G. L., IN: Voprosy astrofiziki [Problems of Astrophysics], "Naukova Dumka" Press, Kiev, 1966, p. 169.

19. Apriamashvili, S. P., Kuznetsov, V. I., Byull. Abastumanskoy observatorii, No. 35, 1967.

20. Kuznetsov, V. I., This collection, p. 102.

21. Whitford, A. E., Ap. J., Vol. 107, 1948.

22. Blanko, V. M., Lennon, C. J., A. J., Vol. 66, 1961, p. 524.

23. Kopylov, I. M., AZh., Vol. 35, No. 3, 1958, p. 390.

24. Pronik, I. I., Izv. KrAO, Vol. 25, 1961.

Translated for the National Aeronautics and Space Administration under contract No. NASw-2038 by Translation Consultants, Ltd., 944 South Wakefield Street, Arlington, Virginia 22204.

NASA-Langley, 1971 —— 30

021 001 C1 U 30 711119 S00903DS
DEPT OF THE AIR FORCE
AF WEAPONS LAB (AFSC)
TECH LIBRARY/WLOL/
ATTN: E LOU BOWMAN, CHIEF
KIRTLAND AFB NM 87117

"The aeronautical and space activities of the United States shall be conducted so as to contribute . . . to the expansion of human knowledge of phenomena in the atmosphere and space. The Administration shall provide for the widest practicable and appropriate dissemination of information concerning its activities and the results thereof."

—NATIONAL AERONAUTICS AND SPACE ACT OF 1958

NASA SCIENTIFIC AND TECHNICAL PUBLICATIONS

TECHNICAL REPORTS: Scientific and technical information considered important, complete, and a lasting contribution to existing knowledge.

TECHNICAL NOTES: Information less broad in scope but nevertheless of importance as a contribution to existing knowledge.

TECHNICAL MEMORANDUMS: Information receiving limited distribution because of preliminary data, security classification, or other reasons.

CONTRACTOR REPORTS: Scientific and technical information generated under a NASA contract or grant and considered an important contribution to existing knowledge.

TECHNICAL TRANSLATIONS: Information published in a foreign language considered to merit NASA distribution in English.

SPECIAL PUBLICATIONS: Information derived from or of value to NASA activities. Publications include conference proceedings, monographs, data compilations, handbooks, sourcebooks, and special bibliographies.

TECHNOLOGY UTILIZATION PUBLICATIONS: Information on technology used by NASA that may be of particular interest in commercial and other non-aerospace applications. Publications include Tech Briefs, Technology Utilization Reports and Technology Surveys.

Details on the availability of these publications may be obtained from:

SCIENTIFIC AND TECHNICAL INFORMATION OFFICE

NATIONAL AERONAUTICS AND SPACE ADMINISTRATION

Washington, D.C. 20546